

KU Leuven
Biomedical Sciences Group
Faculty of Pharmaceutical Sciences
Laboratory for Molecular Biodiscovery

Vrije Universiteit Brussel
Faculty of Pharmacy and Medicine
Neurogenetics Research Group



ZEBRAFISH-BASED MODELING OF HUMAN GENETIC EPILEPSIES: *FHF1* AND *TSC2* GENES

Chloë SCHELDEMAN

Promoter:

Prof. Dr. Peter A.M. de Witte
Prof. Dr. dr. Anna Jansen

Co-promoter:

Prof. Dr. dr. Lieven Lagae

Chair:

Prof. Dr. Myriam Baes

Jury members:

Prof. Dr. Lieve Moons
Prof. Dr. Guy van den Mooter
Prof. Dr. Ilse Smolders
Prof. Dr. Kathrin Thedieck
Dr. Jacek Jaworski

Dissertation presented in partial fulfilment of the requirements for the degree of Doctor in Pharmaceutical Sciences (KU Leuven) and Medical Sciences (VUB)

May 2018

Promotiezaal, Universiteitshallen, Naamsestraat 22, Leuven

Tuesday May 15th 2018

Promotor: Prof. Dr. Peter A.M. de Witte

Prof. Dr. dr. Anna Jansen

Co-promotor: Prof. Dr. dr. Lieven Lagae

TABLE OF CONTENTS

Table of contents	i
Dankwoord	vii
List of abbreviations	xi
Summary	xv
Samenvatting	xix
Chapter I: General introduction	1
1. Epilepsy	2
1.1 Definitions of epilepsy and epileptic seizure	2
1.2 Classification.....	2
1.2.1 Seizure type.....	3
1.2.2 Epilepsy type.....	3
1.2.3 Epilepsy syndrome	4
1.2.4 Etiology	4
2. Genetic diseases	4
2.1 Genetic epilepsies.....	5
2.1.1 Fibroblast growth factor homologues factor 1 (FHF1).....	6
2.1.1.1 Structure and function.....	6
2.1.1.2 Patient data	7
2.1.2 Tuberous sclerosis complex (TSC).....	7
2.1.2.1 Clinical picture.....	7
2.1.2.2 Genetic background	9
2.1.2.3 Mechanistic target of rapamycin.....	10
3. Animal models of seizures and epilepsy	12
4. Zebrafish.....	14
4.1 Origin and introduction to research.....	14
4.2 Biology of the model.....	14
4.3 Advantages of zebrafish.....	16
4.4 Limitations of zebrafish	16
4.5 Zebrafish as a model of epileptic seizures and epilepsy	17
4.5.1 Zebrafish seizure models.....	18
4.5.2 Genetic zebrafish epilepsy models.....	19
4.6 Translational bioinformatics using the zebrafish model	23
Chapter II: Research objectives	27

Chapter III: Gain-of-function <i>FHF1</i> mutation causes early-onset epileptic encephalopathy with cerebellar atrophy	31
1. Abstract	32
2. Introduction	32
3. Methods	33
3.1 Genetic analysis of the EOEE-affected family	33
3.2 Zebrafish overexpression studies	33
3.2.1 Zebrafish maintenance and breeding	33
3.2.2 Overexpression experiments	33
3.2.3 <i>fhlb1</i> mRNA expression analysis	34
3.2.4 Tectal field recordings.....	34
3.3 Standard protocol approvals, registrations and patient consents	34
4. Results	35
4.1 <i>FHF1</i> mutation identified in EOEE with cerebellar atrophy	35
4.1.1 Clinical phenotype	37
4.2 WT vs mutated <i>Fhlb1</i> in zebrafish.....	38
5. Discussion	43
6. Supplementary information.....	45
6.1 Table e-1: Primer sequences of primers used for <i>Fhlb1</i> site-directed mutagenesis and primers for real-time qPCR.....	45
6.2 Figure e-1: Ictal EEG of patient with <i>FHF1</i> mutation.....	46
6.3 Figure e-2: Sequence alignment of human <i>FHF1</i> and zebrafish <i>Fhl1</i> orthologs	47
7. Acknowledgements	48
Chapter IV: mTOR-related neuropathology in mutant <i>tsc2</i> zebrafish: phenotypic, transcriptomic and pharmacological analysis.....	51
1. Abstract	52
2. Introduction	53
3. Methods	54
3.1 Zebrafish strains	54
3.2 Zebrafish maintenance and breeding	54
3.3 Genotyping	55
3.4 Morphological phenotyping	55
3.5 Survival assay.....	55
3.6 Head and body measurements.....	55
3.7 Immunohistochemistry.....	55
3.8 Photomotor response.....	56
3.9 Locomotor behavior	56
3.10 Local field potential (LFP) recordings.....	57
3.11 Zebrafish RNA extraction	57
3.12 RNA-sequencing of zebrafish samples	57

3.13	Bioinformatics analysis.....	57
3.14	Protein-coding potential of novel genes.....	58
3.15	Gene ontology and pathway enrichment analysis.....	58
3.16	RT-qPCR validation.....	58
3.17	Prediction of pharmacological targets for TSC.....	59
3.18	Pharmacological validation.....	59
3.19	Western blot.....	59
4.	Results.....	60
4.1	<i>tsc2</i> homozygous larvae survive until 9 days post fertilization (dpf) and display enlarged brains.....	60
4.2	7 dpf homozygous larvae demonstrate neurobehavioral alterations.....	62
4.3	<i>tsc2</i> homozygous larvae display abnormal brain activity.....	62
4.4	Characterization of the zebrafish transcriptome.....	64
4.4.1	Differentially expressed genes.....	64
4.4.2	RT-qPCR validation of RNA-Seq data.....	66
4.4.3	Enriched gene ontology terms and pathways.....	66
4.4.4	Genes related to inflammation and immune response differentially expressed in the zebrafish model.....	67
4.4.5	Up-regulation of <i>ctss2.1</i> in the <i>tsc2</i> homozygous larvae.....	67
4.4.6	Prediction of pharmacological targets for TSC.....	67
4.5	Pharmacological validation.....	69
5.	Discussion.....	71
6.	Supplementary information.....	75
6.1	S1 fig.: heatmap of the complete transcriptome profile of each sequenced replicate..	75
6.2	S2 fig.: Volcano plot of differentially expressed genes between the <i>tsc2</i> ^{+/+} and the <i>tsc2</i> ^{-/-} zebrafish.....	76
6.3	S3 fig.: Volcano plot of differentially expressed genes between the <i>tsc2</i> ^{+/+} and the <i>tsc2</i> ^{+/-} zebrafish.....	77
6.4	S4 fig.: The expression of <i>tsc2</i> in each of the genotypes.....	78
6.5	S5 fig.: RT-qPCR validation of selected genes.....	79
6.6	Supplementary tables.....	80
7.	Acknowledgements.....	80
	Chapter V: General discussion.....	83
1.	Challenges in anti-seizure drug discovery.....	84
1.1	Potential of genetic zebrafish epilepsy models in anti-seizure drug discovery.....	84
1.2	<i>fhfl</i> mutant zebrafish model.....	85
1.3	<i>tsc2</i> mutant zebrafish model.....	86
1.3.1	Challenges for mutant zebrafish epilepsy models in anti-seizure drug discovery.....	87
1.3.1.1	Sample size.....	88
1.3.1.2	Cost-benefit analysis: genotyping-free vs genotyping.....	90
2.	Conclusion and future perspectives.....	92

References	95
Curriculum vitae	107
Personal contribution.....	111
Conflict of interest statement	113

DANKWOORD

Er zijn heel veel personen die direct of indirect hebben bijgedragen tot mijn doctoraatsopleiding en het tot stand komen van dit werk. Graag wil ik ieder van hen bedanken, met name zij die dit alles van dichtbij hebben meegemaakt.

Peter, ik ben ongelofelijk dankbaar dat ik deel heb mogen uitmaken van uw zebравisteam. Op wetenschappelijk vlak wil ik u, als promotor, bedanken voor uw geloof in mij, uw steun, uw supervisie en het feit dat de deur altijd openstond. Ook prijs ik mezelf gelukkig dat ik in uw labo de mogelijkheid heb gekregen om een portfolio aan technieken te verwerven. Verder koester ik mooie herinneringen aan de vele laboactiviteiten gaande van verjaardagen, BBQs en kerstfeestjes bij u thuis tot meer sportieve uitdagingen, zoals deelname aan de University Trail, intense jogsessies onder de middag (uitzonderlijk weldoend na regen, vermits er dan meer zuurstof in de lucht hing), het afleggen van een hoogteparcours en kanoën op de Lesse. Bedankt voor deze fantastische tijd. *An* en *Lieven*, mijn (co-)promotoren, zonder jullie was er misschien niet eens sprake geweest van dit doctoraat. Ontzettend bedankt dat jullie in mij en mijn project geloofden en dat jullie je schouders er mee onder wilden zetten. Ook wil ik jullie bedanken om mij, als benjamin, te introduceren binnen het Epistop project, wat mijn doctoraat binnen een groter perspectief plaatste.

Naast mijn (co-)promotoren wil ik ook de leden van mijn thesis advisory committee (TAC), *Myriam Baes*, *Lieve Moons*, *Guy Van den Mooter* graag bedanken voor de goede opvolging en constructieve feedback tijdens voorgaande evaluatiemomenten en ook voor het kritisch nalezen en evalueren van mijn thesis. I would also like to thank my (external) jury members, *Ilse Smolders*, *Kathrin Thedieck* and *Jacek Jaworski*, for the critical assessment of my thesis.

Een welgemeend dankjewel aan de dames van het secretariaat Farmaceutische Wetenschappen aan KUL en het secretariaat Geneeskunde en Farmacie aan VUB, *An Haine*, *Chantal Voets*, *Esther Balogh*, *Jenny Vijverman*, *Tamara De Lombaert* en *Irén Varga* om mijn praktische beslommeringen gaande van bestellingen tot de logistiek voor mijn verdediging op een efficiënte manier het hoofd te bieden.

Patrick Augustijns, bedankt om mij te begeleiden en te vertrouwen als chair van het organiserend comité van de ULLA summer school 2017. Ik ben dankbaar voor wat ik geleerd heb uit deze unieke ervaring.

To all my former and current colleagues of the lab, *Angela, Annelii, Arianna, Bac, Daniëlle, Evelien, Hung, Jan, Jing, Jo, Maoxuan, Marly, Michèle, Monika, Niels, Ola, Olivia, Rita, Sanne, Tatiana, Xixin and Yifan*, a big THANK YOU for having contributed to such a nice and cheerful working environment. I really enjoyed working with you.

I would like to especially thank the following people: *Daniëlle, Jan* en *Michèle*, bedankt voor de goeie tijden in het labo en om naast goeie collega's ook vrienden te zijn geworden ☺. *Ola*, I am grateful for everything you taught me as my mentor in molecular biology. *Ola* and *Annelii*, thanks for accepting me in the “post-doc” office. I also want to thank you for our small talk and for always being prepared to answer my questions and give feedback on my practice presentations.

Ook wil ik graag mijn vriendinnen van de Kempen en van Farmacie bedanken om op tijd en stond eens te vragen “En, hoe gaat het met de visjes?” en natuurlijk voor de nodige ontspanning.

Tot slot wil ik mijn familie en schoonfamilie bedanken. *Mama en Papa*, dank voor jullie onvoorwaardelijke steun bij alle belangrijke keuzes in mijn leven. *Lauranne*, bedankt om zo'n goeie zus te zijn. Een speciaal woord van dank gaat naar mijn man *Joost*, om er te altijd te zijn voor mij en mij graag te blijven zien ook wanneer ik over niet veel anders dan mijn thesis kon praten. Dank voor dit en zoveel meer.

LIST OF ABBREVIATIONS

3R	replacement, refinement, reduction
4E-BP	eukaryotic translation initiation factor 4E-binding protein
AML	angiomyolipoma
AMPK	AMP-activated protein kinase
ASD	anti-seizure drug (in clinic referred to as anti-epileptic drug)
Atg13	autophagy-related 13
Cas9	CRISPR-associated protein 9
CNS	central nervous system
CPC	coding potential calculator
CRISPR	clustered regulatory interspaced short palindromic repeats
DAVID	Database for Annotation, Visualization and Integrated Discovery
DEG	differentially expressed gene
Deptor	DEP domain containing mTOR-interacting protein
DGIdb	drug gene interaction database
dpf	days post fertilization
DSB	double strand break
ENU	N-ethyl N-nitrosurea
EOEE	early-onset epileptic encephalopathy
ETSP	epilepsy therapy screening program
FGF	fibroblast growth factor
FGFR	fibroblast growth factor receptor
FHF	fibroblast growth factor homologues factor
FIP200	FAK family kinase-interacting protein of 200 kDa
FKBP12	FK506-binding protein of 12 kDa
FPKM	fragments per kilobase of exon per million fragments mapped
FRB	FKBP12-rapamycin binding
GAERS	genetic absence epilepsy rat from Strasbourg
gRNA	guide RNA

hpf	hours post fertilization
IL1B	interleukin 1 beta
kb	kilobase
kDa	kilo dalton
LAM	lymphangioliomyomatosis
LFP	local field potential
lincRNA	long intergenic non-coding RNA
LOH	loss-of-heterozygosity
MES	maximal electro-shock
mLST8	mammalian lethal with sec-13
MOA	mechanism of action
MO	morpholino
mtDNA	mitochondrial DNA
mSin1	mammalian stress-activated map kinase-interacting protein 1
mTOR	mechanistic target of rapamycin
mTORC1	mechanistic target of rapamycin complex 1
Na _v	voltage-gated sodium channel
NHEJ	non-homologues end joining
NMI	no mutation identified
p70S6K1	p70 ribosomal S6 kinase
PI3K	phospho-inositide 3-kinase
PMR	photomotor response
pmTOR	phosphorylated mTOR
PRAS40	proline-rich AKT1 substrate 40 kDa
Protor	protein observed with Rictor
pS6	ribosomal protein pS6
PTZ	pentylentetrazol
Raptor	regulatory-associated protein of mTOR
Rictor	rapamycin-insensitive companion of mTOR
Rheb-GAP	Ras homolog enriched in brain – GTPase activating protein
RNA-Seq	RNA-Sequencing
RT-qPCR	real-time quantitative PCR
SE	status epilepticus
SEGA	subependymal giant cell astrocytoma

SEN	subependymal nodule
SRS	spontaneous recurrent seizures
TALENs	transcription activator-like effector nucleases
TAND	TSC-associated neuropsychiatric disorders
TBC1D7	Tre2-Bub2-Cdc 1 domain family, member 7
Tel2	telomere maintenance 2
TSC	tuberous sclerosis complex
Tti1	Tel-two interacting protein 1
WES	whole exome sequencing
WISH	whole-mount in situ hybridization
wpf	weeks post fertilization
WT	wild type
ZFNs	zinc finger nucleases

SUMMARY

Epilepsy is one of the most common chronic brain disorders characterized by the occurrence of spontaneous, recurrent epileptiform discharges. The standard therapy consists of anti-seizure drugs, which effectively control seizures in the majority of patients. However, 30% of epilepsy patients continue to suffer from seizures due to drug-resistance. Based on its etiology epilepsy is classified into six different groups: structural, genetic, infectious, metabolic, immune and unknown. A genetic epilepsy results from a variant in a gene that is presumed or known to be pathogenic for epilepsy. Due to the recent emergence of next-generation sequencing, more and more candidate-epilepsy genes are being uncovered at a high rate, necessitating the use of proper animal models to validate their disease-causing potential. Therefore, together with the issue of drug-resistance, there is a high need for ‘personalized’ animal models that closely mimic epilepsy in humans.

The use of zebrafish as a small, non-mammalian model has emerged in the field of epilepsy research. Unique features of this simple vertebrate are the production of hundreds of eggs per week, fast *ex utero* development, ease of genetic manipulation, small size which enables the use of multi-well plate format, and the fact that compounds can be immersed in the swimming medium. Taken together, these advantages allow (i) fast modeling of a human candidate epilepsy gene and therefore rapid translation to the clinic, (ii) elucidation of the pathophysiology of epilepsy and (iii) a moderate- to high-throughput screening of compounds in genetic zebrafish epilepsy models. Therefore, we used zebrafish to model two mutations that are presumed (*FHF1* gene) and known (*TSC2* gene) to result in epilepsy or a syndrome-associated epilepsy.

In the first project, we investigated whether a variant in *FHF1* could be linked to the development of epilepsy. Whole exome sequencing of a family quintet identified a heterozygous missense mutation in the *FHF1* gene of two siblings suffering from early-onset epileptic encephalopathy associated with intellectual disability and cerebellar atrophy. To investigate the functional consequences of the patients’ mutation *in vivo*, we established an Fhf1 overexpression model in zebrafish larvae using Tol2 tissue-specific transgenesis. Local field potential recordings from the midbrain of mutant Fhf1 overexpression larvae revealed a significantly higher incidence of recurrent epileptiform discharges when compared to wild type overexpression and control larvae. Moreover, real-time qPCR confirmed the abnormal brain activity to result from the overexpressed *fhf1* mutation. These results underscore the utility of zebrafish to investigate and validate rapidly the epileptic potential of a human candidate epilepsy gene.

In the second project, we investigated the brain phenotype of tuberous sclerosis complex, a rare genetic disease resulting from loss-of-function mutations in the *TSC1* or *TSC2* genes. For this purpose, the *tsc2^{vu242}* zebrafish model was used. The homozygous (*tsc2^{-/-}*) larvae have enlarged brains, reduced locomotor behavior and display epileptiform discharges at 7 dpf. Rapamycin, a well-known mTOR inhibitor was shown to have a significant rescue effect on selected phenotypic readouts as well as at the molecular level. These results demonstrate that the *tsc2^{-/-}* zebrafish model mirrors certain aspects of the human condition. To acquire more insight into the neuropathology of TSC, transcriptome profiling was performed. Between WT and *tsc2^{-/-}* larvae 1,414 genes were differentially expressed, with genes related to inflammation and immune response being up-regulated in the heads of *tsc2^{-/-}* larvae. This is in line with findings in human brain tissue, where gross transcriptome changes have been reported. Besides, inflammatory and immune responses appear to be major hallmarks of TSC. Interestingly, new areas of investigation, including dysfunction of calcium ion channels and calcium signaling, and up-regulation of *ctss2.1* were discovered using transcriptomics. These findings suggest that the *tsc2^{-/-}* zebrafish model can be an interesting tool to gain further pathomechanistic insights into TSC and TSC-associated epilepsy.

In conclusion, our two studies demonstrate the translational potential of zebrafish in both the fast modeling of newly discovered candidate epilepsy genes and the modeling of existing epilepsy-associated syndromes.

SAMENVATTING

Epilepsie is een van de meest voorkomende chronische hersenziekten en wordt gekenmerkt door spontane, terugkerende epileptische ontladingen in de hersenen. In de standaardtherapie worden anti-epileptica toegediend, die bij de meerderheid van de patiënten de aanvallen effectief onder controle brengen. 30% van de epilepsiepatiënten blijft echter last hebben van aanvallen door hun resistentie tegen geneesmiddelen. Op basis van haar etiologie wordt epilepsie ingedeeld in zes verschillende soorten: structureel, genetisch, infectieus, metabool, immuun en onbekend. Genetische epilepsie is het gevolg van een variant in een gen waarvan wordt verondersteld of waarvan bekend is dat het pathogeen is voor epilepsie. Door de recente opkomst van Next Generation Sequencing, worden aan sneltempo meer en meer kandidaat-epilepsie-genen ontdekt. Het analyseren van die kandidaat-epilepsie-genen vereist de juiste diermodellen om hun ziekteverwekkend potentieel te valideren. Naast het probleem van geneesmiddelenresistentie, is er ook daarom een grote behoefte aan 'gepersonaliseerde' diermodellen die de epilepsie in mensen goed nabootsen.

Zebravissen worden als een klein, niet-zoogdiermodel steeds meer gebruikt in het domein van epilepsieonderzoek. Unieke kenmerken van deze eenvoudige gewervelde dieren zijn dat ze honderden nakomelingen per week produceren, dat ze snel ex-utero ontwikkelen, dat ze makkelijk genetisch te manipuleren zijn, dat ze door hun klein formaat in multi-well platen kunnen worden gebruikt en dat ze verbindingen toegediend kunnen krijgen via het zwemmedium. Al deze voordelen samen zorgen voor (i) snelle modellering van een menselijk kandidaat-epilepsie-gen en dus snelle vertaling naar de kliniek, (ii) opheldering van de pathofysiologie van epilepsie en (iii) een gemiddelde tot hoge-doorvoer screening van verbindingen in genetische zebravis-epilepsiemodellen. Daarom gebruikten we het zebravis proefdiermodel om twee mutaties te modelleren waarvan verondersteld wordt (*FHF1*-gen) of bekend is (*TSC2*-gen) dat ze resulteren in epilepsie of een syndroom-geassocieerde epilepsie.

In het eerste project onderzochten we of een variant in *FHF1* kon gekoppeld worden aan de ontwikkeling van epilepsie. Met whole exome sequencing van een familiëkwintet identificeerden we een heterozygote missense mutatie in het *FHF1*-gen van een broer en zus. Zij leden aan vroeg optredende epileptische encefalopathie geassocieerd met een verstandelijke beperking en cerebellaire atrofie. Om de functionele gevolgen van de mutatie van de patiënten *in vivo* te onderzoeken, hebben we een Fhf1-overexpressiemodel gecreëerd in zebravislarven met behulp van Tol2-weefsel-specifieke transgenese. Opnamen van lokale veld potentialen van de middenhersenen van mutante Fhf1 overexpressie larven

wezen erop dat recidiverende epileptiforme ontladingen significant vaker voorkwamen in vergelijking met wild type overexpressielarven en controlelarven. Bovendien bevestigde real-time qPCR de abnormale hersenactiviteit als gevolg van de tot overexpressie gebrachte *fhf1*-mutatie. Deze resultaten onderstrepen het nut van zebavis om snel het epileptische potentieel van een menselijk kandidaat-epilepsiegen te onderzoeken.

In het tweede project onderzochten we het hersenfenotype van tubereuze sclerose, een zeldzame genetische ziekte als gevolg van loss-of-function mutaties in de *TSC1*- of *TSC2*-genen. Hiervoor werd gebruik gemaakt van het *tsc2^{vu242}* zebavis model. De homozygote (*tsc2^{-/-}*) larven hadden vergrote hersenen, verminderd locomotorisch gedrag en toegenomen epileptiforme ontladingen op 7 dpf. Rapamycine, een bekende mTOR-inhibitor, bleek een significant hersteleffect te hebben op geselecteerde fenotypische readouts evenals op moleculair niveau. Deze resultaten tonen aan dat het *tsc2^{-/-}* zebavismodel bepaalde aspecten van de menselijke conditie weerspiegelt. Om meer inzicht te krijgen in de neuropathologie van TSC, werd ook een transcriptoomstudie gedaan. Tussen WT en *tsc2^{-/-}* larven werden 1,414 genen differentieel tot expressie gebracht, waarbij genen die gerelateerd zijn aan ontsteking en immuunrespons opgeregeerd werden in de hoofden van *tsc2^{-/-}* larven. Dit komt overeen met bevindingen in menselijk hersenweefsel, waar grote transcriptoomveranderingen zijn gerapporteerd. Bovendien blijken ontstekingsreacties en immuunreacties belangrijke kenmerken van TSC te zijn. Interessant is dat er nieuwe onderzoeksgebieden zijn gevonden met behulp van transcriptomics, waaronder disfunctie van calciumionkanalen en calciumsignaling, en up-regulatie van *ctss2.1*. Deze bevindingen suggereren dat het *tsc2^{-/-}* zebavismodel een interessant hulpmiddel kan zijn om verdere pathomechanistische inzichten te verkrijgen in TSC en TSC-geassocieerde epilepsie.

Besluitend: onze twee studies illustreren het translationele potentieel van het zebavis proefdiermodel in zowel de snelle modellering van nieuw ontdekte kandidaat-epilepsie-genen als de modellering van bestaande epilepsie-geassocieerde syndromen.

CHAPTER I

General introduction

1. Epilepsy

1.1 Definitions of epilepsy and epileptic seizure

Epilepsy originates from the Greek word “επιλαμβάω” which signifies ‘to be taken over’ and refers to the clinical expression (i.e. epileptic seizure) of the disease (1). According to the International League Against Epilepsy (ILAE), an epileptic seizure is defined as a transient occurrence of signs and/or symptoms due to abnormal excessive or synchronous neuronal activity in the brain (ILAE 2005) (2). More recently, the definition of epilepsy was updated with epilepsy being defined as a disease of the brain characterized by any of the following conditions: (I) at least two unprovoked (or reflex) seizures > 24h apart, (II) one unprovoked (or reflex) seizure and a probability of having another seizure similar to the general recurrence risk after two unprovoked seizures ($\geq 60\%$) over the next 10 years, or (III) an epilepsy syndrome (ILAE 2014) (2). With worldwide more than 70 million people being affected, epilepsy is one of the most common chronic neurologic conditions (1).

1.2 Classification

According to ILAE, the classification of epilepsies requires a multilevel approach combining information on seizure type, epilepsy type and epilepsy syndrome (3). Ideally, a diagnosis should be made at all three levels and also include information on the etiology of the epilepsy (Fig. 1) (3, 4). This classification improves understanding (patient), communication and discussion (clinicians) and allows investigation to optimize treatments (researchers) (5).

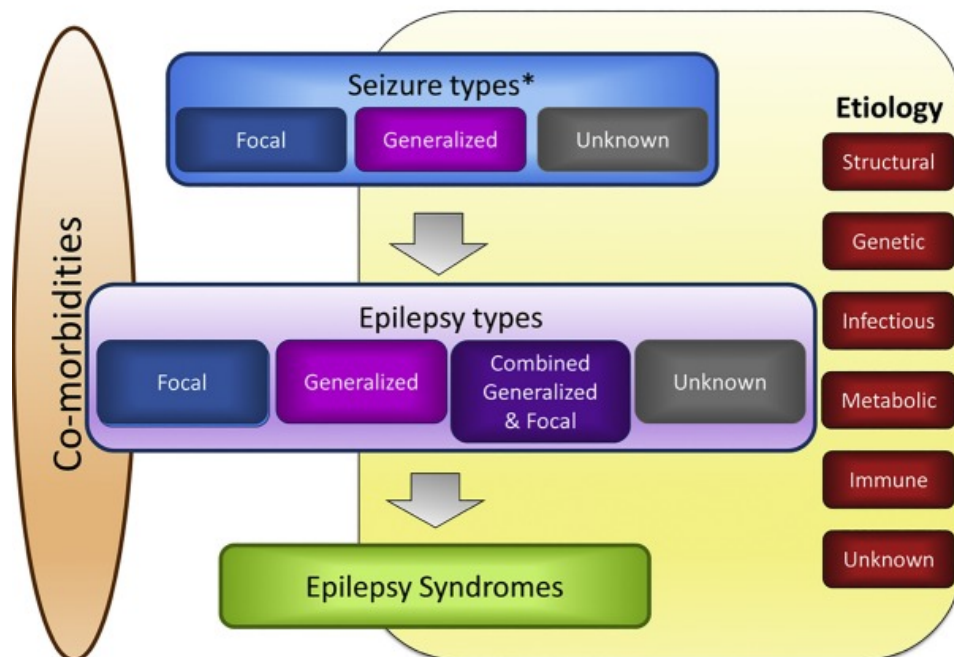


Figure 1: ILAE 2017 classification of the epilepsies. From Scheffer et al. 2017 *Epilepsia* (4).

1.2.1 Seizure type

Based on their type of onset epileptic seizures are classified as focal, generalized, unknown or unclassifiable (Fig 1) (5). A focal onset indicates that the seizure arises from a part of only one cerebral hemisphere, whereas generalized seizures necessitate involvement of both cerebral hemispheres (6). When information on the origin of seizures is not available, although clear manifestations are observed, they are classified as unknown (5). A further sub-classification is based on the level of awareness (Fig. 2). The terms ‘aware’ or ‘impaired awareness’ are clinically more relevant with regards to focal onset seizures, since generalized seizures mostly imply a loss or impairment of awareness. The next level to be considered for all three types of seizure onsets is whether the onset can be classified as ‘motor’ or ‘non-motor’. These categories can be expanded with different classifiers based on the first sign or symptom of the seizure (Fig.2) (5).

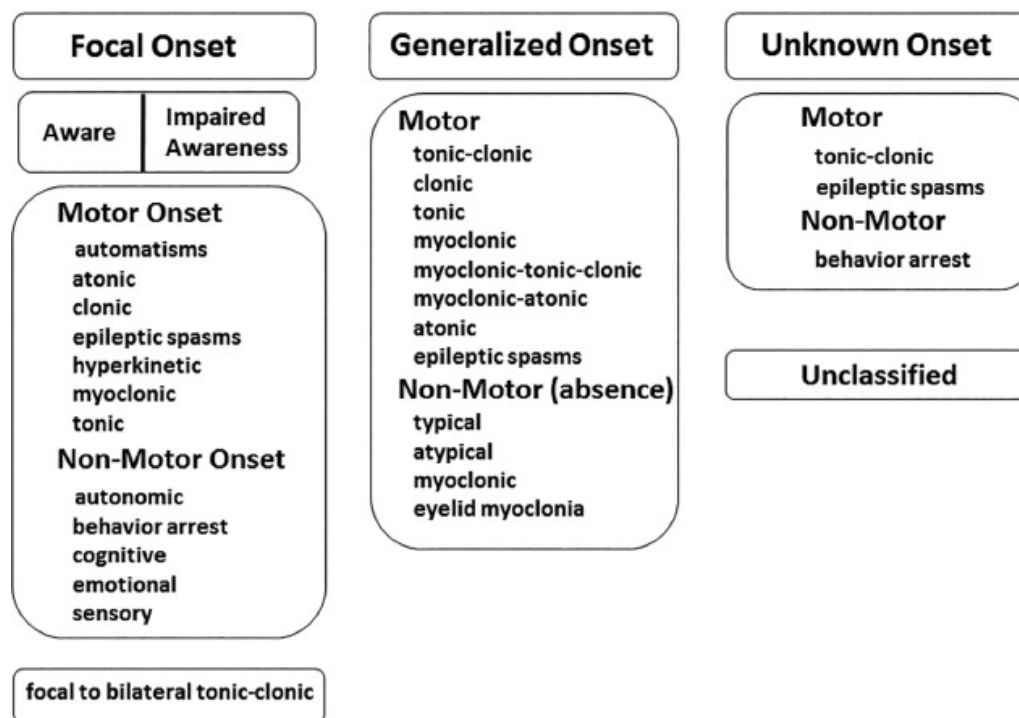


Figure 2: ILAE 2017 classification of seizure types. From Fisher et al. 2017 *Epilepsia* (3).

1.2.2 Epilepsy type

In order to classify the epilepsy type, a patient needs to be diagnosed with epilepsy according to the 2014 definition (4). The epilepsy type can be divided into 4 categories: focal, generalized, combined generalized – focal and unknown (Fig. 1). The second level of epilepsy type is broader than the seizure classification, since one epilepsy type can consist of multiple seizure types (4, 5). Besides the seizure type(s), also information on the clinical picture, laboratory tests and imaging contribute to the determination of the epilepsy type (5).

1.2.3 Epilepsy syndrome

The third level comprises the diagnosis of an epilepsy syndrome (Fig. 1). An epilepsy syndrome refers to a cluster of features (including seizure type(s), EEG and imaging findings, comorbidities, age at onset and remission, prognosis) that tend to occur together (4, 5). Although several epilepsy syndromes are well recognized (e.g. Dravet syndrome), a formal ILAE classification of these syndromes is not (yet) available (4).

1.2.4 Etiology

Besides the multilevel classification of epilepsy, information on the etiology of the patients' epilepsy is important since it can influence the treatment options (e.g. epilepsy surgery in case of structural etiology) (4). Based on its etiology epilepsy is classified into six different groups: structural, genetic, infectious, metabolic, immune and unknown (Fig. 1). A patients' epilepsy might belong to more than one etiological group (4, 5). A structural etiology is characterized by the presence of a structural abnormality visible on neuroimaging, which is likely to cause the patients' seizures. This abnormality can be acquired (e.g. stroke, trauma) or genetic (e.g. malformations of cortical development or tuberous sclerosis complex) (4, 5). A patients' epilepsy is likely to be genetic when the patient has a mutation in a gene that is presumed or known to be pathogenic for epilepsy. 'Genetic' here is not used as a synonym for 'inherited', since an increasing number of patients present with *de novo* mutations. An example of an epilepsy with genetic etiology is Dravet syndrome, where a pathogenic variant in the *SCN1A* gene gives rise to seizure development (4, 5). An infectious etiology assumes the epilepsy to result directly from an infection, e.g. development of epilepsy after resolved meningitis. However, seizures triggered by an acute infection are not considered to fall within this category (4, 5). A patients' epilepsy that results directly from a metabolic disturbance is categorized as having a metabolic etiology. Most of these metabolic disorders have a genetic cause, e.g. porphyria, although some might be acquired, e.g. cerebral folate deficiency (4, 5). An immune epilepsy directly results from an autoimmune disease, where antibodies lead to encephalitis resulting in seizures (e.g. anti-NMDA receptor encephalitis) (4, 5). Finally, an unknown etiology means that the cause of a patients' epilepsy remains unclear (4, 5).

2. Genetic diseases

A genetic disease or disorder results from abnormalities in an individuals' genome. Three different types of chromosomal abnormalities can occur: point, chromosomal and genomic mutations (7). Point mutations (i.e. one nucleotide change) often give rise to a single-gene disorder, whereas chromosomal rearrangements affect a larger area of the chromosome and therefore are often more severe (7). Genomic mutations are characterized by a change in the total number of chromosomes present (7). Recently, more than 10,000 human diseases have been described as being genetic (8).

Based on their inheritance pattern, genetic disorders are classified as Mendelian or non-Mendelian (9). The Mendelian disorders, which are also known as single-gene disorders, are estimated to affect 1% of the general population (7). Within this Mendelian category of inheritance four subtypes can be distinguished: autosomal dominant, autosomal recessive, X-linked and Y-linked inheritance (7, 9). The term autosomal indicates that the mutated allele or pair of alleles is located on a non-sex chromosome (autosome). In autosomal disorders males and females are equally affected (7). An autosomal dominant disorder refers to the fact that a single affected allele suffices to result in illness (e.g. Huntington's disease). Recessive autosomal disorders require both alleles to be affected in order to have the disease or disorder (e.g. cystic fibrosis). When the affected allele or pair of alleles is located on a sex chromosome, the terms X-linked or Y-linked are used (9). X-linked disorders can be dominant (e.g. Fragile X syndrome) or recessive (e.g. Duchenne muscular dystrophy) (9). Males are more prone to a X-linked disorder since they only have one copy of the X-chromosome. Y-linked disorders only affect males and are transmitted from father to son (e.g. Y-chromosome infertility) (7, 9).

Non-Mendelian patterns of inheritance include complex (or multifactorial) inheritance, mitochondrial inheritance and chromosomal abnormalities (7, 9). In contrast to Mendelian disorders, a complex disorder is not caused by a single gene mutation but is the result of an interplay of multiple genes, lifestyle and environmental factors (e.g. diabetes mellitus) (9). Mitochondrial inheritance implies mutations or abnormalities in the mitochondrial DNA (mtDNA). mtDNA is only inherited from the mother and differs from nuclear DNA. Leber hereditary optic neuropathy is the most common mtDNA disorder (7, 9, 10). One of the best known examples of chromosomal abnormalities is Trisomy 21 or Down syndrome, where the patient has 3 copies of chromosome 21 instead of 2 (7).

Besides inheritance, genetic diseases can be caused by the occurrence of *de novo* mutations. These *de novo* mutations are often more deleterious compared to the inherited variation (11). The *de novo* mutation rate is higher in males than females and increases with age (12). Most of the *de novo* mutations are single-nucleotide variants (SNVs), although small insertions and deletions (indels) and larger copy-number variations (CNVs) can occur as well (11). Recently, the emergence of high-throughput next-generation sequencing (NGS) boosted the study of *de novo* mutations, since it allowed high-throughput large scale sequencing at single-nucleotide resolution (11, 13).

2.1 Genetic epilepsies

A genetic epilepsy is caused by a known or presumed gene mutation in which seizures are a main symptom of the disorder (4). This thesis focuses on 2 genes that, when mutated, are presumed (i.e. *FHF1*) or known (i.e. *TSC2*) to result in epilepsy.

2.1.1 Fibroblast growth factor homologues factor 1 (FHF1)

2.1.1.1 Structure and function

Fibroblast growth factor homologues factor 1 (FHF1) is also known as fibroblast growth factor 12 (FGF12) (14). Fibroblast growth factors (FGFs) are involved in development, wound healing, tissue repair, metabolism and homeostasis (15-17). The family of FGFs consists of 22 members and can be divided into 7 subfamilies belonging to 3 different groups based on their mechanism of action: the intracellular FGF11/12/13/14 group, the endocrine FGF19/21/23 group and the canonical FGF group comprising of 5 subfamilies (i.e. FGF1/2/5, FGF3/4/6, FGF7/10/22, FGF8/17/18 and FGF9/16/20) (15). The intracellular subfamily members, also known as fibroblast growth factor homologues factors, where FHF1 = FGF12, FHF2 = FGF13, FHF3 = FGF11 and FHF4 = FGF14, are mainly expressed in the developing and mature nervous system (14, 18). All FGFs contain a homologous region of approximately 120-130 amino acids, also known as the core homology domain which assumes a β -trefoil fold consisting of 12 β -strands (β 1 – β 12) (Fig. 3A and 3B) (16, 18). The FHF1s show 30-50% amino acid sequence identity with other FGFs and up to 70% identity with other members of the FHF subfamily (15, 18). FHF1s appear in two different isoforms, with the A-type isoform having a longer amino-terminal sequence and bearing a bipartite nuclear localization signal, responsible for its nuclear distribution. B-type isoforms are localized predominantly in the cytoplasm (18). While both the endocrine and canonical FGFs function extracellularly to activate the tyrosine kinase FGF-receptors (FGFRs), FHF1s lack the N-terminal signaling peptide for secretion and function in an intracrine manner (15, 18). These intracellular signaling molecules play a role in neuronal functions by binding to the intracellular domains of the voltage-gated sodium channels (Na_v s) (more specifically to the cytoplasmic C-terminal tails of the sodium channel alpha subunits) and interaction with the protein kinase scaffold protein islet brain-2 (IB-2) (14, 15). The interaction of FHF1s with the Na_v s suggests that they might play a role in neuronal excitability and *FHF* gene defects might result in the development of epilepsy.

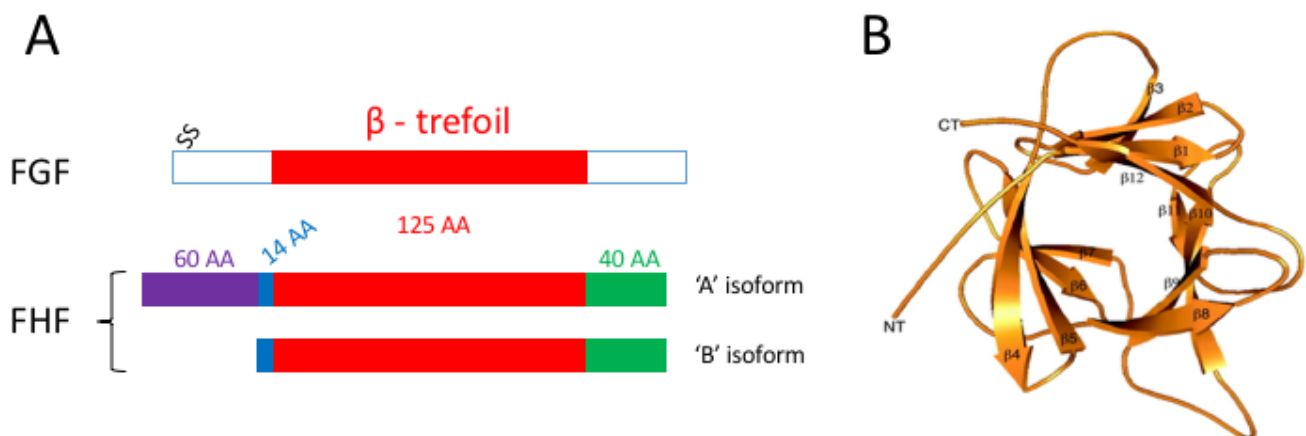


Figure 3: Structure of FGF and FHF. (A) Both FGFs and FHF1s contain a homologous region of 120-130 AA (β -trefoil fold, consisting of 12 β -strands). FHF1s exist in an A- and B-type isoform, that are highly related, although the A-isoform is longer than the B-isoform and bears a nuclear localization signal. (B) Ribbon representation of human FHF1B. The β -trefoil fold domain consists of 12 β -strands. (A) From Goldfarb et al. 2005 *Cytokine Growth Factor Rev* (16). (B) From Olsen et al. 2003 *The Journal of Biological Chemistry* (16)

2.1.1.2 Patient data

Whole-exome sequencing was performed by geneticists and neurologists at the UZ Leuven in a family quintet and identified a *de novo* heterozygous *FHFI* missense mutation in two affected siblings, suffering from cerebellar atrophy, peripheral neuropathy, generalized tonic seizures (early-onset) and microcephaly. Unfortunately, both died very young (7 and 3,5 years old) (19). These data suggested the discovery of a new candidate epilepsy gene.

2.1.2 Tuberous sclerosis complex (TSC)

2.1.2.1 Clinical picture

Tuberous sclerosis complex (TSC) also known as Bourneville disease or syndrome is a rare, genetic disease resulting from loss-of-function mutations in either the *TSC1* or *TSC2* gene. The incidence of TSC is estimated to be one in 6000 to one in 10,000 live births (20). One of the hallmarks of the disease is the development of hamartomas (i.e. benign tumor growths) leading to impaired function of multiple organs of which brain, skin, heart, lungs (in females) and kidneys are the most important (20-22). Examples of these non-neurological manifestations are facial angiofibromas, cardiac rhabdomyoma, pulmonary lymphangiomyomatosis (LAM) and renal angiomyolipomas (AMLs) (20-22).

In most patients (>90%) the central nervous system (CNS) is affected due to the presence of structural developmental abnormalities in the brain, including cortical dysplasias (i.e. tubers and white matter radial migration lines), subependymal nodules (SENs) and subependymal giant cell astrocytomas (SEGAs) (23). Functional CNS abnormalities consist of epilepsy and TSC-associated neuropsychiatric disorders (TAND). TAND is an umbrella term used to refer to a wide range of behavioral, psychiatric, intellectual, academic, neuropsychologic and psychosocial difficulties (24, 25). Examples of difficulties at the different levels are given in Fig. 4. Approximately 90 % of the individuals with TSC will experience one of these TAND features at some stage during life (24).

As epilepsy is the most common presenting symptom of TSC, it affects up to 90% of TSC patients (26-28). In the majority of cases (60 – 70%), seizures emerge within the first year of life (27). Multiple seizure types have been observed in children with TSC, with infantile spasms and focal seizures being the most common ones (26). Infantile spasms are highly prevalent in TSC infants (33 – 75%) and are often associated with intellectual disability and poor neurological prognosis (26). Children suffering from infantile spasms often develop other types of seizures leading to drug-resistant epilepsy in 75% of cases (23). The first-line treatment for seizures in TSC patients consists of anti-epileptic drugs, although two thirds of patients remain unresponsive to therapy (21).

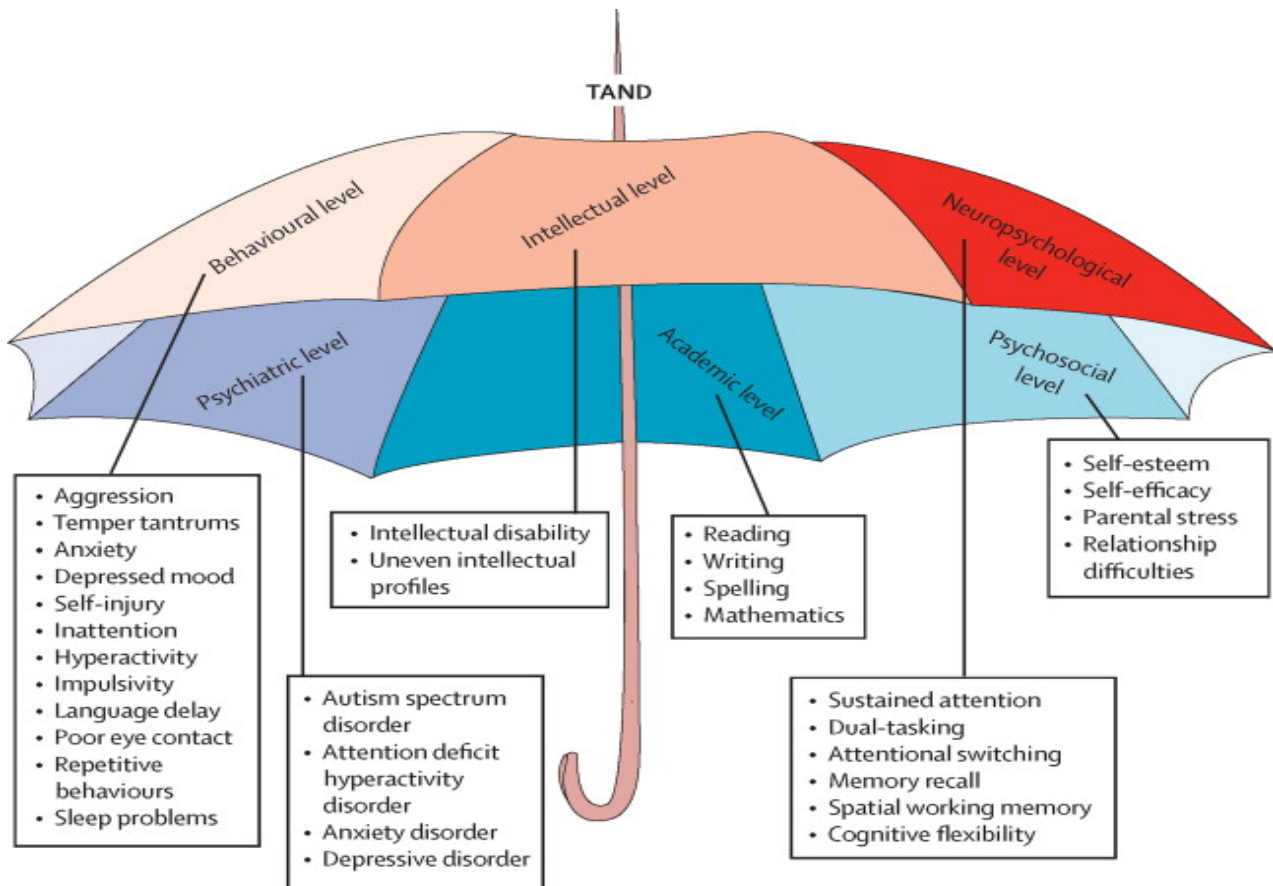
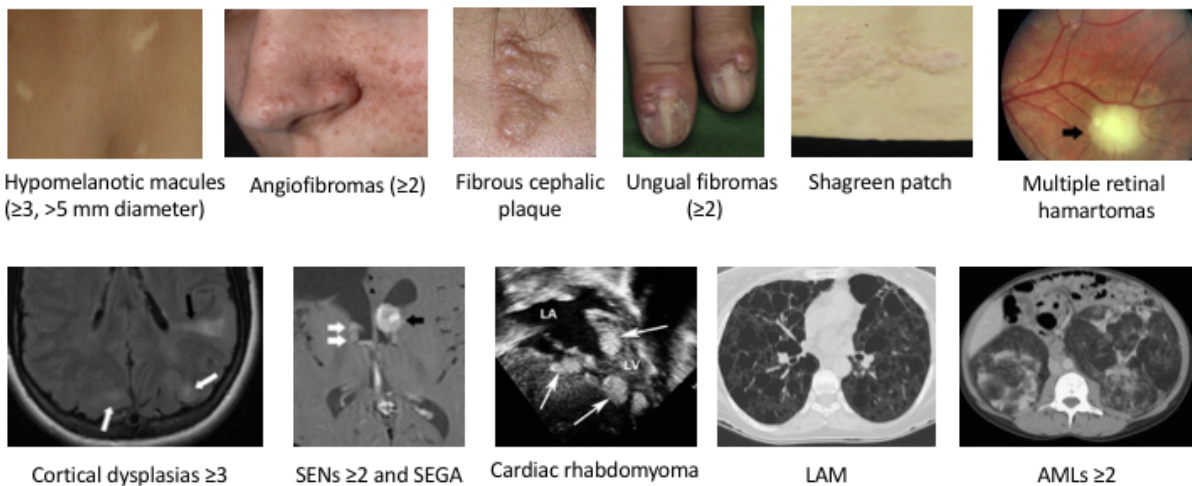


Figure 4: TAND. TAND refers to TSC-associated neuropsychiatric disorders and encompasses a wide range of difficulties situated at the behavioral, intellectual, neuropsychosocial, psychiatric, academic and psychosocial levels. From Curatolo et al. 2015 *Lancet Neurology* (23).

The diagnosis of TSC is made based on genetic and/or clinical diagnostic criteria (20, 23, 29). A definite diagnosis of TSC requires the identification of a pathogenic variant in the *TSC1* or *TSC2* gene (genetic diagnostic criterion) or the detection of two major features or one major feature with two or more minor features (clinical diagnostic criterion) (20, 23, 29). A possible diagnosis is made when there is one major feature or two or more minor features (20, 23, 29). An overview of the different major and minor features can be found in Fig. 5. TSC is characterized by a very heterogeneous manifestation of the disease. Therefore, an individuals' prognosis depends on the disease severity, ranging from mild skin lesions to drug-resistant epilepsy, severe intellectual disability and kidney failure (20).

MAJOR FEATURES



MINOR FEATURES



Figure 5: Overview of the major and minor features used to clinically diagnose TSC. A definite diagnosis of TSC requires two major features or 1 major feature with 2 or more minor features. A possible diagnosis of TSC is made when 1 major feature or 2 or more minor features are detected. Major features include hypomelanotic macules (≥3, at least 5 mm in diameter), facial angiofibromas (≥2), fibrous cephalic plaque, unguinal fibromas (≥2), shagreen patch, multiple retinal hamartomas, cortical dysplasias (tubers indicated by the white arrows; white matter radial migration lines indicated by the black arrow), subependymal nodules (SENs, ≥2) indicated by the white arrows, subependymal giant cell astrocytoma (SEGA) indicated by the black arrow, cardiac rhabdomyoma indicated by the white arrows, lymphangiomyomatosis (LAM) and renal angiomyolipomas (AMLs, ≥2). Minor features include confetti skin lesions, dental enamel pits (≥3), intraoral fibromas (≥2), retinal achromatic patch, multiple renal cysts and nonrenal hamartomas. Adapted from Northrup et al. 2013 *Pediatric Neurology* (29).

2.1.2.2 Genetic background

TSC is a genetic disease caused by variants in one of the tumor suppressor genes *TSC1* or *TSC2* (20, 22, 30, 31). The *TSC1* gene is located on chromosome 9q34.3 and encodes an 8.6 kilobase (kb) transcript and a 130 kDa protein, named hamartin (20, 30, 32). The *TSC2* gene is located on chromosome 16p13.3 and encodes a 5.5 kb transcript and a 198 kDa protein, known as tuberin (30, 33). Both genes are ubiquitously expressed and show a high conservation across different species (20, 32, 33).

Pathogenic variants in *TSC1* or *TSC2* can be inherited in an autosomal dominant manner, although the majority occurs *de novo* during embryo development (20). Sporadic cases of TSC are more often resulting from *TSC2* variants than from *TSC1* variants, while in case of inheritance both genes are equally involved (20). Remarkably, in 10 – 15% of TSC patients, no disease-causing mutation can be

identified (NMI) (20, 23). To date, approximately 850 DNA variants have been described on the *TSC1* gene and 2500 on the *TSC2* gene (20, 23). Variants in *TSC1* are mostly indels resulting in a truncated protein, whereas the variant type of the *TSC2* gene is broader and includes large deletions, indels, nonsense and missense mutations (20). The manifestation of the disease in terms of age at seizure onset, tuber load and degree of intellectual disability is generally more severe in case of *TSC2* gene variants (20). An important concept to understand the hamartoma development and the variable disease manifestation in TSC is the “two-hit” hypothesis or loss of heterozygosity (LOH) model. This model assumes the presence of an acquired or inherited variant in one allele of the *TSC1* or *TSC2* gene, meaning that patients are heterozygous (except for mosaic individuals) (20). Subsequently, at some point in life, the occurrence of a somatic “second-hit” variant in the other unaffected allele results in a biallelic inactivation or LOH of *TSC1* or *TSC2*. Lesion formation in the brain (SEGAs) and kidneys (AMLs) requires a biallelic inactivation of *TSC1* or *TSC2*, while this is not the case for cardiac rhabdomyomas and cortical tubers (20).

2.1.2.3 Mechanistic target of rapamycin

The *TSC1* and *TSC2* gene products (TSC1 or hamartin and TSC2 or tuberin) are upstream regulators of mechanistic target of rapamycin (mTOR) complex 1 (mTORC1) (34). mTOR is a serine/threonine protein kinase of 289 kDa and belongs to the phospho-inositide 3-kinase (PI3K)-related kinase family (34). In order to be active, mTOR needs to associate with several other proteins to form two distinct multiprotein complexes, named mTORC1 and mTORC2 (34-36). These mTOR complexes can be distinguished by their different upstream and downstream in- and outputs and by their difference in sensitivity to rapamycin (with mTORC1 being more rapamycin-sensitive) (37). However, these complexes also show similarity since they have some protein partners in common: the catalytic mTOR subunit, mammalian lethal with sec-13 (mLST8), DEP domain containing mTOR-interacting protein (Deptor), Tel-two interacting protein 1 (Tti1) and telomere maintenance 2 (Tel2) (36, 37). In addition to the shared proteins, mTORC1 consists of regulatory-associated protein of mTOR (Raptor) and proline-rich AKT1 substrate 40 kDa (PRAS40) (36, 37). Specific to mTORC2 are rapamycin-insensitive companion of mTOR (Rictor), mammalian stress-activated map kinase-interacting protein 1 (mSin1) and protein observed with Rictor (Protor) (36, 37). The composition of the mTORC protein complexes is shown in Fig. 6.

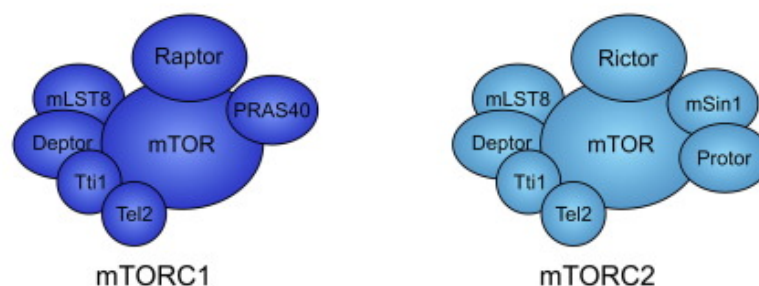


Figure 6: Composition of the mTORC1 and mTORC2 complexes. From Switon *et al.* 2017 *Neuroscience* (36).

mTOR is, as a central regulator within a wide signaling network, responsible for the control of major cellular processes including cell metabolism, growth, proliferation and survival (34, 37). One of the most important sensors involved in the regulation of the activity of mTORC1 are the proteins derived from the *TSC1* and *TSC2* genes. They act by integrating signals from different cues: both growth factors (e.g. insulin) and high glucose and cellular energy levels lead to mTORC1 activation through PI3K and Ras signaling mediated inhibition of TSC2 and inhibition of AMP-activated protein kinase (AMPK) respectively (Fig. 7) (34, 36). One of the best-known downstream effects of mTORC1 is stimulation of protein translation via phosphorylation of eukaryotic translation initiation factor 4E-binding protein (4E-BP) and p70 ribosomal S6 kinase 1 (p70S6K1) (Fig. 7) (36).

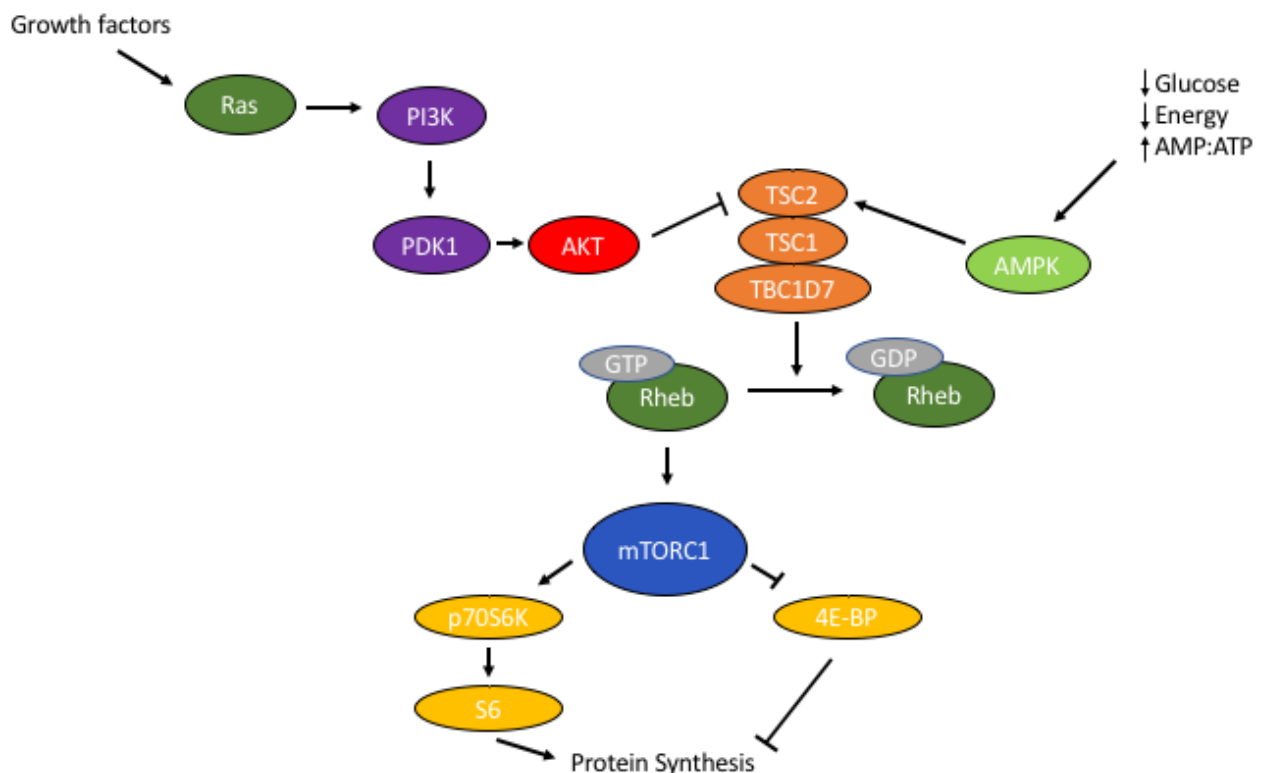


Figure 7: TSC1/TSC2 dependent regulation of mTORC1. Growth factors and hormones lead to mTORC1 activation via Ras and PI3K signaling mediated inhibition of TSC2. Low glucose and low cellular energy levels stimulate AMPK which in turn phosphorylates and activates TSC2, resulting in mTORC1 inhibition. PI3K = phospho-inositide 3-kinase, PDK1 = phospho-inositide-dependent kinase-1, AKT = protein kinase B, TBC1D7 = Tre2-Bub2-Cdc16 1 domain family member 7, AMPK = AMP-activated protein kinase, Rheb = Ras homolog enriched in brain, p70S6K1 = p70 ribosomal S6 kinase 1, 4E-BP = eukaryotic translation initiation factor 4E-binding protein. Adapted from Switon *et al.* 2017 *Neuroscience* (36).

TSC1 and TSC2 physically associate together with a third subunit Tre2-Bub2-Cdc16 (TBC) 1 domain family, member 7 (TBC1D7) to form the TSC1-TSC2-TBC1D7 complex. This complex functions as a negative regulator of mTORC1 due to its Ras homolog enriched in brain – GTPase activating protein (Rheb-GAP) activity (Fig. 7) (30, 31, 38, 39). More specifically, it inactivates Rheb-GTP, which is a potent stimulator of mTORC1, by conversion to the inactive Rheb-GDP. The GAP activity of this

complex originates from TSC2, which contains a GAP domain near its C-terminus. TSC1 is known to stabilize TSC2 and increase the GAP activity, whereas TBC1D7 by binding to TSC1 strengthens the association of TSC1 and TSC2 (30, 31, 38, 39). When a variant is present in one of the two *TSC* genes, the TSC1-TSC2-TBC1D7 complex loses its GAP function and results in hyperactive mTORC1 signaling (38). Therefore, mTOR inhibitors such as rapamycin and everolimus have been successfully used to treat the following TSC manifestations in patients: SEGAs, renal angiomyolipomas, pulmonary lymphangiomyomatosis, facial angiofibromas and epilepsy (40-43). Rapamycin is a macrolide antibiotic that blocks mTORC1 by the formation of a complex with FK506-binding protein of 12 kDa (FKBP12), after which the complex binds to the FKBP12-rapamycin binding (FRB) domain on mTOR. Consequently, the mTOR protein is no longer able to interact with the other regulatory proteins to form the mTORC1 complex, resulting in inhibition of its kinase activity (36).

3. Animal models of seizures and epilepsy

Over 100 different *in vitro* and *in vivo* models exist to capture the heterogeneity of epilepsy with different types of epileptic seizures, multiple syndromes and etiologies (44). Animal models of seizures and epilepsy have been, and still are, of great importance firstly to improve our understanding of the basic mechanisms underlying seizure generation and epilepsy development, and secondly to aid the development of novel anti-seizure drugs (ASDs, in clinical context referred to as anti-epileptic drugs) or anti-epileptogenic drugs (44).

Countless models of epileptic seizures and epilepsy have been generated and characterized so far. In general, these models can be classified as two main classes: i) genetic models and ii) induced seizure models (45) (Fig. 8). Genetic models are characterized by the occurrence of spontaneous recurrent seizures as seen in the GAERS rat (Genetic Absence Epilepsy Rat from Strasbourg), epileptic dogs, mutant mice and simpler non-mammalian organisms such as the roundworm (i.e. *Caenorhabditis elegans*), the fruit fly (*Drosophila melanogaster*) and the zebrafish (*Danio rerio*) (46). Models in which reflex seizures develop in response to a visual (e.g. photosensitive baboons) or acoustic (e.g. DBA/2 mice with audiogenic absence seizures) stimulus are also classified as genetic (45, 47). Seizures can be induced chemically or electrically. The induced models can be subdivided in three groups based on the type of induced seizures: acute seizures, chronic seizures and post-status epilepticus models with spontaneous recurrent seizures (SRS). The best-known examples of acute seizure models are the mouse maximal electro-shock (MES) model and the mouse or zebrafish pentylenetetrazol (PTZ) model (46, 47). Chronic seizures result from electrical or chemical kindling (i.e. repeated application of electrical or chemical stimuli). Finally, kainate-induced status epilepticus (SE) followed by the development of SRS is an example of a chemically induced epilepsy model (45, 48).

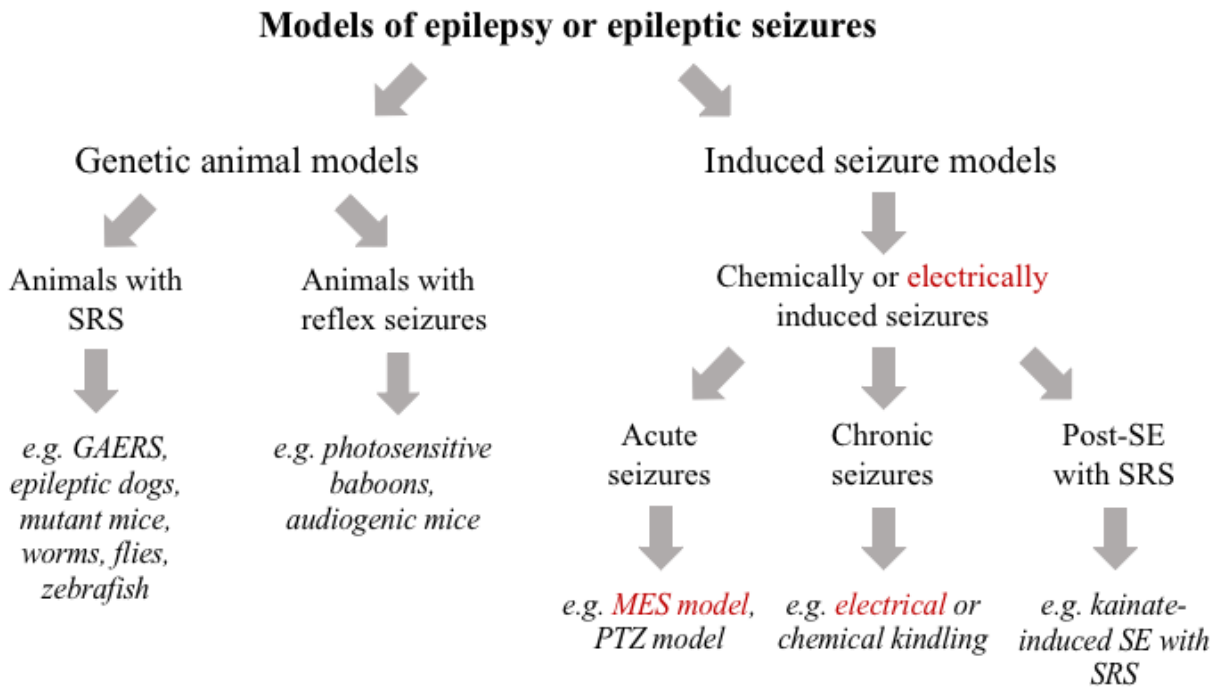


Figure 8: Classification of animal models of epilepsy and epileptic seizures. Models of epilepsy and epileptic seizures are either genetic animal models either induced seizure models. Both animals with spontaneous SRS and animals with reflex seizures are classified as being genetic. Seizures can be induced in normal animals chemically or electrically (examples in red) and depending on the type of seizures can be classified as acute, chronic or post-SE with SRS. SRS = spontaneous recurrent seizures, post-SE = post-status epilepticus. Adapted from Löscher *et al.* 2011 *Seizure* (45).

Traditionally, different animals have been used for epilepsy and seizure modeling. Nowadays, rodents are considered to be the gold standard due to a number of reasons. First, they show a close genetic, physiologic and pharmacologic similarity to humans (49). Second, a plethora of genetic tools is available to generate rodent models that closely mimic human epilepsy and therefore can be used to study the pathophysiology of epilepsy (50). Third, with respect to ASD discovery the use of rodents as an *in vivo* model allows phenotype-based drug discovery and therefore discovery of compounds with a wide range of mechanisms of action (MOA) (51). Fourth, rodents have a small size, reproduce fast and are easy to handle when compared to other mammalian models like dogs and baboons (49).

Despite the availability of a range of rodent models and 150 years of research, still 30% of epilepsy patients do not respond to the existing ASDs (47, 48). Therefore, the Epilepsy Therapy Screening Program (ETSP) includes several rodent models of seizures and epilepsy to find drugs that are efficacious for the treatment of drug-resistant epilepsy (47). However, the biggest drawback of this approach is the use of induced seizure and epilepsy models. To strive towards a personalized medicine, the need for models that (i) represent each specific epileptic syndrome (genetic models) and (ii) are amenable to high-throughput screening remains. Another limitation of the rodent models is that they are not suitable as a fast, *in vivo* model for rapid translation to the clinic, i.e. to rapidly verify the effects of

a potential disease-causing gene, as discovered in the clinic. Hence, there is a high need for new animal models that cover these shortcomings.

Recently, the use of smaller non-mammalian models is emerging in epilepsy research (49). Zebrafish larvae have been proven useful in both modeling of acute evoked seizures (PTZ test) and modeling of genetic epilepsies (46, 52). Compared to rodents they offer some unique advantages: (i) one zebrafish female produces hundreds of offspring per week that develop very fast and *ex utero*, (ii) the ease of genetic manipulation compared to rodents (53), (iii) use of multi-well plate format due to their small size and (iv) compounds can be easily administered to the swimming medium (i.e. immersion) (49, 54). Taken together, these advantages allow (i) fast modeling of a human candidate epilepsy gene and therefore rapid translation to the clinic, (ii) elucidation of the pathophysiology of epilepsy and (iii) a moderate- to high-throughput screening of compounds in genetic epilepsy zebrafish models (49). An example is the discovery of clemizole by using a *scn1lab* mutant zebrafish model (Dravet syndrome) to screen a re-purposed drug library of more than 300 compounds (55).

4. Zebrafish

4.1 Origin and introduction to research

Zebrafish are tropical freshwater fish belonging to the minnow family (Cyprinidae) of the class Actinopterygii and originate from shallow waters in South – Southeast Asia (Fig. 9) (56) (57). In the late 1960's zebrafish were introduced to the laboratory environment by George Streisinger, whose major interest was to understand the genetics of neurodevelopment (58). He established zebrafish as a new *in vivo* non-mammalian



Figure 9: Adult zebrafish. Picture taken by Thierry Marysael

vertebrate genetic model and therefore may be considered as the father of 'modern' zebrafish research (57). Moreover, recent decades are characterized by a rapidly growing interest in zebrafish as a simple vertebrate model for use in biomedical research (57). To date, zebrafish have been successfully used to model a range of human diseases including hematological diseases, melanoma, heart, muscle, kidney and central nervous system (CNS) disorders (59).

4.2 Biology of the model

Zebrafish development occurs very fast and *ex utero* (as is the case for fertilization), allowing embryogenesis to be studied in the developing transparent embryo (57, 59, 60). Embryogenesis can be divided into seven defined periods: zygote (0 – 0.75h), cleavage (0.75 – 2.25h), blastula (2.25 – 5.25h), gastrula (5.25 – 10h), segmentation (10 – 24h), pharyngula (24 – 48h) and hatching (48 – 72h) periods.

This time frame for development assumes incubation of the embryos without crowding at an optimal temperature of 28.5°C (61). Examples of embryonic development during each of these phases are represented in Fig. 10. The zygote will undergo a first cleavage at about 40 minutes post fertilization with subsequent divisions every 15 minutes. When the embryo enters the pharyngula period at 24 hours post fertilization (hpf), it already possesses the classic vertebrate structure. Furthermore, the heart starts beating and the embryo displays an early touch response with subsequent development of spontaneous movements (61). Hatching occurs at different rates, but in general during the whole third day of development (61, 62). At the end of this day, all major developmental processes are completed and the embryos (3,5 mm in length) are now referred to as ‘larvae’ (61). Around 45 dpf the larvae develop into juveniles that in their turn reach adulthood by 3 – 4 months of age (56). From that time point onwards the animals are considered to be sexually mature (62). Interestingly, zebrafish do not possess a pair of highly differentiated sex chromosomes and their final sex is only determined around 3 – 4 weeks post fertilization (wpf) (56). All zebrafish larvae start to develop ‘juvenile ovaries’ around 10 dpf and from 21 dpf onwards these ovaries are transformed either into a functional ovary in case of females either into male testis (56, 63). Sex determination mechanisms are not yet fully understood in zebrafish. However, it is suggested that sex determination is predominantly polygenic, but may be influenced by the number of germ cells (loss of germ cells favors male fate) and environmental factors (e.g. high temperature leads to male bias) (64).

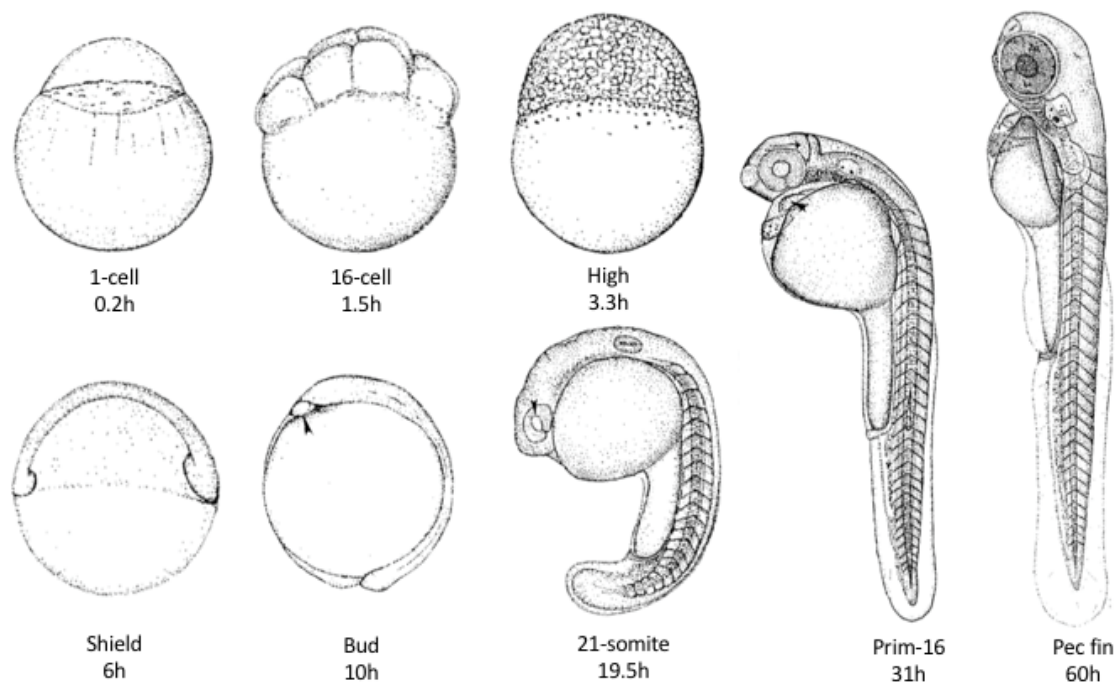


Figure 10: Embryonic zebrafish development. Examples of each period of embryonic development: zygote (1-cell), cleavage (16-cell), blastula (high), gastrula (shield), segmentation (bud and 21-somite), pharyngula (prim-16) and hatching (pec fin). Adapted from Kimmel *et al.* 1995 *Developmental Dynamics* (61).

4.3 Advantages of zebrafish

Nowadays, zebrafish are established as an invaluable animal model for the investigation of human pathogenesis (57, 59, 60, 65-67). They owe their rising popularity as a model organism to a series of advantages, outlined below.

- Zebrafish are vertebrates that share a high genetic and physiologic similarity to humans. Noteworthy, with respect to their genome 69% of the protein coding genes has at least one human orthologue, while up to 82% of the genes associated with human disease has at least one zebrafish orthologue (51, 68). This underscores the utility of zebrafish to model most of the human pathologies (60).
- Zebrafish are lower-order vertebrate animals and are protected as laboratory animals from 6 dpf onwards. Therefore, the use of larval stages up to and including 5 dpf is in line with the 3R (Replacement, Reduction, Refinement) principle of humane animal research (69). Beyond 6 dpf their use requires ethical approval (70).
- Zebrafish are small (3 cm in case of the adults) and are easy to maintain at a low cost. Moreover, they show a high fecundity with a pair of adult zebrafish producing up to 300 eggs per week (59).
- The optical transparency of the embryos (until 24 hpf) together with their fast development outside of the mother allows embryogenesis to be studied easily and (genetic) manipulations to be performed at the early embryonal stage (57, 60). Moreover, by 4 dpf most organs are functional and the nervous system is active (57).
- Zebrafish larvae (3 – 7 dpf) are amenable to high-throughput compound/drug testing for human diseases, since they only measure 3.5 – 4.5 mm enabling the use of 96 well-plates (71). In contrast to mice, small amounts of compounds can be administered by simply adding them to the swimming medium, followed by dermal or enteral (from 3dpf onwards) absorption (57, 72).
- Zebrafish can be easily modified genetically by means of forward (e.g. ENU mutagenesis) and reverse (morpholino-mediated gene knockdown, transgenesis, targeted mutagenesis) genetic tools (57). Moreover, the developing larval zebrafish brain consists of numerous structures, cell types and neurotransmitters similar to those found in mammals (72, 73). Hence, zebrafish larvae are well suited to investigate genetic CNS diseases/disorders, ranging from Parkinson's disease to autism spectrum disorder and epilepsy (57).

4.4 Limitations of zebrafish

To be complete, zebrafish possess some limitations as well.

- Although a high genetic and physiological homology to humans is observed, zebrafish as a non-mammalian model are evolutionarily more distant when compared to rodents. Moreover, in

contrast to mammals, zebrafish lack some organs (e.g. lungs, stomach, lymph nodes, heart only consists of 2 chambers), parts of the brain are not as developed (e.g. only rudimentary cortex) and for some CNS structures in zebrafish finding the mammalian counterparts is hard (54, 57).

- Concerning drug discovery the major advantage of medium- to high- throughput screening is restricted to zebrafish embryos and larvae and excludes adults based on their ‘large’ size (74). A potential problem here in case of a water-insoluble compound might be the administration of the drug via water immersion, possibly leading to false-negative screening results (54).
- Zebrafish possess numerous duplicate genes due to a whole-genome duplication that took place early in the evolution of the teleosts (circa 300 million years ago) (75). These genes, also called paralogs, may hamper the modeling of human genetic diseases in zebrafish, i.e. when the paralogs exert a similar function, knockdown of both genes might be necessary to generate a full loss-of-function phenotype.

4.5 Zebrafish as a model of epileptic seizures and epilepsy

Within the last decade both larval and adult zebrafish have been increasingly used to model epileptic seizures and epilepsy (53). Each has its own advantages and limitations. Larval zebrafish benefit from their transparency, small size (amenable to high-throughput screening in a 96-well plate), functional organs by 4 dpf and the fact that recessive homozygous mutations resulting in embryonic lethality can be investigated (57). While larval zebrafish are extremely well suited for the investigation of early-onset (e.g. pediatric) epilepsy, compared to the adults they possess somewhat underdeveloped neural and endocrine systems and simple locomotor responses (53, 76). Therefore, the use of adults to model more complex behaviors and endocrine biomarkers, complements the strengths of the larval models (76).

Zebrafish models can be classified as models of epileptic seizures (induced) and epilepsy models (genetic) (Fig. 11) (77). Similar to rodent models, although typified by a higher throughput, zebrafish models of induced epileptic seizures are useful for ASD discovery and investigation of ictogenesis. Given the multiplicity of different human genetic epilepsies, there is a need for genetic zebrafish epilepsy models that mimic each of the human epilepsies more closely. These genetic models serve to gain more insights into the process of epilepsy development (i.e. epileptogenesis) and can be implemented in high-throughput screens for anti-epileptogenic drug discovery (77).

Studying epileptic seizures or epilepsy in zebrafish involves firstly the assessment of seizure-like behavior using manual scoring and/or an automated tracking device (e.g. Viewpoint, France). Secondly, a non-behavioral seizure or epilepsy biomarker is used to confirm that the observed change in behavior is due to epileptic seizures. To this end, an electrophysiological marker can be used, i.e. local field potential recordings (LFPs) to investigate the brain activity for the occurrence of epileptiform-like discharges. Besides a molecular biomarker can be quantified, i.e. detection of expression levels of a marker of neuronal activation by means of RT-qPCR (real-time quantitative PCR) or WISH (whole-mount in situ hybridization) (53, 77).

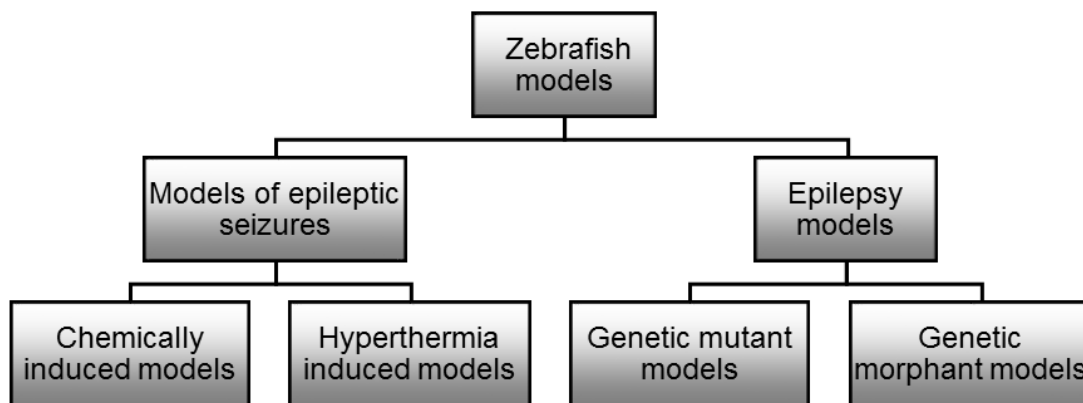


Figure 11: Classification of zebrafish models of epileptic seizures and epilepsy. Zebrafish models can be classified on the one hand into models of epileptic seizures, which are either chemically either hyperthermia induced. On the other hand, genetic epilepsy models can be generated using transient (morphant) or permanent (mutant) gene knockdown. From Pitkänen *et al.* 2017 *Models of Seizures and Epilepsy*, 2nd edition (77).

4.5.1 Zebrafish seizure models

In zebrafish seizure models, seizures are induced either chemically by the administration of a proconvulsant, e.g. PTZ either via hyperthermia, which is defined as an elevation of body temperature (Fig. 11) (77).

The first zebrafish model reported was the larval zebrafish PTZ seizure model in 2005 (78). The authors showed that, after exposure of 7 dpf larvae to PTZ via water immersion, the larvae display a series of locomotor behaviors starting with a steep increase in their swimming activity, followed by ‘whirlpool-like’ circling swim behavior and evolving into clonus-like convulsions resulting in loss of posture. Moreover, spontaneous epileptiform discharges were obtained from the optic tectum of PTZ-treated larvae using LFP recordings, validating the behavioral observations. Finally, the seizure activity was confirmed as well by a threefold upregulation of the expression of *c-fos* (78). This first larval seizure model paved the way for many more larval and adult models of chemically induced seizures. The high speed ‘whirlpool-like’ movements followed by loss of posture, typically seen after PTZ treatment (78,

79), are also observed in an adult kainate model (80) and a larval allylglycine model (81). Other types of models are the larval domoic acid model (82, 83), the larval pilocarpine model (84) and the adult picrotoxin model (76) that all show more subtle convulsive behaviors such as spasms, twitching, jerking, tremor and/or loss of posture. In most studies, the focus is on the behavior, i.e. the occurrence of seizures and to a lesser extent on the investigation of a non-behavioral parameter, i.e. electrophysiological recordings or a molecular biomarker. However, with regards to the aforementioned models epileptiform discharges have been shown in case of treatment with PTZ (larval and adult) (78, 79) and allylglycine (larval) (81). Moreover, upregulation of *c-fos* has been demonstrated in the larval pilocarpine model (84). Concerning routes of administration, exposure to a proconvulsant mostly occurs through water immersion, even though injection into the peritoneum in case of adults is possible (80).

With regards to the chemically induced larval PTZ seizure model, a pharmacological characterization has been performed by investigating the effects of ASDs on seizure-like behavior and epileptiform discharges (78, 85). Afrikanova *et al.* demonstrated that the effects of 13 ASDs in the larval PTZ seizure model resulted in a similar response in both the behavioral and electrophysiological assays. Moreover, a good correlation was obtained between acute PTZ zebrafish and rodent data (85). Furthermore, the EEG data were found to correlate well with those described by Baraban *et al.* (78). Taken together, these observations highlight the potential of the larval PTZ seizure model for ASD discovery.

Besides chemical induction of seizures, hyperthermia can be used as well. In humans, hyperthermia occurs in case of fever (possibly leading to febrile seizures, mostly in children below 5 years of age) or when taking a hot water bath. The only zebrafish model of febrile seizures, i.e. hyperthermia-induced seizures, reported to date was generated by Hunt and colleagues (86). In brief, 3 – 7 dpf larvae were immobilized in agarose and perfused with water of increasing temperature (whether or not containing a drug). Simultaneously local field potentials were recorded from the forebrain while the temperature gradually increased from $22.5 \pm 0.3^\circ\text{C}$ (room temperature) to $33.5 \pm 0.3^\circ\text{C}$, with the first electrographic seizure occurring at $25.5 \pm 0.3^\circ\text{C}$. Since this zebrafish model showed electrographic seizures to be age-dependent (with a peak at 5 dpf), reproducible, strain-independent and not resulting into death, it is considered to mimic well key features of human febrile seizures (86).

4.5.2 Genetic zebrafish epilepsy models

A variety of human genetic epilepsies have been successfully modeled using zebrafish (Table 1). Based on the extent to which a model was characterized, three groups can be considered.

The first group consists of models where seizures or epileptiform discharges were observed as biomarkers for epilepsy. Examples are the *lgila* morphant (87) and the *kcnq3* morphant (88). The generation of these models was based on the fact that mutations in *LGII* and *KCNQ3* in humans are

associated with autosomal dominant partial epilepsy with auditory features (ADPEAF) and benign familial neonatal convulsion (BFNC), respectively (87, 88). *lgila* morphants were characterized morphologically by smaller brains and eyes, reduced body length and abnormal tail shapes. Moreover, they displayed hyperactivity characterized by circling movements and jerky directional swimming (87). *kcnq3* morphants displayed abnormal epileptiform discharges (88).

The second group includes models where epilepsy was characterized both by seizures and epileptiform discharges. Examples are the *ocr11* mutant (89), the *chd2* mutant (90), the *stx1b* morphant (52) and the *stxbp1b* mutant (91). The *ocr11* mutant is a model of Lowe syndrome that affects the CNS, eyes and kidneys. CNS symptoms include intellectual disability and increased susceptibility to fever-induced seizures. The *ocr11* zebrafish mutants displayed smaller brains and eyes, a more subtle seizure behavior typified by twitching and rigor, and sensitivity to heat-induced epileptiform discharges (89). Mutations in *CHD2* have been associated with a Dravet-like syndrome, which is characterized by early-onset fever-sensitive seizures that are drug-resistant (90). *chd2* morphants displayed certain morphological features, such as pericardial edema, microcephaly, body curvature and lack of swim bladder. Seizures were observed as whirlpool-like activity, whole body trembling and twitching of the pectoral fin and jaw. Additionally, epilepsy was confirmed by the presence of epileptiform discharges (90). The *stx1b* zebrafish morphant is a model for febrile seizures and epilepsy (52). Besides minor morphological abnormalities (lack of swim bladder, slight tail curvature), seizures consisted of more subtle movements (pectoral fin fluttering, orofacial movements and myoclonus-like jerks) and spontaneous epileptiform discharges were shown to be enhanced by hyperthermia (52). Mutations in *STXBPI* are associated with different drug-resistant childhood epilepsies (91). The *stxbp1b* zebrafish mutant successfully modeled epilepsy on the behavioral level by showing a reduced locomotor response and non-behaviorally by the occurrence of epileptiform discharges (91). Despite differences in seizure behavior, local field potential recordings revealed epileptiform discharges in all models mentioned, underscoring the validity of zebrafish in modeling human genetic epilepsies.

The third group of zebrafish epilepsy models brings together those models with a more detailed characterization of the observed seizures and/or epilepsy by integrating a pharmacological analysis and/or a transcriptomic approach. Examples are the *kcnj10a* morphant (92, 93), the *mind bomb* mutant (94), the *scn1lab* morphant (95) and the *scn1lab* mutant (55). The *kcnj10a* morphant aims at modeling EAST (epilepsy, ataxia, sensorineural deafness, tubulopathy) syndrome (92, 93). Seizure behavior was observed as an increased frequency of spontaneous contractions at the embryonal stage and as circling behavior and speed bursts at the larval stage (92). Spontaneous epileptiform discharges confirmed the epileptic nature of this behavior. To provide a first characterization of the pharmacological profile of this zebrafish EAST model, two ASDs (diazepam and pentobarbitone) were tested, of which only pentobarbitone successfully suppressed the electrical brain activity (93). The zebrafish *mind bomb*

mutant is a model for Angelman syndrome, a genetic disorder that mainly affects the CNS leading to developmental delay, intellectual disability, motor impairment and epilepsy (94). The mutants were morphologically characterized by a curled body, small and misshapen brains and smaller eyes. Moreover, seizures characterized by hyperactive behavior and spontaneous epileptiform discharges were observed. To better understand the mechanisms/pathways underlying the epileptic phenotype, a transcriptome analysis was performed, revealing a downregulation of genes involved in GABA-signaling and an up-regulation of seizure markers (e.g. *c-fos*) (94). The *scn1lab* morphant and mutant aim at modeling Dravet syndrome, a drug-resistant debilitating childhood epilepsy syndrome (55, 95). In both models, epilepsy is characterized by seizures consisting of hyperactivity, whole-body convulsions and rapid undirected movement and by the presence of epileptiform discharges. Pharmacological characterization of the *scn1lab* morphant revealed that only two out of six tested ASDs (sodium valproate and fenfluramine) could significantly reduce the epileptiform discharges. These results are in line with findings from the *scn1lab* mutant where 4 out of 11 tested ASDs (valproate, diazepam, potassium bromide and stiripentol) showed a significant improvement in brain activity (55, 95). These data demonstrate that the zebrafish *scn1lab* model mimics well the drug-resistant profile of Dravet syndrome. Additionally, a transcriptome analysis was carried out on the *scn1lab* mutants, but failed to detect an up-regulation of seizure markers (e.g. *bdnf*) (55). Finally, this mutant model was used for drug screening and led to the discovery of clemizole, which provides a proof-of-concept for the suitability of genetic zebrafish epilepsy models for high-throughput ASD discovery (55).

Table 1: Overview of genetic zebrafish epilepsy models

Model	Genetic tool	Human gene	Functional target or function	Seizures	Non-behavioral epilepsy biomarker	Ref.
<i>mind bomb</i> mutant	retroviral insertional mutagenesis	<i>KIAA1323</i>	E3 ubiquitin ligase	yes	epileptiform discharges, TA	(94)
<i>lgi1a</i> morphant	MOs	<i>LGII</i>	synapse transmission	yes, also sensitized to PTZ	NI	(87)
<i>kcnq3</i> morphant	MOs	<i>KCNQ3</i>	K _v 7.3 channel	NI	epileptiform discharges	(88)
<i>ocr1l</i> mutant	retroviral insertional mutagenesis	<i>OCRL1</i>	phosphoinositide 5-phosphatase OCRL1	yes	sensitized to heat-induced epileptiform discharges	(89)
<i>scn1lab</i> mutant	ENU mutagenesis	<i>SCN1A</i>	Na _v 1.1 channel	yes	epileptiform discharges, TA	(55)
<i>kcnj10a</i> morphant	MOs	<i>KCNJ10</i>	K-channel	yes	epileptiform discharges	(92) (93)
<i>chd2</i> morphant	MOs	<i>CHD2</i>	gene transcription modification	yes	epileptiform discharges	(90)
<i>stx1b</i> morphant	MOs	<i>STX1B</i>	GABA and glutamate release	yes	epileptiform discharges	(52)
<i>scn1lab</i> morphant	MOs	<i>SCN1A</i>	Na _v 1.1 channel	yes	epileptiform discharges	(95)
<i>stxbp1b</i> mutant	CRISPR/Cas9	<i>STXBP1</i>	neurotransmitter release	not observed	epileptiform discharges	(91)

Abbreviations: MOs = morpholinos, ENU = N-ethyl-N-nitrosurea, K_v-channel = voltage-gated potassium channel, Na_v-channel = voltage-gated sodium channel, TA = transcriptome analysis, NI = not investigated. Adapted from Pitkänen *et al.* 2017 *Models of Seizures and Epilepsy*, 2nd edition (77)

Where previously zebrafish mutants were discovered using ENU or proviral-insertional mutagenesis screens to select mutants with a specific phenotype or behavior (forward genetics), the rise of whole-exome sequencing (WES) combined with the availability of genome engineering tools opens avenues for the generation of ‘personalized’ zebrafish models (reverse genetics) (96). As such, a novel candidate epilepsy gene, identified using WES in a cohort of patients, can be modeled in zebrafish. Subsequently after validation of behavioral and/or electrophysiological seizure activity, this newly developed genetic epilepsy model can (i) improve insights into the pathophysiology of epilepsy and (ii) serve in moderate- to high-throughput screens for novel ‘personalized’ ASDs and anti-epileptogenic drugs (96).

Currently, a wide range of reverse genetic tools is available to obtain efficient knockdown (transient or permanent) or overexpression of a gene of interest.

Morpholinos (MOs) have been extensively used for the generation of genetic zebrafish epilepsy models by transiently knocking down the gene of interest (52, 88, 90, 92, 95). MOs are antisense morpholino oligonucleotides that, when compared to DNA, possess a six-membered morpholine ring instead of the deoxyribose ring and a non-ionic phosphorodiamidate backbone instead of the anionic phosphodiester bond. MOs are typically 25 base pairs (bps) in length and bind the RNA of interest via complementary base pairing with high affinity due to the neutral charged backbone. After microinjection of the fertilised egg into the yolk at the one- or two-cell stage MOs lead to partial or full gene knockdown by (i) interfering with the correct splicing of the mRNA (splice-blocking MO) or (ii) inhibiting ribosome assembly and thus translation-initiation of the mRNA (translation-blocking MO) (57, 97, 98). MOs owe their popularity to the fact that they are inexpensive and allow a fast investigation of gene function in normal wild type (WT) larvae. However, more recently MOs were criticized for the induction of possible off-target effects (99, 100). To respond to this drawback, proper controls such as a second MO targeting a non-overlapping sequence and/or a mRNA rescue should be included to validate the specificity of the used MO (57).

In recent years, the general interest has shifted from the MO approach, which resulted in a transient knockdown of gene expression, to the use of targeted genome editing tools like zinc finger nucleases (ZFNs) (101, 102) or transcription activator-like effector nucleases (TALENs) (103, 104). Although these tools have been proven useful in the generation of stable genetic zebrafish models, a newer and more efficient method of targeted mutagenesis has been developed, namely clustered regulatory interspaced short palindromic repeats (CRISPR). CRISPR is derived from a defense mechanism of bacteria using small RNAs guiding the nuclease CRISPR-associated 9 (Cas9) to target invading foreign DNA (i.e. viruses and plasmids) (105, 106). To obtain targeted mutagenesis *in vivo* only two components are needed: a guide RNA (gRNA) designed to bind to a complementary DNA target sequence in the gene of interest and the nuclease Cas9 that binds to the gRNA (107, 108). At the target site a Cas9-

mediated double strand break (DSB) will be induced, which subsequently will be repaired by the cell's DNA repair mechanisms either by non-homologous end joining (NHEJ) leading to indels either by homology-directed repair (107). The latter repair mechanism is well suited to introduce a patient-specific mutation by providing a complementary DNA template harboring this mutation. Co-injection of the gRNA and Cas9 mRNA into the cytoplasm of the fertilized egg at the one-cell stage leads to the generation of F0 mosaic individuals (107). These fish are raised until adulthood and outcrossed with WT animals to determine germline transmission in the F1 offspring. Next, F1 adults carrying the same mutation can be incrossed to obtain F2 homozygotes or further outcrossed with WT to get F2 heterozygotes (in the latter case, the experiments would be performed on the F3 generation). Of interest, the first genetic zebrafish epilepsy model generated by means of the CRISPR/Cas system was the homozygous *stxbp1* mutant reported by Grone *et al* (91).

In order to overexpress a gene and study its function, the most commonly used method in zebrafish is the Tol2 method of transgenesis (109, 110). The tools needed are (i) a donor plasmid containing the Tol2 construct, i.e. a tissue-specific promoter, the gene of interest and a fluorescent tag, flanked by Tol2 sites and (ii) a transposase enzyme that recognizes the Tol2 sites. The transposon-donor plasmid and transposase mRNA are co-microinjected into the cytoplasm of the fertilized egg at the 1-cell stage. Subsequently, after translation of the transposase mRNA, this enzyme will cleave the donor plasmid at the Tol2 sites and integrate the Tol2 construct at a random place into the genome. Successful integration and thus overexpression of the gene of interest can be verified by visualization of the fluorescent tag in the transparent embryos/larvae (109, 110).

4.6 Translational Bioinformatics using the zebrafish model

Bioinformatics research aims at processing large amounts of basic biological data (on DNA, RNA, proteins and small molecules) and subsequently representing them in a comprehensive way. Translational bioinformatics integrates molecular and clinical (e.g. patients, disease, symptoms) information working towards an improvement of both clinical care and our understanding of biology or pathophysiology (111). Due to recent technological advances, i.e. Next Generation Sequencing, biological data are generated at a high speed underscoring the associated need for user-friendly tools to structure, analyze and visualize those big data sets (112, 113). Examples of such open access services for visualization, integration and enrichment of biological information are Cytoscape, BioGPS and Database for Annotation, Visualization and Integrated Discovery (DAVID) (112). These services provide tools for the bioinformatics analyses at the genomic, transcriptomic, proteomic and metabolic levels (112).

Zebrafish are a good model to study systems biology, which can be defined as “the systematic examining and understanding of various variables and components making the system (reductionist approach) and the understanding of the biological system as a whole (holistic approach)” (114, 115). Therefore, systems biology can be regarded as a sort of data integration approach with information from different fields. The omics approach with characterization of the model at the levels of genes, mRNA, proteins and metabolites forms the basis of systems biology (115). In reality, however, often a reductionist approach is followed using a zebrafish model to whether or not confirm a certain hypothesis by performing a set of experiments (115).

In general, data management in transcriptomics studies follows a sequence of steps (Fig. 12) (116). First, a large dataset on gene regulation is obtained via microarray (or any other method used to measure RNA transcripts). Next, a number of tools are available for data mining (i.e. extract information using mathematical methods) and cleaning of the data in order to obtain a profile of the differentially expressed genes (DEGs). Subsequently, clustering of DEGs based on their expression allows visualization of co-regulated genes. Additionally, by functional clustering of DEGs using gene ontology, pathways involved in the studied disease process might be identified (116). One of the tools frequently used to test DEGs for gene ontology and pathway enrichment is DAVID (117). Pathway analysis is one of the major outputs of bioinformatics at the transcriptomic level, since it provides insight into the pathways underlying the disease and therefore may help the identification of possible treatment targets (116).

In the field of genetic zebrafish epilepsy models, only two examples have been reported that include valuable information obtained from a transcriptomic approach, i.e. the *scn1lab* mutant and the *mind bomb* mutant (55, 94). The *scn1lab* zebrafish model harbors a mutation in the alpha subunit of the voltage-gated sodium channel 1.1, leading to a decrease in mRNA expression. The authors hypothesized this downregulation to be associated with an upregulation of other *scn* subunits. However, microarray analysis proved this hypothesis wrong since no differences in expression of the voltage-gated sodium channel subunits could be detected when comparing WT siblings with *scn1lab* mutants. Although 1099 DEGs were uncovered using bioinformatics, they did not show obvious CNS-related function (55). Hortopan *et al.* have demonstrated that the *mind bomb* zebrafish mutant, which carries a mutation in the gene encoding the E3 ubiquitin ligase, showed both behavioral and electrographic seizure activity. They incorporated a transcriptomics approach to unravel the molecular pathways underlying the observed epileptic phenotype and as such found a downregulation of genes necessary for GABA-mediated signaling.

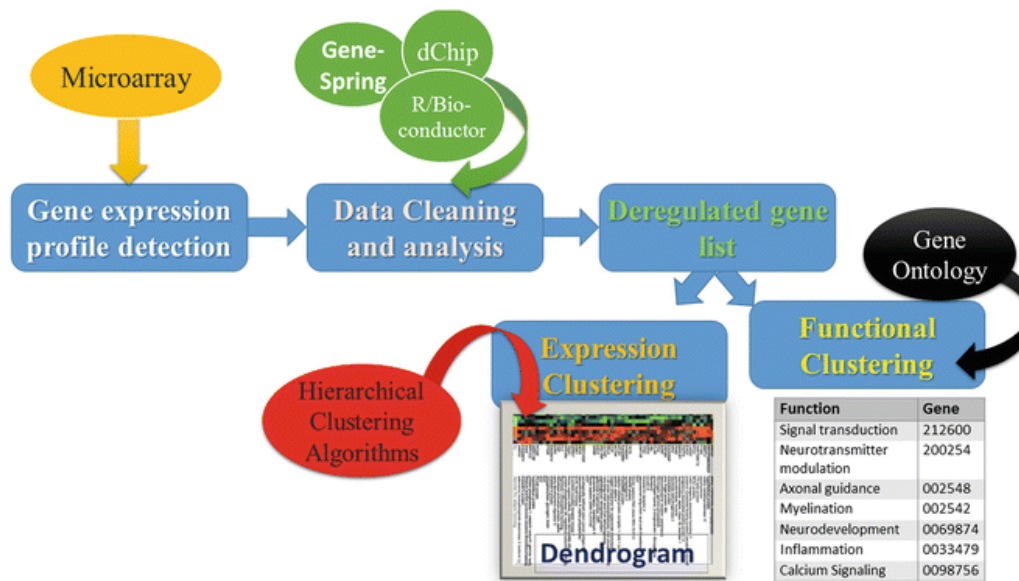


Figure 12: Workflow of data management in transcriptomics studies. Microarrays are used to obtain gene expression profiles. Subsequently the wealth of data is cleaned and analyzed using online tools (e.g. GeneSpring offers accessible statistic tools) to result in a list of differentially expressed genes. Next, clustering of genes occurs based on their expression using hierarchical clustering algorithms or based on biological function using gene ontology. From Alawieh *et al.* 2014 *Methods in Molecular Biology* (116).

These studies show the utility of bioinformatics to extract relevant information from a huge dataset obtained using transcriptomics. Since zebrafish are often used to model human diseases, insights gained from transcriptomics might be directly translatable to the clinic (translational bioinformatics).

CHAPTER II

Research objectives

Recently, more and more mutations are identified as a cause underlying epilepsy or a syndrome associated with epilepsy. This is partly due to the emergence of Next-Generation Sequencing technologies that allow fast, high resolution sequencing of the whole genome or exome of patients giving rise to the identification of *de novo* mutations. Zebrafish are a tractable genetic organism permitting easy and fast modeling of a genetic disease *in vivo*. With regards to genetic epilepsy research in zebrafish, standardized procedures are available to assess seizure activity on the molecular, behavioral and electrographic level. Moreover, zebrafish as a simple vertebrate model may provide valuable insights into the pathogenesis of a disease. Finally, genetic zebrafish models may be included in high-throughput assays to screen for disease-modifying drugs and as such contribute to a more personalized medicine.

The presented doctoral research focuses on the modeling of two mutations in zebrafish, that are presumed (*FHF1* gene) or known (*TSC2* gene) to give rise to epilepsy or a syndrome-associated epilepsy in humans.

A variant in the *FHF1* gene was identified using whole-exome sequencing (WES) on patients suffering from severe generalized tonic seizures among other symptoms. Given the need for a fast clinical diagnosis, i.e. linking a specific gene mutation to a disease phenotype, we aimed at modeling the *FHF1* pathogenic variant in zebrafish in order to confirm its role in epileptogenesis (Chapter III).

Tuberous sclerosis complex, caused by pathogenic variants in the *TSC1* or *TSC2* genes, is an orphan disease with epilepsy as the most common neurological symptom (90% of patients). Since epilepsy in two thirds of patients remains uncontrolled, despite proper treatment with ASDs, the need for effective drugs is high. Recently, mTOR inhibitors have been shown effective in the treatment of TSC-associated epilepsy. Nonetheless, the side effects related to mTOR treatment necessitate the discovery of new drugs with a higher tolerability. To this end, animal models are needed to further unravel the pathogenesis of the disease in the search for new drug targets and/or drug discovery purposes. Therefore, we investigated an already established, however, not yet functionally characterized *tsc2* mutant zebrafish model, developed by Kim *et al.* (118). We aimed to determine whether this zebrafish model serves (i) to further investigate the patients' phenotype, (ii) to gain more insights into the pathogenesis of TSC and identify possible targets for treatment, and (iii) to be pharmacologically validated using an mTOR inhibitor (Chapter IV).

CHAPTER III

Parts of this chapter have been published in the following publication:

“Gain-of-function *FHFI* mutation causes early-onset epileptic encephalopathy with cerebellar atrophy”

1. Abstract

Objective: Voltage-gated sodium channel (Na_v)-encoding genes are among early-onset epileptic encephalopathies (EOEE) targets, suggesting that other genes encoding Na_v -binding proteins, such as fibroblast growth factor homologous factors (FHF), may also play roles in these disorders.

Methods: To identify additional genes for EOEE, we performed whole-exome sequencing in a family quintet with two siblings with a lethal disease characterized by EOEE and cerebellar atrophy. The pathogenic nature and functional consequences of the identified sequence alteration were investigated *in vivo* using zebrafish. To this end, both *fhlb* loss-of-function and gain-of-function experiments have been performed.

Results: A *de novo* heterozygous missense mutation was identified in the *FHF1* gene (*FHF1A*_{R114H}, *FHF1B*_{R52H}) in the two affected siblings. Transgenic overexpression of mutant FHF1B in zebrafish larvae enhanced epileptiform discharges, demonstrating the epileptic potential of this *FHF1* mutation in the affected children.

Conclusions: Our data demonstrate that gain-of-function *FHF* mutations can cause neurologic disorder, and expand the repertoire of genetic causes (*FHF1*) underlying EOEE and cerebellar atrophy.

2. Introduction

Early-onset epileptic encephalopathies (EOEEs) are characterized by progressive diffuse brain dysfunction with recurrent seizures starting during the neonatal or early infantile periods. These epilepsies are among the most severe, with the child typically experiencing multiple seizure types which are often refractory to anti-epileptic drugs, in the setting of developmental delay or regression. Epileptic encephalopathies can worsen over time, and the epileptic activity itself may contribute to severe cognitive, neurological and behavioral impairments above and beyond what might be expected from the underlying pathology alone (119). EOEE represent a broad spectrum of phenotypes that are highly heterogeneous at the clinical and molecular levels. Whereas a number of genetically determined (monogenic) forms have been recognized, in clinical practice many cases remain of unknown etiology (120). Of the genetic mutations known to be linked to EOEE, several are missense mutations in *SCN8A* encoding the alpha pore-forming subunits of the voltage-gated sodium channel $\text{Na}_v1.6$ (121-123), with some of these mutations acting in a gain-of-function manner to enhance sodium channel current (121, 122). So far there had been no report of EOEE caused by mutation of sodium channel-binding proteins, such as fibroblast growth factor homologous factors (FHF), although *FHF* loss-of-function mutations have been associated with unrelated neurological disorders (spinocerebellar ataxia and Wildervanck syndrome). We have now identified a new EOEE gene (*FHF1*) by whole-exome sequencing in a family quintet with two affected siblings, and we validated the disease-causative nature *in vivo* using zebrafish.

3. Methods

3.1 Genetic analysis of the EOEE-affected family

Pathogenic copy number variants were excluded by conventional karyotyping and array comparative genomic hybridization. DNA of parents, their two affected children, and one unaffected child was extracted from peripheral blood lymphocytes. All five samples were used for library preparation and exome enrichment using the TruSeq DNA library prep kit (Illumina, San Diego, CA) and NimbleGen SeqCap EZ Human Exome Library v3, respectively. Paired-end sequencing (2x100bp) was performed on the HiSeq 2000 platform (Illumina). Sequence reads were mapped to the human reference genome (hg19) with BWA and variant calling was performed using the GATK framework (124, 125). Variants were annotated in Annovar and filtered in Microsoft (Redmond WA) Excel based on inheritance pattern, location, function and presence in the 1000 Genomes dataset (126). Candidate variants obtained from exome sequencing were validated using Sanger sequencing. Primers covering all exons and exon-intron boundaries were designed using Primer3Plus (127). PCR was performed using GoTaq DNA Polymerase (Promega Corporation, Madison, WI) and products were sequenced on an ABI3130xl sequencer (Life Technologies, Carlsbad, CA).

3.2 Zebrafish overexpression studies

3.2.1 Zebrafish maintenance and breeding

Adult zebrafish (*Danio rerio*) of the AB strain (ZIRC) were maintained at 28.5 °C on a 14-hour light/10-hour dark cycle under standard aquaculture conditions. Embryos were raised in embryo medium, containing (in mM) 1.5 HEPES, pH 7.6, 17.4 NaCl, 0.21 KCl, 0.12 MgSO₄ and 0.18 Ca(NO₃)₂, in an incubator on a 14-hour light/10-hour dark cycle at 28.5 °C.

3.2.2 Overexpression experiments

Wild-type (WT) zebrafish *fhf1b1* cDNA (ENSDART00000090596) under the control of the zebrafish CNS-specific *her4* promoter was cloned into the Tol2 expression vector (gift from G. Weidinger; University of Ulm, Germany) using *PacI* and *NotI* sites (WT-*fhf1b1*-Tol2). The mutation encoding R56H in zebrafish was cloned into the *fhf1b1* sequence via site-directed mutagenesis (primers: table e-1) (R56H-*fhf1b1*-Tol2). Empty Tol2 vector expressing the fluorescent reporter mCherry alone was used as a control (ctrl-Tol2). The overexpression experiment was performed by cytoplasmic microinjection of 10 pg of WT-*fhf1b1*-Tol2, R56H-*fhf1b1*-Tol2 or ctrl-Tol2 and 50 pg of transposase (1-nl volume) into embryos at one-cell stage.

3.2.3 *fhf1b1* mRNA expression analysis

Total RNA from 5 dpf larvae was extracted using TRIzol (Ambion; Thermo Fischer Scientific, Waltham, MA). Reverse transcription of total RNA to single-stranded cDNA was performed using the High Capacity cDNA Reverse Transcription Kit (Applied Biosystems, Foster City, CA). Measurements of *fhf1b1* mRNA were performed using *fhf1b1*-specific primers (table e-1) combined with SsoAdvanced Universal SYBR Green Supermix (Bio-Rad, Hercules, CA) using CFX96 Touch Real-Time PCR Detection System (Bio-Rad) and analyzed using CFX Manager Software (Bio-Rad). *fhf1b1* transcripts were normalized against β -2 microglobulin and β -actin controls (table e-1). The results consist of data from three separate experiments run in triplicates. Pairwise statistical significance was determined with Student's unpaired *t* test (Prism 6, Graphpad, La Jolla, CA).

3.2.4 Tectal field recordings

Open-field recordings were obtained from zebrafish larval tecta at 5 dpf at room temperature, as described previously (128). Single recordings were performed for 10 minutes. Spontaneous events were taken into account when the amplitude exceeded baseline by at least threefold. The analysis of spikes was carried out using Clampfit 10.2 software (Molecular Devices). The statistical significance between 2 conditions was calculated by Fisher exact test (GraphPad Prism 6).

3.3 Standard protocol approvals, registrations and patient consents

This study was approved by the UZ Leuven institutional review board and written patient informed consent was obtained. All zebrafish experiments were approved by the KU Leuven Ethics Committee and the Belgian Federal authority.

4. Results

4.1 *FHF1* mutation identified in EOEE with cerebellar atrophy

Whole-exome sequencing was carried out on a family quintet with two affected siblings (EOEE with cerebellar atrophy) and unaffected parents and sibling, where extensive neurometabolic investigations and directed mutagenesis analysis of known genes (including *STXBP1*, *KCNQ2*, *SLC2A1*) were all negative. Exome data analysis identified a heterozygous missense mutation in *FHF1* on chromosome 3 (NM_021032, 192053223 C>T based on Hg19, p.R114H in A-isoform, p.R52H in B-isoform; figure 1A). This was the only variant present in the two affected siblings but not in the unaffected sibling, their parents (pointing towards germline mosaicism), or in normal population databases including 1000 Genomes, the NHLBI Exome Variant Server and the EXaC browser. No other pathogenic mutations were yielded by filtering variants for recessive (homozygous or compound heterozygous) inheritance present in both affected individuals and absent in the unaffected sibling. The affected arginine residue is part of the highly conserved surface region that binds voltage-gated sodium channels (figure 1, B-D) (129, 130), and the mutation was presumed to be damaging by the PolyPhen-2 and Mutationtaster *in-silico* prediction software (Grantham score 29; GERP-score 5.16) (131, 132). A disease-causative nature of the mutation was further supported by the physiological role of *FHF1* in controlling neuronal excitability (14, 133, 134), the patients' phenotype being dominated by a hyperexcitable CNS state with epilepsy/EOEE and cerebellar atrophy assumed secondary to chronic excitotoxicity.

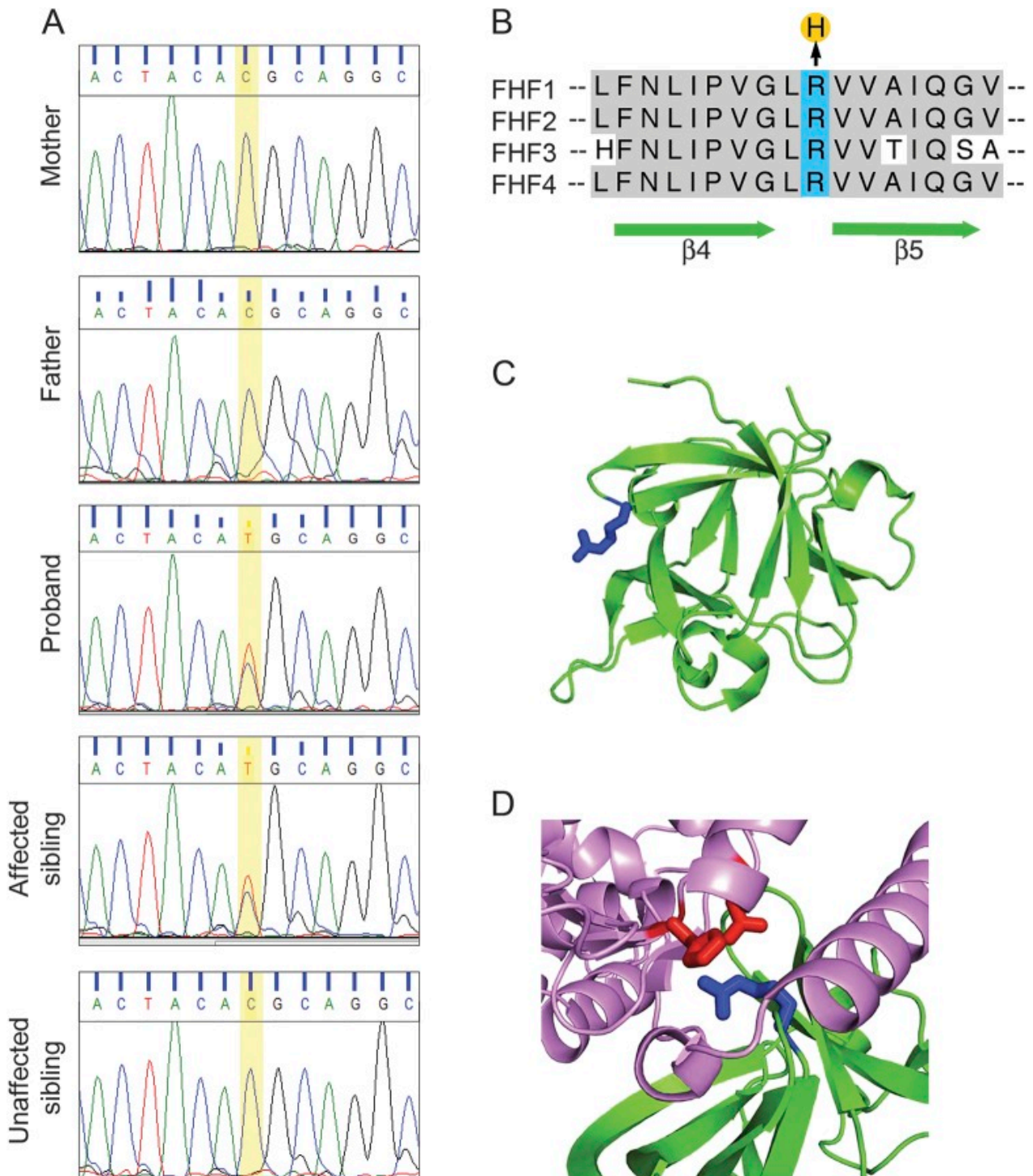


Figure 1: Heterozygous missense mutation (C > T) in *FHF1* in 2 siblings with early-onset epileptic encephalopathy (EOEE) with cerebellar atrophy. (A) Whole-exome sequencing on a family quintet with 2 affected siblings (EOEE with cerebellar atrophy) and unaffected parents and sibling identified a heterozygous missense mutation in *FHF1* (p.R114H in A-isoform, p.R52H in B-isoform). (B) Alignment of fibroblast growth factor homologues factor (FHF) sequences in the region of the mutation. The FHF amino acid sequence contributing to the $\beta 4$ and $\beta 5$ strands and the $\beta 4/\beta 5$ loop is highly conserved among the 4 FHF core domains (shaded residues), including the $\beta 4/\beta 5$ loop arginine (blue) that is mutated to histidine (yellow) in the affected siblings. (C) Ribbon diagram of the FHF1 core structure (14). The affected arginine residue side chain (blue) in the $\beta 4/\beta 5$ loop projects to the protein surface. (D) Ribbon diagram of the FHF/voltage-gated sodium channel (Nav) interface (126). The FHF $\beta 4/\beta 5$ loop arginine (blue) interacts with aspartate and histidine residues (red) in the Nav cytoplasmic tail.

4.1.1 Clinical phenotype

The proband (female) was born at term (birthweight 2,920 g) as the first child of non-consanguineous Caucasian parents. It was a spontaneous twin pregnancy with *in utero* loss of the other fetus around the end of the first trimester (no medical information available). Tonic seizures developed from the age of 14 days, mostly during sleep. She was a normal neonate prior to the onset of the seizures. There was no epileptic myoclonus or other seizure types. Very rapidly, a clear encephalopathic EEG developed with severe background slowing and multifocal epileptic abnormalities. Seizures were tonic, generalized or focal with a typical ictal EEG pattern of low voltage fast activity (Figure e-1), followed by long suppression of the background. This evolution resulted in an hypersarrhythmia pattern at the age of 5 months, without clinical epileptic spasms. Her epilepsy proved refractory to multiple anti-epileptic drugs. She developed profound intellectual disability, acquired microcephaly, axial hypotonia, ataxia (limbs), severe feeding difficulties necessitating tube feeding, cerebral visual impairment and absent speech development. Unsupported sitting was achieved at age 24 months, she never came to standing and walking. Visual evoked potentials were normal at age 4 months; fundoscopy was normal initially and showed pale optic discs and narrow vessels at age 5 years. Brain MRI was normal at age 5 months, but showed cerebellar atrophy at age 6 years (figure 2A). The disease course seemed degenerative (decrease in alertness, general condition and skills, appearance of discomfort and agitation, increase in epilepsy) prior to death at age 7 years due to status epilepticus. The proband had two younger brothers. The youngest was healthy, the other showed an identical clinical course as his sister with refractory epilepsy (onset at age 4 weeks, tonic seizures) with similar seizure semiology and EEG abnormalities, hypotonia, ataxia, acquired microcephaly, poor visual contact, feeding problems and profound intellectual disability. Brain MRI was normal at age 2 months but showed cerebellar atrophy at age 3 years (figure 2B). He died at age 3.5 years (cause of death unknown). At the age of 5 years, the father had one epileptic seizure (unknown whether febrile or not), further family history was negative for epilepsy and neurodegenerative disease.

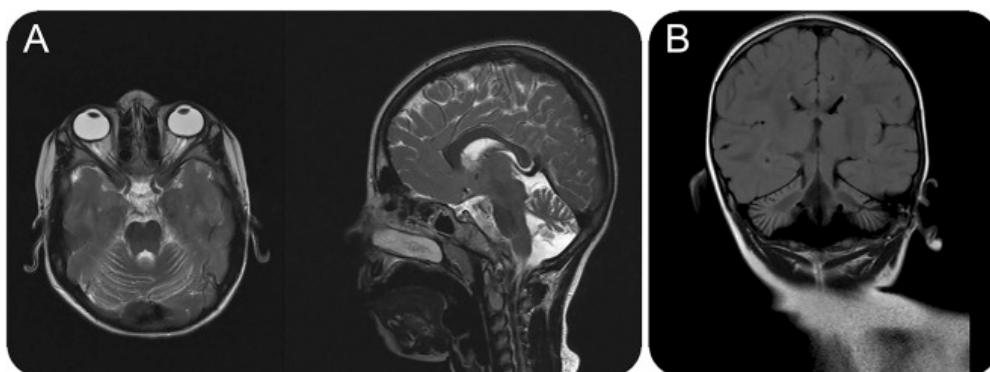


Figure 2: Cerebellar atrophy in 2 siblings with a gain-of-function *FHF1* mutation. MRI of the brain was normal at infant age in both affected siblings. However, repeat MRI in their further disease course, which was degenerative, showed the emergence of cerebellar atrophy in both children: (A) proband at age 6 years: axial and sagittal image show prominent fissures between shrunken cerebellar folia; (B) younger brother of proband at age 3 years: coronal image shows cerebellar atrophy.

4.2 WT vs mutated Fhf1b in zebrafish

To investigate the pathogenic nature and functional consequences of the patients' *FHF1* R→H mutation *in vivo*, a bilateral zebrafish approach was used consisting of both *fhf1b* loss-of-function and gain-of-function experiments. The approach outlined below, is applicable for the *in vivo* modeling and characterization of newly identified candidate-epilepsy genes in general.

Zebrafish have two *fhf1* genes (due to genome duplication), termed *fhf1a* and *fhf1b*. The A-type protein isoforms (Fhf1a, Fhf1b2) encoded by these two zebrafish genes share 81.8-90.9% identity with human FHF1A, whereas the B-type protein isoform Fhf1b1 encoded by an alternatively spliced mRNA from the zebrafish *fhf1b* is 84.4% identical to human FHF1B. The zebrafish *fhf1b* gene expresses both A- (Fhf1b2) and B-type (Fhf1b1) zebrafish isoforms (figure e-2). The arginine residue mutated in the EOOE siblings is conserved in zebrafish *fhf1* orthologs and corresponds to R112 in A-isoform Fhf1a, R116 in A-isoform Fhf1b2, and R56 in B-isoform Fhf1b1 (figure e-2).

First, we studied the *fhf1b* expression in different tissues (brain, spinal cord, eye, muscle, intestines, liver and heart) of adult zebrafish using RT-PCR. *fhf1b* was highly expressed in brain and spinal cord compared to the other organs and thus proves the validity of our model system to study *fhf1*-related neurological deficits. Our findings are in line with expression data obtained from murine tissues, where *fhf1* was expressed predominantly in the developing and mature central nervous system (135). Next, whole mount *in situ* hybridization (WISH) was performed on 12 hpf, 1 dpf and 2 dpf embryos to detect the spatiotemporal expression pattern of *fhf1b*. Unfortunately, the generated antisense probe showed a non-specific staining.

The first approach used to investigate the function of FHF1 consisted of a morpholino (MO)-mediated knockdown of the *fhf1b* gene. This gene leads to two alternatively spliced isoforms *fhf1b1* and *fhf1b2*. To obtain a full knockdown of the *fhf1b* gene, a splice blocking MO was designed to target the exon 3-intron 3 boundary, a region conserved in both isoforms. Different amounts of *fhf1b* and control MOs were microinjected into the yolk of 1-2 cell stage embryos. Splice blocking MOs interfere with correct pre-mRNA processing by inhibiting the binding of splice-regulatory proteins, giving rise to intron-inclusions or exon-exclusions (136). Here, an exclusion of exon 3 was detected by RT-PCR in the *fhf1b*-MO-injected larvae, confirming a sustained knockdown of *fhf1b* up till 5 dpf.

Morphological assessment was done until 6 dpf and revealed at higher doses (6.75 and 9 ng) the occurrence of a curved trunk in up to 70% of the *fhf1b*-MO-injected larvae. Although this curved trunk might be a gene-specific effect, it should be noted that body curvature is quite commonly observed as non-specific phenotype related to the morpholino approach (97). By non-specific activation of p53,

morpholinos can lead to what is known as “the morpholino phenotype” characterized by, but not limited to, neuronal cell death, shortened body axis and spinal curvature (137). Moreover, several studies reported a curved trunk phenotype in zebrafish morphants (138-141), while the corresponding mutants appeared to be normal, suggesting it to be a non-specific effect of the MOs tested (100). In our case, since no mutant was available, a *p53*-MO could have been co-injected together with *fhflb*-MO to determine the specificity of this morphological trait. For further experiments the doses used were 6.75 ng and 9 ng, since these did not result in severe toxicity. Head and brain size measurements were performed at 3 dpf to examine whether the microcephaly phenotype of the children could be mimicked in zebrafish larvae. To this end, different parameters were measured including head area, brain area and body length. Our results indicated a consistent reduction in brain size in the *fhflb*-MO-injected larvae compared to control-MO-injected larvae. In our study, the larvae were imaged from the lateral view with both eyes perfectly overlapping. Reference points used to ensure a reproducible surface selection were the otic vesicle and the jaw (head size) or the otic vesicle and the upper lining of the eye (brain size). Another approach could be to image the larvae from the dorsal view and measure head diameter, distance between the convex tips of the eye cups or predetermined brain surface area consisting of the area between the eye cups (142-145). Next, behavioral tracking performed at 4 dpf in both light and dark conditions failed to detect differences in behavior between *fhflb*- and control-MO-injected larvae. Finally, brain activity assessed by invasive local field potential (LFP) recordings from the optic tectum of 5 dpf larvae did not reveal any epileptiform activity in the *fhflb*-MO-injected larvae.

The second approach consisted of transient overexpression of WT and mutant *fhflb1* (R56H-*fhflb1*) by microinjecting these mRNAs into the cytoplasm of 1-cell stage embryos. EGFP-mRNA was used as a control. The full-length *fhflb1* mRNA probes were generated by (i) amplification of the full-length *fhflb1* cDNA from a cDNA clone using attB₁- and attB₂-flanked primers, (ii) recombination of the Gateway attB sites with attP sites of the pDONR221 vector, i.e. BP reaction resulting in pENTR221 insert, (iii) recombination of the Gateway attL sites of the pENTR221 insert with attR sites of the pCSDest vector, i.e. LR reaction resulting in insertion of the *fhflb1* sequence into the final vector, named pCSFinal, (iv) site-directed mutagenesis using a pair of complementary mutagenic primers bearing the R56H point mutation to amplify the entire pCSFinal vector to obtain the mutant *fhflb1* sequence, and (v) linearization and transcription of the pCSFinal vectors resulting in the production of WT-*fhflb1* mRNA and R56H-*fhflb1* mRNA. At each step of this cloning procedure, generated plasmids were transformed in *E.coli* TOP10 cells, plated, purified and sent for sequencing to ensure effective recombination. Morphological phenotyping revealed severe eye defects ranging from no eyes to cyclopia and a proboscis-shaped mouth in up to 25% of the WT- and R56H-*fhflb1* overexpression (OE) larvae, while control larvae developed normally. Finally, some preliminary local field potential recordings were performed on larval optic tecta at 3 dpf. Unfortunately, no significant epileptiform activity was detected.

In our final approach (as described in the published article), Tol2 transgenesis was used to obtain a more stable overexpression of WT and mutant *fhf1b1* (110). Zebrafish *fhf1b1* was cloned under the CNS-specific promoter *her4* and mCherry was used to identify the embryos with Fhf1b1 expression (figure 4A). One-cell stage zebrafish embryos were microinjected with WT and R56H-*fhf1b1*-Tol2 overexpression constructs. *fhf1b1*-Tol2-injected larvae did not exhibit any gross dysmorphologies compared to control larvae (i.e. injected with empty Tol2 vector and expressing mCherry only) (figure 4A). For further experiments, normal looking embryos displaying touch response were selected. To investigate whether overexpression (OE) of R56H *fhf1b1* resulted in abnormal brain activity, we performed local field potential recordings (128) on larval optic tecta on 5 days post-fertilization WT-*fhf1b1*-OE (n=54), R56H-*fhf1b1*-OE (n=54) and control larvae (n=40). Recurrent epileptiform discharges occurred in 50% of R56H-*fhf1b1*-OE larvae, which was of significantly greater incidence than in WT-*fhf1b1*-OE and control groups (27.8% and 17.5%, respectively) (figure 4B). Larvae were classified as having epileptiform activity when the following criteria were met: (i) at least 3 events per 10-minute recording, (ii) duration of the event exceeding 50 ms, and (iii) amplitude of the event exceeding the baseline by at least threefold. When only the larvae with epileptiform activity were included, the mean frequency, duration and cumulative duration of events did not significantly differ among tested groups (figure 4C-E). A similar mean duration indicates that the same type of epileptiform discharge was observed in the different groups, which has been reported in other models as well, e.g. the *scn1lab* morphant (95). Real-time qPCR experiments confirmed that both WT and R56H *fhf1b1* were effectively and equally overexpressed in the OE larvae (figure 4G), confirming that the difference between the number of seizing fish was a result of the *fhf1b1* alteration and not due to the differences in the mRNA expression. These results demonstrate the epileptic potential of the *fhf1b1* mutation in an *in vivo* zebrafish model, supporting FHF1 gain-of-function as the disease mechanism in our EOEE patients with *FHF1* missense mutation.

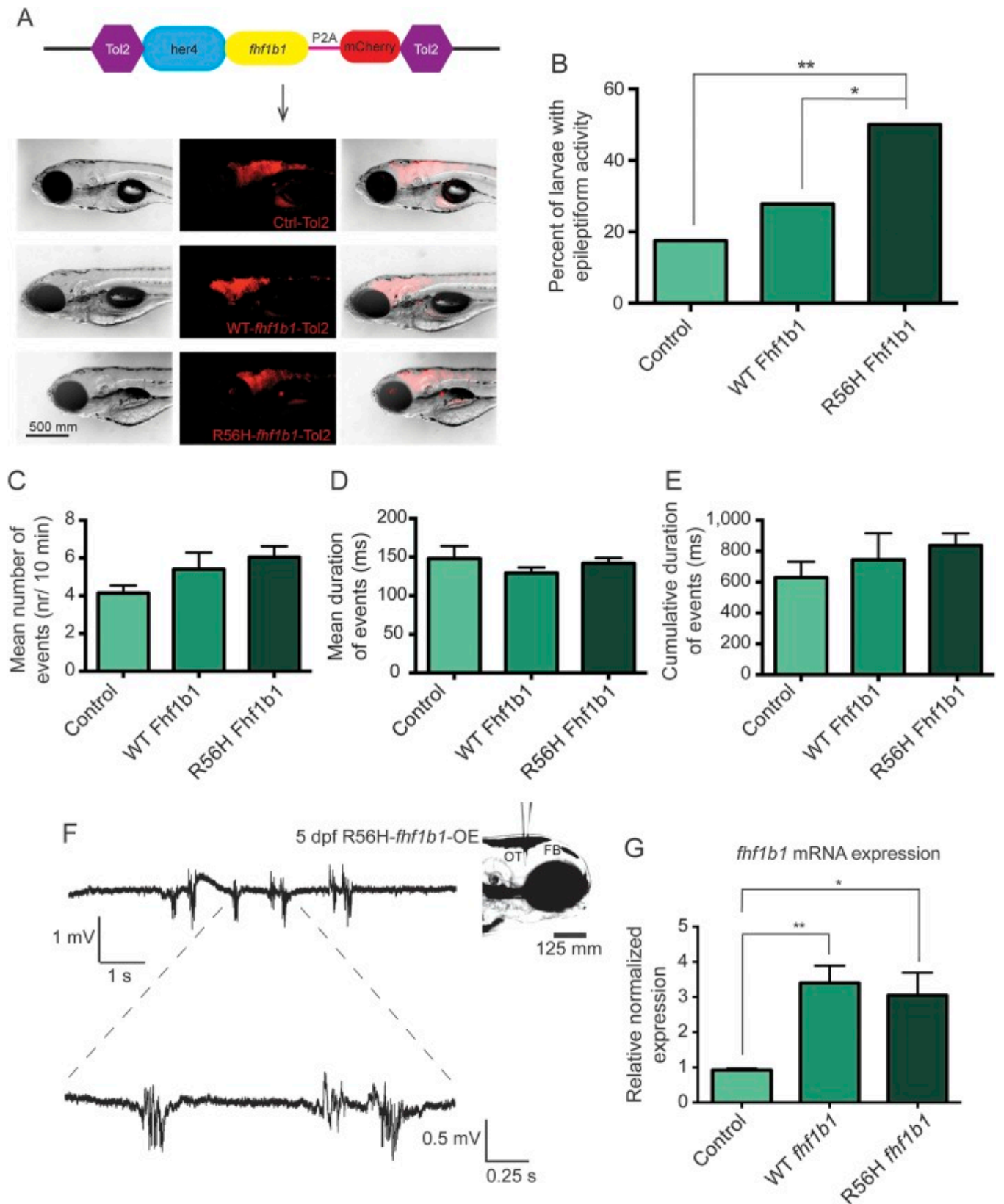


Figure 4: caption on the next page

Figure 4: R56H *fhlb1* overexpression (OE) causes epileptiform discharges in transgenic zebrafish larvae. (A) The Tol2 system was used to transiently overexpress WT and R56H mutant zebrafish *fhlb1*. WT and R56H zebrafish *fhlb1* cDNA was expressed under the control of the zebrafish CNS-specific *her4* promoter. A fluorescent reporter mCherry was used to identify larvae with *fhlb1* expression. Self-cleaving peptide, P2A, enabled the separation between *fhlb1* and mCherry in order to avoid possible disadvantages of a fusion protein. Representative images of 5 dpf larvae microinjected with zebrafish cDNA encoding WT and mutated *fhlb1*, selected for tectal field recordings and mRNA analysis. Red fluorescence depicts the brain-specific expression of Fhlb. Scale bar, 500 μ m. (B) Percentage of larvae with abnormal epileptiform activity after overexpression of WT and R56H *fhlb1*. Overexpression of mutant Fhlb led to a significant increase of the number of larvae with seizure-like events in comparison to WT-*fhlb1*-OE and control larvae (27/54 larvae with R56H-*fhlb1*-OE vs 15/54 larvae with WT-*fhlb1*-OE and 7/40 control larvae; * $p = 0.0293$ and ** $p = 0.0012$, respectively, Fisher exact test). Overexpression of mCherry alone resulted in 17.5% of seizing larvae, which was not statistically different from 27.8% for WT-*fhlb1*-OE larvae ($p = 0.3261$, Fisher exact test). (C) Occurrence of epileptiform events/recording in WT-*fhlb1*-OE (5.4 ± 0.9), R56H-*fhlb1*-OE (6.0 ± 0.6), and control larvae (4.1 ± 0.4) ($p = 0.3237$, one-way ANOVA). Results are mean \pm SEM. (D) Mean duration of epileptiform events in WT-*fhlb1*-OE (129.4 ± 7.1 ms), R56H-*fhlb1*-OE (141.9 ± 7.0 ms), and control larvae (148.2 ± 16.0 ms) ($p = 0.4112$, one-way ANOVA). Results are mean \pm SEM. (E) Cumulative duration of epileptiform events in WT-*fhlb1*-OE (743.6 ± 172.1 ms), R56H-*fhlb1*-OE (836.5 ± 78.3 ms), and control larvae (629.3 ± 102.1 ms) ($p = 0.5556$, one-way ANOVA). Results are mean \pm SEM. (F) Representative spontaneous epileptiform activity recorded from 5 dpf R56H-*fhlb1*-OE larvae. Top trace represents typical epileptiform pattern as seen in gap-free recordings. Bottom trace shows high-resolution magnification of the selected epileptiform events. Next to the traces, an agar immobilized 5 dpf zebrafish with the recording electrode placed in the optic tectum (OT) is shown. FB = forebrain. (G) *fhlb1* mRNA expression in WT and R56H-*fhlb1*-OE larvae. *fhlb1* was expressed approximately 3-fold higher in WT and mutant-OE larvae in comparison to *fhlb1* baseline level in control larvae. ** $p = 0.0080$ WT-*fhlb1*-OE vs control; * $p = 0.0293$ R56H-*fhlb1*-OE vs control (2-tailed Student t-test). β -2 microglobulin and β -actin were used as normalizing controls. Values are mean \pm SEM (triplicate samples with triplicate qPCR experiments).

5. Discussion

The *de novo* heterozygous missense *FHF1* mutation identified in 2 siblings, with a lethal disorder characterized by EOEE and cerebellar atrophy, was the only variant present in the affected siblings but not in the unaffected family members or in normal population databases, and no other pathogenic variants were identified.

The zebrafish-based approach underscores the ease with which zebrafish can be genetically manipulated and their suitability for the fast modeling of newly discovered gene variants. However, it should be noted that the modeling of *FHF1* in zebrafish, in particular, was challenging due to the existence of multiple isoforms and genes. In humans only one *FHF1* gene exists that gives rise to two alternatively spliced isoforms *FHF1A* and *FHF1B*. Zebrafish possess two genes *fhf1a* and *fhf1b*, resulting in three isoforms of which *fhf1a* and *fhf1b2* are A-type isoforms, whereas *fhf1b1* is a B-type isoform. Our first approach, knockdown of the *fhf1b* gene using morpholino oligos, failed to detect any abnormal brain activity in 5 dpf *fhf1b* morphants, which could possibly be explained by a compensatory effect of the A-type isoform *fhf1a*. Next, it was decided to perform mRNA overexpression studies with the B-type isoform *fhf1b1*, since *in vitro* studies (performed by the group of Prof. Goldfarb) had shown a stronger effect on neural excitation of the human B-type isoform *FHF1B* compared to *FHF1A*. Moreover, in contrast to a MO-mediated knockdown these studies allowed to investigate the specific patients' mutation by comparing the overexpression of WT-*fhf1b1* to R56H-*fhf1b1*. Unfortunately, no epileptiform activity was detected at 3 dpf. A possible reason is that detecting epileptiform activity in the developing brain can be difficult to interpret, as the brain is only fully functional at 4 dpf (55, 86). Moreover, fast degradation of 5' capped mRNA *in vivo* complicates study of the effect after 48 hpf (57, 146, 147). Another drawback of this method is the ubiquitous overexpression of the injected mRNAs (57). To address these issues, Tol2 transgenesis was used to obtain a sustained CNS-specific overexpression of WT- and R56H-*fhf1b1*. Using this system, a significantly higher number of R56H-*fhf1b1*-OE larvae showed epileptiform activity compared to WT-*fhf1b1*-OE and control larvae. Importantly, the 50% of R56H-*fhf1b1*-OE larvae showing abnormal brain activity is most probably an underestimation due to the presence of endogenously expressed *fhf1b1* WT mRNA and the A-type isoforms *fhf1a* and *fhf1b2*. Moreover, since the LFP experiments were done directly in the injected larvae, they may show a mosaic expression pattern that has been frequently described for the founder generation of transgenic animals (148), which could lead to heterogeneous phenotypes. A possible limitation of Tol2 transient transgenesis is that Tol2 construct is randomly integrated into the genome, which might interfere with the expression of the gene in which the construct was inserted; however, mostly introns are targeted due to their larger cumulative size (149). Nonetheless, Tol2 transgenesis

proved to be valuable since it allowed us to investigate the effect of the patient-specific mutation *in vivo* in a relatively short timeframe.

Cerebellar atrophy, a component of the disease phenotype associated with mutated *FHF1* (this report), has previously been reported in EOEE caused by mutations in several other genes including those encoding voltage-gated sodium channels such as *SCN8A* (123, 150, 151). Currently, it is not clear how mutations in these genes cause brain atrophy, but one possible mechanism is through a hyperexcitotoxic mechanism. The cerebellar-specific atrophy associated with *FHF1* mutation mirrors the preferential cerebellar functional deficit associated with *FHF1* gene deletion (14) and could reflect preferential expression of an FHF1 protein isoform compared to other FHF1s in this brain region.

Our findings offer a causal link between familial EOEE with cerebellar atrophy and *FHF1* mutation. Early-onset epileptic encephalopathies are severe neurological disorders, which in clinical practice often remain of undetermined etiology. In recent years progress in molecular diagnostics has revealed that a significant proportion of EOEEs are single-gene disorders. Identification of a causative gene defect is important for prognostic and genetic counseling, and may also carry treatment implications. The current study adds *FHF1* and altered Na_v gating to the list of EOEE genes and mechanisms, and our findings support the inclusion of *FHF* genes into the panels of candidate genes used to query the genetic basis of EOEE in additional affected individuals.

6. Supplementary information

6.1 Table e-1: Primer sequences of primers used for *fhf1b1* site-directed mutagenesis and primers for real-time qPCR

Primers for zebrafish *fhf1b1* site directed mutagenesis:

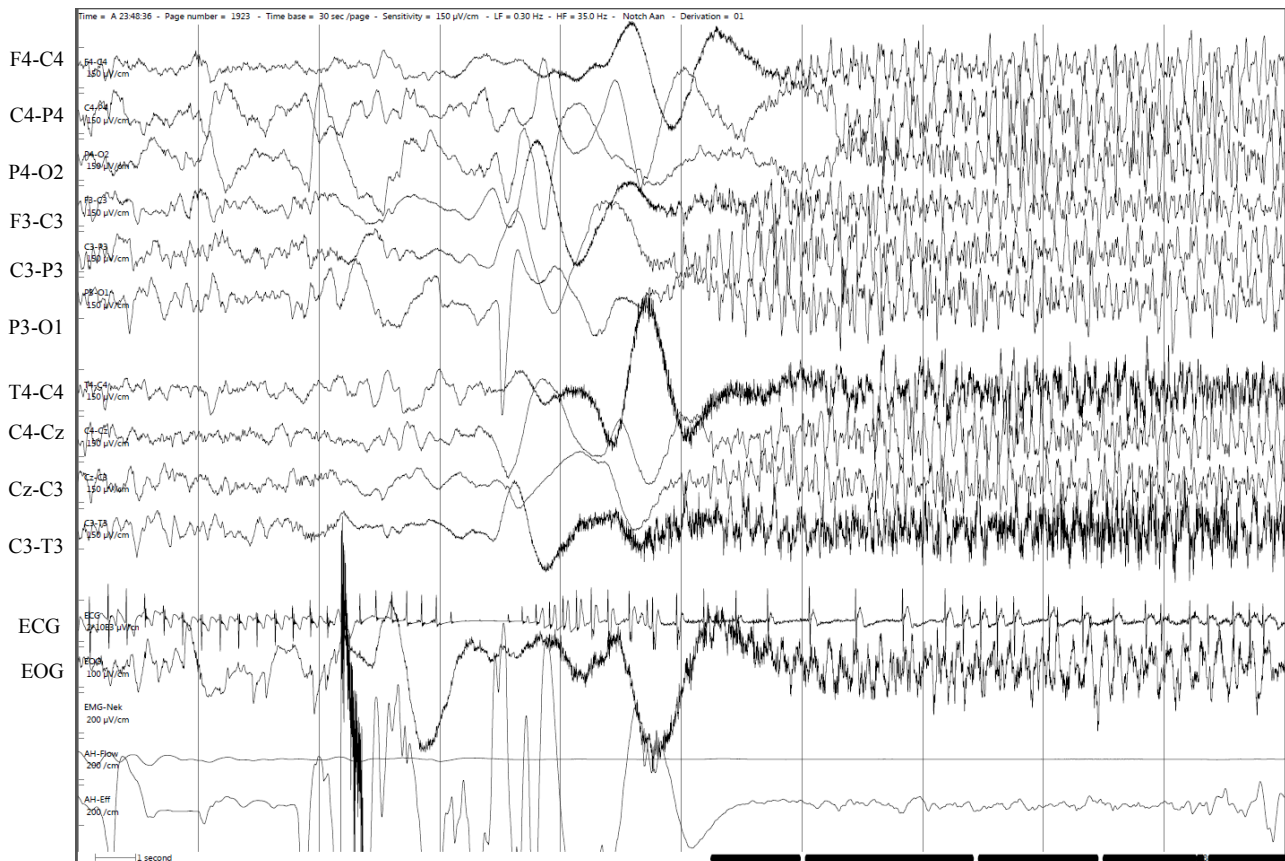
Primer name	Sequence (from 5' to 3')
<i>fhf1b1</i> R56H forward	CCGGTGGGTTTGCACGTCGTGGCGATT
<i>fhf1b1</i> R56H reverse	AATCGCCACGACGTGCAAACCCACCGG

Primers for real-time qPCR:

Primer name	Sequence (from 5' to 3')
<i>fhf1b1</i> _E4 forward	CCTGGTTCCTCGGACTCAAT
<i>fhf1b1</i> _E4 reverse	TCAATGGGTCTGGGTACGAA
<i>Bactin I</i> forward	CGAGCAGGAGATGGGAACC
<i>Bactin I</i> reverse	CAACGGAAACGCTCATTGC
<i>B2m</i> forward	GCCTTCACCCCAGAGAAAGG
<i>B2m</i> reverse	GCGGTTGGGATTTACATGTTG

6.2 Figure e-1: Ictal EEG of patient with *FHF1* mutation

Ictal EEG of a tonic seizure at age 3 months: left centrotemporal ictal onset followed by rapid secondary generalization. Clinically the seizure started with a cry and tonic flexion of the right arm, followed by a generalized tonic phase with opisthotonus, apnea, desaturation and bradycardia.



6.3 Figure e-2: Sequence alignment of human FHF1 and zebrafish Fhfl1 orthologs

An asterisk (*) indicates a fully conserved residue. A colon (:) indicates strongly similar amino acid properties and a period (.) weakly similar amino acid properties. The red shading highlights the arginine (R) substituted in our patients, conserved in zebrafish orthologs. FHF1 sequences taken from Ensemble database: *Homo sapiens* FHF1A, ENST00000454309; *Homo sapiens* FHF1B, ENST00000445105; *Danio rerio* Fhfla, ENSDART0000028390; *Danio rerio* Fhflb1, ENSDART0000090596; *Danio rerio* Fhflb2, ENSDART00000100332. Clustal Omega 1.2.1 used to generate the sequence alignment.

```

CLUSTAL O(1.2.1) multiple sequence alignment

human FHF1A      MAAAIASSLIRQKRQARENSDRVSASKRRSSPSKDG---RSLCERHVLGVFSKVRFCSG
danio Fhfla     -MAAIASSLIRQKRQARENSDRVSASKRRSSPSKDP---RSLCERHFLGVFSKVRFCSG
danio Fhflb2    MAAAIASSLIRQKRQARENSERAATGKRRSSPGKEPTGRGSLCERHLFGLFGKVRFCSG
human FHF1B     -----
danio Fhflb1    -----

human FHF1A      KRKRVRRRPEPQLKGIIVTRLFSEQGYFLQMHPDGTIDGTDKDNSDYTLFNLIPVGLRVVA
danio Fhfla     KRKRVRRRPEPQLKGIIVTRLFSEQGYFLQMHPDGTIDGTDKDNSDYTLFNLIPVGLRVVA
danio Fhflb2    KRKRVRRRPEPQLKGIIVTRLFSEQGYFLQMHPDGTISGTDKDNSDYTLFNLIPVGLRVVA
human FHF1B     -----MESKEPQLKGIIVTRLFSEQGYFLQMHPDGTIDGTDKDNSDYTLFNLIPVGLRVVA
danio Fhflb1    -MESKDKSAEPQLKGIIVTRLFSEQGYFLQMHPDGTISGTDKDNSDYTLFNLIPVGLRVVA
.      *****:***:* **:*:*.* *****

human FHF1A      IQGVKASLYVAMNGEGYLYSSDVFTPECKFKESVFENYYVIYSSSTLYRQQESGRAWFLGL
danio Fhfla     IQGVKAGFYIGMNGEGFLYSSEMFTPECKFKESVFENYYVIYSSSTMYRQQESGRAWFLGL
danio Fhflb2    IQGVKAGLYVAMNGEGFLFSSETFTAECKFKESVFENYYVIYSSSTLYRQHESGRAWFLGL
human FHF1B     IQGVKASLYVAMNGEGYLYSSDVFTPECKFKESVFENYYVIYSSSTLYRQQESGRAWFLGL
danio Fhflb1    IQGVKAGLYVAMNGEGFLFSSETFTAECKFKESVFENYYVIYSSSTLYRQHESGRAWFLGL
*****.:*:.*****:***:* ** *****:***:*****

human FHF1A      NKEGQIMKGNRVKTKPSSHVFPKPIEVCMYREPSLHEIGEKQGRSRKSSGTPMTNNGKV
danio Fhfla     TKEGQVMKGNRVKTKPSSHVFPKPIEVCMYREPSLHEIEEKQ-RSRKSSGTPMTNNGKV
danio Fhflb2    NKEGIIMKGNRVKTKPCSHVFPKPIEVCMYREPSLHDIDEKQ-RSRKNSGTPMTSTRKE
human FHF1B     NKEGQIMKGNRVKTKPSSHVFPKPIEVCMYREPSLHEIGEKQGRSRKSSGTPMTNNGKV
danio Fhflb1    NKEGIIMKGNRVKTKPCSHVFPKPIEVCMYREPSLHDIDEKQ-RSRKNSGTPMTSTRKE
.*. :*****.*****:*****:*****:* *** ***,*****. *

human FHF1A      VNQDST-----
danio Fhfla     VNQDST-----
danio Fhflb2    LNLGWGEGLVNNSAL
human FHF1B     VNQDST-----
danio Fhflb1    LNQDSTDHEGS----
:*

```

Percent Identity Matrix - created by Clustal2.1

1: human FHF1A	100.00	90.87	81.82	97.79	82.07
2: danio Fhfla	90.87	100.00	81.33	88.33	81.52
3: danio Fhflb2	81.82	81.33	100.00	81.67	91.01
4: human FHF1B	97.79	88.33	81.67	100.00	84.44
5: danio Fhflb1	82.07	81.52	91.01	84.44	100.00

7. Acknowledgements

G.M. Buyse and H. Van Esch are Senior Clinical Investigators of the Research Foundation-Flanders (FWO Vlaanderen, Belgium). The authors thank Patrik Verstreken (VIB, KU Leuven) for providing access to the electrophysiology equipment and Jan Maes (LMB, KU Leuven) for help with zebrafish cytoplasmic microinjections.

CHAPTER IV

This chapter has been published in the following paper:

“mTOR-related neuropathology in mutant *tsc2* zebrafish:
Phenotypic, transcriptomic and pharmacological analysis”

1. Abstract

Tuberous sclerosis complex (TSC) is a rare, genetic disease caused by loss-of-function mutations in either *TSC1* or *TSC2*. Patients with TSC are neurologically characterized by the presence of abnormal brain structure, intractable epilepsy and TSC-associated neuropsychiatric disorders. Given the lack of effective long-term treatments for TSC, there is a need to gain greater insight into TSC-related pathophysiology and to identify and develop new treatments.

In this work, we show that homozygous *tsc2*^{-/-} mutant zebrafish larvae, but not *tsc2*^{+/-} and WT larvae, display enlarged brains, reduced locomotor behavior and epileptiform discharges at 7dpf. In addition, we pharmacologically validated the TSC model by demonstrating the dramatic rescue effect of pericardially injected rapamycin, a well-known mTOR inhibitor, on selected behavioral read-outs and at the molecular level.

By means of transcriptome profiling we also acquired more insight into the neuropathology of TSC, and as a result were able to highlight possible new treatment targets. The gene expression profiles of WT and *tsc2*^{+/-} larvae revealed 117 differentially expressed genes (DEGs), while between WT and *tsc2*^{-/-} larvae and *tsc2*^{+/-} and *tsc2*^{-/-} larvae there were 1,414 and 1,079 DEGs, respectively. Pathway enrichment analysis from the WT and *tsc2*^{-/-} DEGs, identified 14 enriched pathways from the up-regulated genes and 6 enriched pathways from the down-regulated genes. Moreover, genes related to inflammation and immune response were up-regulated in the heads of *tsc2*^{-/-} larvae, in line with the findings in human brain tissue where inflammatory and immune responses appear to be major hallmarks of TSC.

Taken together, our phenotypic, transcriptomic and pharmacological analysis identified the *tsc2*^{-/-} zebrafish as a preclinical model that mirrors well aspects of the human condition and delineated relevant TSC-related biological pathways. The model may be of value for future TSC-related drug discovery and development programs.

2. Introduction

Tuberous sclerosis complex (TSC), also called Bourneville disease/syndrome, is a rare, genetic disease caused by loss-of-function mutations in either *TSC1* or *TSC2*. These genes are classified as tumor suppressor genes that encode hamartin and tuberin, respectively (30, 31). The latter proteins physically associate together with a third subunit TBC1D7 to form the TSC1-TSC2-TBC1D7 complex (31). This complex negatively regulates the mTOR pathway since the GTPase activating protein (GAP) activity of tuberin inactivates Ras homolog enriched in brain (Rheb) kinase, an activator of mTOR (31). Upon activation, mTOR phosphorylates multiple downstream mediators, of which 40S ribosomal protein S6 kinase (p70S6K) and eIF4E-binding protein 1 (4E-BP) are among the best characterized (152, 153).

A prominent characteristic of TSC is the activation of the mTOR pathway followed by the formation of hamartomatous lesions in multiple organs resulting in dermatological, renal, cardiac, ophthalmic and pulmonary manifestations (30, 31, 154-156). Besides these non-neurological clinical features, the central nervous system (CNS) of most patients is affected due to the presence of focal malformations of cortical development (termed tubers), subependymal nodules, giant cell astrocytomas and white matter pathology (156). As a result TSC patients commonly present with neurological disorders such as epilepsy and TSC-associated neuropsychiatric disorders (TAND) including autism and intellectual disability (30, 31, 154-156).

The mechanism underlying tuber development in TSC remains controversial; accordingly, loss of heterozygosity (LOH) and second hit mutations in *TSC1* and *TSC2* in humans are very rare in TSC cortical tubers (157). However, preclinical data support the role of the TORC1 signaling in epilepsy development, even in the absence of major brain pathology (158). Moreover, it has been shown that mTORC1 signaling plays a direct role in epilepsy development via induction of functional and microstructural changes eventually leading to network alterations (158-161). Epilepsy is the most common neurological manifestation, present in up to 85% of TSC patients (155). The first-line treatment for seizures in TSC patients consists of anti-epileptic drugs, although two thirds of patients remain unresponsive to therapy (155).

Given the lack of effective long-term treatments for TSC, there is a need to gain greater insight into TSC-related pathophysiology. Small animal models like zebrafish can help to speed up our understanding of the human disease like TSC and to identify and develop new treatments. Zebrafish are rapidly emerging as a promising small vertebrate animal model for use in biomedical research (162). Besides their small size, easy maintenance, high fecundity, and *ex utero* development, they can be easily modified genetically and implemented as mutant or transgenic fish in medium- to high throughput platforms to interrogate compound activity (57, 162-165). Moreover, zebrafish show a relatively high

degree of physiological and genetic similarity to humans (162), for instance genes associated with human disease have a zebrafish orthologue up to 82% (68). Developing larval zebrafish brain consists of numerous structures and cell types similar to those found in mammals e.g. the telencephalic organization, neuronal cell subtypes, and major anatomical structures such as cortex and hippocampus (73, 166, 167). This emphasizes the relevance of zebrafish as a model for neurological diseases.

Here we show that *tsc2*^{-/-} homozygous larvae display neurobehavioral alterations and epileptiform discharges at 7 days post fertilization (dpf). By means of transcriptome profiling we also acquired more insight into the neuropathology of TSC, and as a result were able to highlight possible new treatment targets. In addition, we pharmacologically validated the TSC model by demonstrating the dramatic rescue effect of pericardially injected rapamycin using genotyping-free assays that possibly can be deployed in future TSC-relevant drug screens.

3. Methods

3.1 Zebrafish strains

Zebrafish embryos, heterozygous for the *tsc2*^{vu242} mutation backcrossed with Tupfel longfin wild type fish, were a generous gift of Malgorzata Wiweger, head of the Zebrafish Core Facility of the International Institute of Molecular and Cell Biology (Warsaw, Poland). This zebrafish strain has been generated and characterized previously by the group of K. Ess (118). For experiments, *tsc2*^{vu242/vu242} (hereafter called *tsc2*^{-/-}), *tsc2*^{vu242/+} (hereafter called *tsc2*^{+/-}) and *tsc2*^{+/+} (hereafter called WT) were used.

3.2 Zebrafish maintenance and breeding

Adult zebrafish were maintained at 28.5°C in UV-sterilized water on a 14h light/10h dark cycle under standard aquaculture conditions. Fertilized eggs were collected via natural spawning. Embryos and larvae (*tsc2*^{+/+}, *tsc2*^{+/-} and *tsc2*^{-/-}) were kept in embryo medium, containing 1.5mM HEPES, pH 7.6, 17.4mM NaCl, 0.21mM KCl, 0.12mM MgSO₄ and 0.18mM Ca(NO₃)₂ in an incubator on a 14h light/10h dark cycle at 28.5°C. For all experiments described, larvae at 0-10 dpf were used. All zebrafish experiments were approved by the Ethics Committee of the University of Leuven (Ethische Commissie van de KU Leuven, approval number 061/2013) and by the Belgian Federal Department of Public Health, Food Safety and Environment (Federale Overheidsdienst Volksgezondheid, Veiligheid van de Voedselketen en Leefmilieu, approval number LA1210199).

3.3 Genotyping

Zebrafish larvae were lysed at 55°C for 3h followed by 95°C for 10 min using a lysis buffer containing 10 mM Tris-EDTA pH8, 2 mM EDTA 0.5 M pH8, 0.2% Triton-X-100 and 200 µg/ml Proteinase K in MilliQ water. The larval lysates served as template for the subsequent PCR in which a 500 bp fragment was amplified using *Pfu* polymerase (Thermo Scientific) and the following primers: GTAACACAGAATCAGTGAATCGGA (forward primer) and CACACACAGAAAACACTTGAAGC (reverse primer). The PCR products were digested with the *Hpy*CH4IV restriction enzyme (New England Biolabs) and afterwards visualized on a 2% agarose gel containing 0.5 µg/ml ethidium bromide.

3.4 Morphological phenotyping

WT, *tsc2*^{+/−} and *tsc2*^{−/−} larvae from 3 dpf until 10 dpf were screened for obvious morphological defects including gross deformation, oedema, apoptosis, lack of swim bladder, abnormalities of head, eye, tail and fin by visual assessment using a stereo microscope. Moreover, touch response behavior was assessed and scored positive when the larva displayed a rapid escape response upon tactile stimulation of the tail.

3.5 Survival assay

Larvae were cultured in 200 µl Danieau's medium in a 96 well plate and followed from 0 dpf until 10 dpf.

3.6 Head and body measurements

Larvae were positioned laterally in 3% methylcellulose on a microscope depression slide. Images were taken using a Leica MZ 10F fluorescence microscope with a Leica DFC310 FX digital color camera and Leica Application Suite V3.6 software. The head area and brain area were measured using the ImageJ software and normalized against the body length. To ensure a reproducible surface selection, the following reference points were used: otic vesicle and jaw (head size) or otic vesicle and upper lining of the eye (brain size).

3.7 Immunohistochemistry

7dpf zebrafish heads were dissected and fixed in 4% PFA/PBS, then transferred to a 30% sucrose/PBS solution and subsequently embedded in optimum cutting temperature (OCT) compound (AGR1180, Scigen) and stored at -80°C. Cross sections (10µm) of the zebrafish heads, obtained using a Bright cryostat (OTF5000, Bright Instrument Co Ltd) and collected onto Superfrost Plus microscope slides (10149870, Thermo Fischer Scientific), were first blocked for 2 hours followed by overnight incubation with a primary antibody against the phospho-S6 Ribosomal protein (Ser235/236) (#2211, Cell Signaling

Technology; 1:500), at 4°C. Next, following several rinses slides were incubated with goat anti-rabbit Alexa Fluor-647 (A-21245, Invitrogen; 1:1000) and counter-stained with DAPI (D1306, Thermo Fisher Scientific; 1:10000). After rinsing, slides were left to dry and mounted using DPX Mountant (44581, Sigma). Non-consecutive sections were imaged using a Zeiss AxioImager microscope, and pictures taken using the AxioVision software and a 20X objective. Exposure time was determined based on the background present in a slide incubated only with the secondary antibody, and kept constant during image acquisition. Images were prepared using Fiji ImageJ and mounted with Adobe Photoshop CS6.

3.8 Photomotor response

Protocol was adapted from Copmans and colleagues (168) and based on a study of Kokel *et al* (169). In brief, the photomotor response of zebrafish embryos was investigated by automated behavioral tracking (Zebrabox, Viewpoint) at 32 hpf. Embryos were individually placed in a 96-well plate in embryo medium at approximately 31 hpf (prim-15 stage), followed by a dark incubation of 50 minutes prior to tracking, including 20 minutes of habituation in the Zebrabox chamber. Total motion was recorded for 30 seconds at 15 frames per second (fps) in fully dark conditions with a high intensity light pulse (5.2 mW/cm², 38 000 lux) given at 10 and 20 seconds lasting one second. Raw data of total movement per well was used and is defined as the sum of all image pixel changes detected during the time interval of 0.067 seconds, corresponding to one frame. Total motion was plotted in function of time and average motion was plotted per time period. The PMR was divided in 8 time periods: the pre-stimulus phase and the latency phase were considered as one time period each (PRE; seconds 0-10, L; seconds 10-11), while the excitatory phase and the refractory phase were divided in three periods each (E1; seconds 11-14, E2; seconds 14-17, E3; seconds 17-20, R1; seconds 20-22, R2; seconds 22-25, R3; seconds 25-30). Data were pooled from five independent experiments with 4 to 19 replicate wells per genotype.

3.9 Locomotor behavior

To evaluate the locomotor behavior of 7 dpf WT, *tsc2*^{+/-} and *tsc2*^{-/-} larvae, an automated tracking device was used (ZebraboxTM, Viewpoint, Lyon, France). Zebrafish larvae were placed in a 24-well plate containing 400 µl embryo medium per well, followed by an incubation period in the Zebrabox consisting of 10 min light (0.264mW/cm², 1983 lux) and 10 min dark respectively. Subsequently, the total locomotor activity was quantified during a 5 min light and 10 min dark phase using the ZebralabTM software (Viewpoint, Lyon, France). The total movement was expressed in “actinteg” units, which are defined as the sum of all image pixel changes detected during the time of the tracking experiment. One experiment consisted of the subsequent tracking of three 24-well plates.

3.10 Local field potential (LFP) recordings

Local field potential recordings were performed at room temperature on larval optic tecta of 7 dpf WT, *tsc2*^{+/−} and *tsc2*^{−/−} larvae. Larvae were immobilized in 2% low melting point agarose (Invitrogen). A glass pipet (the recording electrode), filled with artificial cerebrospinal fluid (124mM NaCl, 2mM KCl, 2mM MgSO₄, 2mM CaCl₂, 1.25mM KH₂PO₄, 26mM NaHCO₃ and 10mM glucose), was positioned in the optic tectum using a stereomicroscope. 10-minute recordings were performed in current clamp mode, low-pass filtered at 1kHz, high-pass filtered at 0.15Hz, digital gain 100 and sampling rate of 10kHz (EPC 10 USB patch clamp amplifier, HEKA Elektronik Dr. Schulze GmbH, Germany; Kemo VBF 8 dual variable filter, Kemo Ltd., United Kingdom). Both the LFP recordings and the analysis were performed in a blinded manner, since genotyping occurred afterwards. For the analysis of the recordings, Clampfit 10.2 software (Molecular Devices Corporation, USA) was used.

3.11 Zebrafish RNA extraction

10 heads were pooled in quadruplicate for each condition. RNA was extracted with Trizol at 4°C, followed by the phenol-chlorophorm extraction and the isopropanol precipitation. After ethanol washes, the RNA pellet was air-dried and dissolved in nuclease-free water (Fermentas).

3.12 RNA-sequencing of zebrafish samples

RNA concentration and purity were determined spectrophotometrically using the Nanodrop ND-1000 (Nanodrop Technologies) and RNA integrity was assessed using a Bioanalyser 2100 (Agilent). Per sample, an amount of 500 ng of total RNA was used as input. Using the Illumina TruSeq® Stranded mRNA Sample Prep Kit (protocol version "Rev.E - October 2013") poly-A containing mRNA molecules were purified from the total RNA input using poly-T oligo-attached magnetic beads. In a reverse transcription reaction using random primers, RNA was converted into first strand cDNA and subsequently converted into double-stranded cDNA in a second strand cDNA synthesis reaction using DNA Polymerase I and RNase H. The cDNA fragments were extended with a single 'A' base to the 3' ends of the blunt-ended cDNA fragments after which multiple indexing adapters were ligated introducing different barcodes for each sample. Finally, enrichment PCR was carried out to enrich those DNA fragments that have adapter molecules on both ends and to amplify the amount of DNA in the library. Sequence-libraries of each sample were equimolarly pooled and sequenced on a NextSeq500 v2 High75 flow-cell.

3.13 Bioinformatics analysis

Read quality was assessed using FastQC v0.11.2 software produced by the Babraham Institute (Babraham, Cambridgeshire, UK). Trimmomatic v0.36 was used to assess the quality of each read and

filter reads of low quality (170). Low quality leading and trailing bases were removed from each read. If any of the reads dropped below 50 nts in length they were excluded.

Reads were aligned to the zebrafish reference genome, GRCz10 using TopHat2 v2.0.13 using the default settings (171). The aligned reads were then passed to Cufflinks v2.2.1 (172). Cufflinks assembled the RNA-Seq reads into individual transcripts, along with estimating abundance of each transcript. Expression levels were calculated as fragments per kilobase of exon per million fragments mapped (FPKM). The Cufflinks transcript assembly was guided using the zebrafish reference annotation (GRCz10 v84) downloaded from Ensembl (www.ensembl.org). The transcript assemblies from each replicate were passed to Cuffmerge, and amalgamated into a single unified transcript catalog (172). The merged transcript file along with the original alignment files produced were fed to Cuffdiff for differential expression testing (172). Library sizes were first normalised using the quartile method. The false discovery rate was controlled for using a Benjamini-Hochberg correction, gene expression changes with an adjusted p -value <0.05 and an absolute fold-change >2 were considered statistically significant. A gene was considered expressed if it had an FPKM >1 in at least one condition.

3.14 Protein-coding potential of novel genes

The protein-coding potential of all novel genes was assessed using the coding potential calculator (CPC) (173). The transcript sequences were extracted from the merged .gtf files as fasta files using the cufflinks gffread utility, these sequences were then passed to the CPC. CPC assesses protein-coding potential of a transcript based on six biological meaningful sequence features. Based on these features a protein-coding potential score is assigned to each transcript, and it is classified as non-coding, non-coding (weak), coding (weak) or coding.

3.15 Gene ontology and pathway enrichment analysis

The Database for Annotation, Visualization and Integrated Discovery (DAVID) version 6.8 (<http://david-d.ncifcrf.gov>) was used to test DEGs for gene ontology and pathway enrichment (117). As DAVID can only handle annotated genes, the DEG lists were curated to remove all novel genes and indecisively annotated genes. The enriched GO term list produced by DAVID, was processed using the 'Enrichment Map' plugin for Cytoscape (<http://www.cytoscape.org/>) to produce a visual output of the text based GO term list (174).

3.16 RT-qPCR validation

One microgram of total RNA was reverse-transcribed into cDNA using oligo dT primers. PCR primers (Eurogentec, Belgium) were designed using the Universal ProbeLibrary of Roche (<https://www.roche-applied-science.com>) on the basis of the reported mRNA sequences in the National Center for

Biotechnology Information database (NCBI, Bethesda MD, USA). The list of primers and their sequences are included in Supplementary Table 1. For each PCR, a mastermix was prepared on ice, containing per sample: 1 μ l cDNA, 2.5 μ l of 2x SensiFAST™ SYBR Green Reaction Mix (Bioline Inc, Taunton, MA, USA) and 0.4 μ M of both reverse and forward primers. The PCRs were run on a Roche Lightcycler 480 thermocycler (Roche Applied Science, Basel, Switzerland). Quantification of data was performed using the computer program LinRegPCR in which linear regression on the Log (fluorescence) per cycle number data is applied to determine the amplification efficiency per sample (175, 176) and to determine the starting concentration (N_0) of the product. This N_0 value for each specific product was divided by the geometric mean of the N_0 values of reference genes, elongation factor 1 alpha (*ef1a*), β actin 1 and β actin 2 (*bactin1*, *bactin2*) and this ratio was compared between WT, *tsc2*^{+/-} and *tsc2*^{-/-} larvae.

3.17 Prediction of pharmacological targets for TSC

The human orthologs of the DEGs from the WT and *tsc2*^{-/-} transcriptome analysis were identified using BioMart (177). All duplicate genes were removed then fed into the ‘Drug Gene Interaction Database’ (DGIdb) (178). DGIdb is a web resource that consolidates available data sources describing drug-gene interactions and gene druggability, it outputs all genes in which some level of evidence exists for a drug-gene interaction.

3.18 Pharmacological validation

Larvae were micro-injected pericardially (1 nl) at 3 dpf with vehicle, 0.3 mg/kg rapamycin and 1 mg/kg rapamycin. Rapamycin was dissolved in vehicle (50% DMSO/50% water containing 5% rhodamine B dextran). Larvae were selected based on their uniformly spread fluorescence and arrayed into 24 well plates (vehicle, n=38; 0.3 mg/kg rapamycin, n=44; 1 mg/kg rapamycin, n=59). The survival analysis and locomotor behavior were carried out as described before.

3.19 Western blot

SDS-PAGE and immunoblotting were performed on heads of 7dpf vehicle or rapamycin (1mg/kg) micro-injected larvae (injected at 3dpf). Therefore, in each condition 10 heads were homogenized in RIPA buffer supplemented with protease inhibitors. Following the BCA assay, equal amounts (25 μ g) of proteins were separated by SDS-PAGE (NuPage System, Invitrogen) using a 4-12% Bis-Tris gel (Novex, Life Technologies) in MOPS running buffer (Novex, Life Technologies). After wet transfer (Mini Trans-Blot Cell, Bio-Rad) of the proteins to a nitrocellulose membrane, the membrane was blocked for 1h at RT in Odyssey blocking buffer (Li-Cor) and subsequently incubated with primary antibodies against pS6 (1:1000 dilution, Cell Signaling, 2211S), pmTOR (1:1000 dilution, Cell Signaling, 2971S) and LC3B (1:3000 dilution, Abcam, ab51520) overnight at 4°C and Dylight

secondary goat antibody to rabbit IgG (1:10000 dilution, ThermoScientific, 35571) for 1h at room temperature. A rabbit antibody against GAPDH (1:1000 dilution, Sigma-Aldrich, SAB2701825) was used as loading control. Proteins were visualized using the Odyssey 2.1 imaging system (Li-Cor). Semi-quantification was done using Image Studio Lite Ver 5.2.

4. Results

4.1 *tsc2* homozygous larvae survive until 9 days post fertilization and display enlarged brains

The zebrafish strain used in this study is identical to the one used before by the group of K. Ess, who generated and characterized this mutant line (118). Upon receipt of the heterozygous *tsc2*^{+/-} mutant zebrafish, we confirmed the phenotype as observed by Kim and colleagues (118). For instance, it was shown that by 7 dpf the homozygous larvae completely deflated their swim bladders and that they died by 11 dpf. Here, we provide a more quantitative analysis of the mutant phenotype. A visual inspection of the wild type (WT), heterozygous (*tsc2*^{+/-}) and homozygous (*tsc2*^{-/-}) larvae was performed by following their development from 3 dpf until 10 dpf. No obvious differences in appearance such as gross deformation, oedema or necrosis were detected when the different genotypes were compared (data shown at 7 dpf, Fig 1, Panel A). Moreover, no significant differences in touch response were observed (data shown at 7 dpf, Fig 1, Panel B). Swim bladder development, however, was impaired in *tsc2*^{-/-} larvae. At 7 dpf, a significantly lower percentage of *tsc2*^{-/-} larvae inflated their swim bladders when compared to WT and *tsc2*^{+/-} larvae ($p \leq 0.001$; *tsc2*^{-/-} 10%, n=20; WT 65%, n=78; *tsc2*^{+/-} 55%, n=102) (data shown at 7 dpf, Fig 1, Panel B). To investigate the viability of larvae, the survival rate curves of WT, *tsc2*^{+/-} and *tsc2*^{-/-} larvae were compared. The curve of the *tsc2*^{-/-} larvae significantly differed from those of WT and *tsc2*^{+/-} larvae ($p < 0.0001$, Fig 1, Panel C). At 10 dpf, a significantly higher percentage of the *tsc2*^{-/-} larvae were dead compared to the WT and *tsc2*^{+/-} larvae (*tsc2*^{-/-} 100%, n=28; WT 7%, n=57; *tsc2*^{+/-} 16%, n=89). We also confirmed hyperactivation of mTOR in the brains of 7 dpf homozygous larvae. Phosphorylated ribosomal protein S6 (pS6) is a commonly used marker for mTOR hyperactivation. In this study, immunohistochemical analysis was used to examine the presence of pS6 in the brains of 7dpf WT, *tsc2*^{+/-} and *tsc2*^{-/-} larvae. We confirmed that the brains of *tsc2*^{-/-} larvae showed increased pS6 staining when compared to WT and *tsc2*^{+/-} larvae who exhibited similar levels of pS6 (Fig 2), as found before by the group of K. Ess (118).

Additionally, to examine whether *tsc2*^{-/-} larvae display a macrocephaly and/or megalencephaly phenotype, both the head and brain area of 7 dpf larvae were measured and normalized to the body length. Body lengths did not differ significantly between the different groups. Although the head/body length ratio was not distinct between the different groups (data not shown), the brain/body length ratio

differed significantly showing that *tsc2*^{-/-} larvae had significantly larger brains when compared to WT and *tsc2*^{+/-} siblings (5.5% and 4.2% increase, respectively, Fig 1, Panel D).

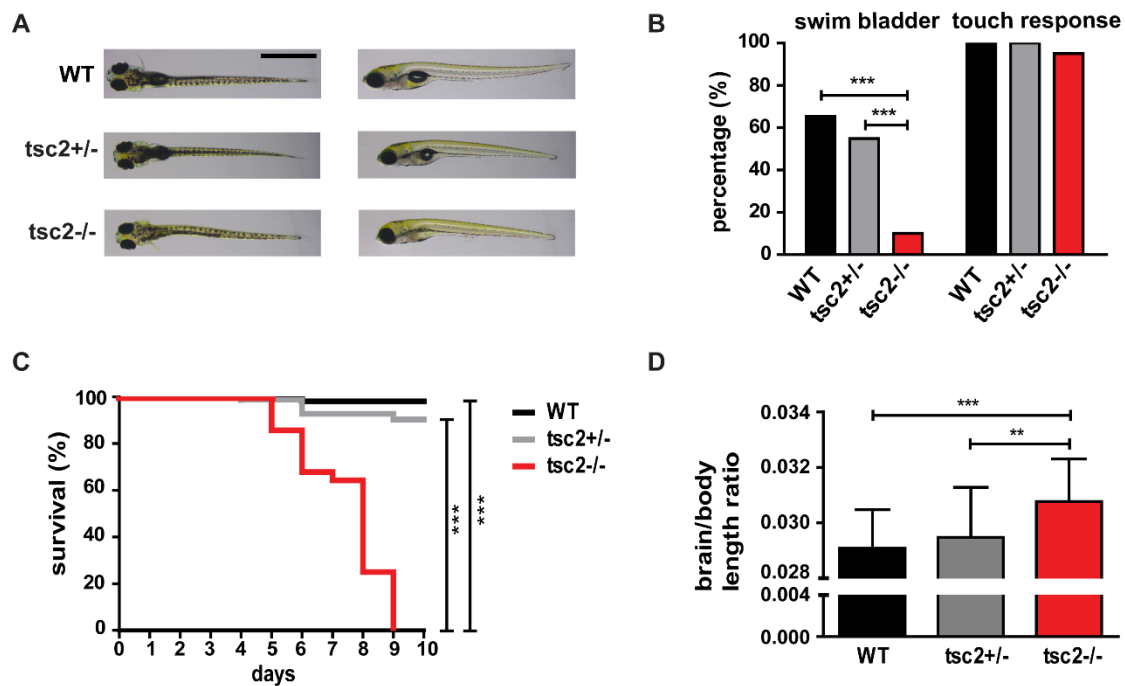


Figure 1: *tsc2* homozygous larvae survive until 9 dpf and display enlarged brains. (A) Gross morphology of 7 dpf WT, *tsc2*^{+/-} and *tsc2*^{-/-} larvae (scale bar, 1 mm). (B) Percentage of 7 dpf WT (n = 78), *tsc2*^{+/-} (n = 102) and *tsc2*^{-/-} (n = 20) larvae with developed swim bladder and touch response. (C) Survival rate curves of WT (n = 57), *tsc2*^{+/-} (n = 89) and *tsc2*^{-/-} (n = 28) larvae. (D) Brain/body length ratios of 7 dpf WT (n = 25), *tsc2*^{+/-} (n = 28) and *tsc2*^{-/-} (n = 46) larvae. Data are expressed as mean ± SEM. Statistical analyses: (B – C) Chi square test with Bonferroni correction for multiple testing, (D) one-way ANOVA (Graphpad Prism 5). ***p* ≤ 0.01; ****p* ≤ 0.001.

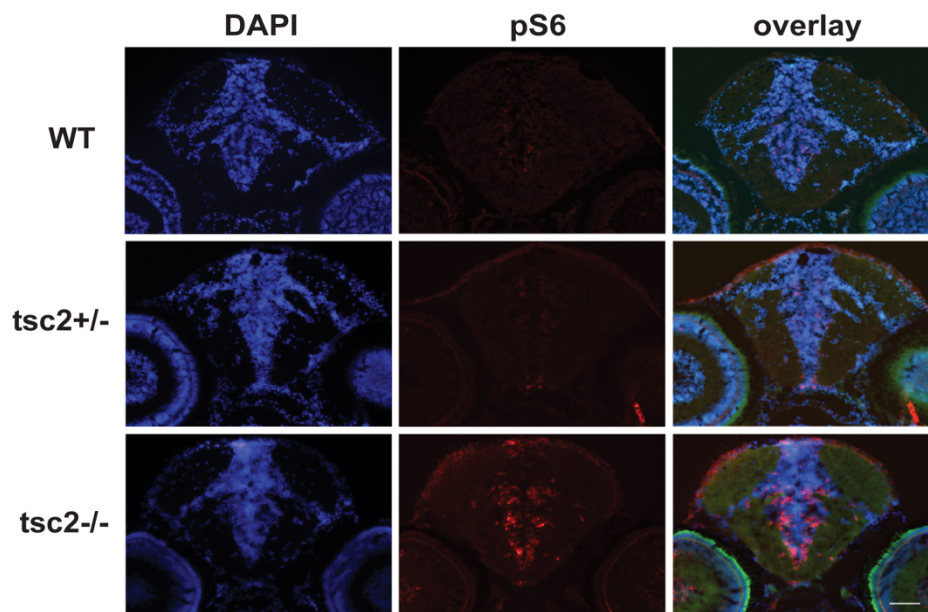


Figure 2: Brains of 7dpf *tsc2* homozygous larvae show hyperactivation of mTOR. Immunohistochemical analysis of pS6 presence in the brains of 7dpf WT, *tsc2*^{+/-} and *tsc2*^{-/-} larvae. Representative cross-sections of the optic tectum of WT (A-C), *tsc2*^{+/-} (D-F) and *tsc2*^{-/-} (G-I) stained for DAPI (blue) and pS6 (red). Composite pictures (C, F, I) include tissue autofluorescence (green). Data are representative of at least three different larvae per group. Scale bar, 50µm.

4.2 7 dpf homozygous larvae demonstrate neurobehavioral alterations

To investigate the impact of the *tsc2* mutation on behavior, the larval locomotor activity of WT, *tsc2*^{+/-} and *tsc2*^{-/-} larvae was evaluated at 32 hours post fertilization (hpf) and 7 dpf. The photomotor responses (PMR) of WT, *tsc2*^{+/-} and *tsc2*^{-/-} embryos were similar in all time periods (Fig 3, Panel A and B). Also at 7 dpf no significant differences in locomotor behavior were obtained during the light phase. However, during the dark phases we observed significantly reduced locomotor behavior in *tsc2*^{-/-} larvae when compared to WT and *tsc2*^{+/-} siblings ($p < 0.001$, Dark1 and $p < 0.05$, Dark2, Fig 3, Panel C and D).

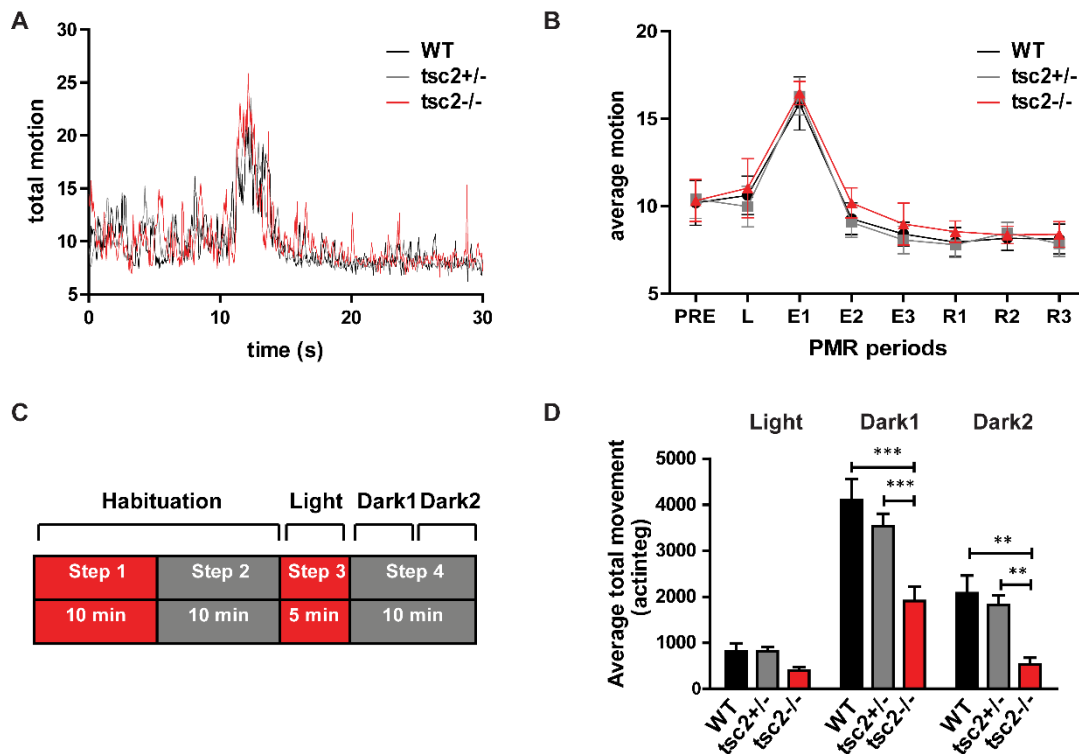


Figure 3: 7dpf *tsc2* homozygous larvae demonstrate neurobehavioral alterations. (A-B) Photomotor response of 32 hpf WT (n=36), *tsc2*^{+/-} (n=81) and *tsc2*^{-/-} (n=32) embryos. (A) Total motion. (B) Average motion during different PMR periods. Data are expressed as mean \pm SEM. (C-D) Locomotor behavior of 7dpf WT (n=63), *tsc2*^{+/-} (n=93) and *tsc2*^{-/-} (n=43). (C) Schematic overview of the protocol used for the evaluation of locomotor behavior at 7 dpf. Red color indicates the light phases. Grey color indicates the dark phases. (D) Average total movement during the behavioral tracking. Data are expressed as mean \pm SEM. Statistical analyses: (B-D): two-way ANOVA (Graphpad Prism 5). * $p \leq 0.05$; *** $p \leq 0.001$.

4.3 *tsc2* homozygous larvae display abnormal brain activity

To investigate the impact of the *tsc2* mutation on brain activity, local field potential recordings were performed on larval optic tecta of WT, *tsc2*^{+/-} and *tsc2*^{-/-} larvae at 7 dpf, as represented in Fig 4 (Panel A). A representative fragment of a 10-minute recording is presented, together with a magnification of the selected polyspiking discharge. The percentage of larvae with epileptiform activity is shown in Panel B. A larva was considered to have epileptiform activity when it met the following criteria: (i) duration of the polyspike exceeding 50 ms and (ii) at least three or more polyspiking discharges per 10-minute

recording. The incidence of recurrent epileptiform discharges was significantly greater in the *tsc2*^{-/-} larvae when compared to *tsc2*^{+/-} and WT larvae (*tsc2*^{-/-} 54%, n=26; *tsc2*^{+/-} 0%, n=12 and WT 0%, n=18). Epileptiform discharges consisted of polyspiking events that exceeded the amplitude of the baseline by at least threefold. Significant differences were observed between the groups tested for the mean frequency (Fig 4, Panel C), mean cumulative duration of seizures per larva (Fig 4, Panel D) and the mean duration of seizures (Fig 4, Panel E).

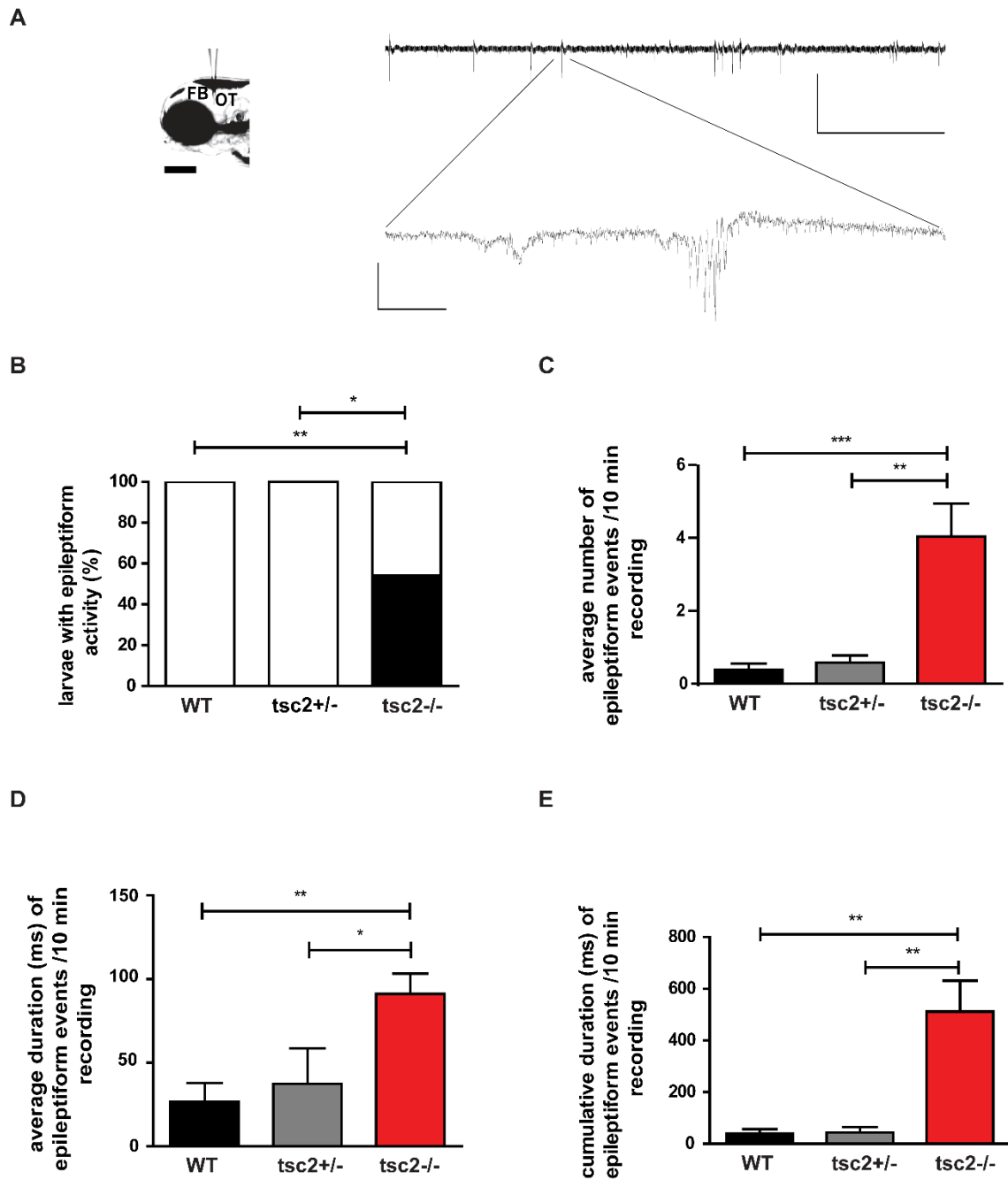


Figure 4: caption on the next page

Figure 4: *tsc2* homozygous larvae display abnormal brain activity. (A) Positioning of the glass pipet into the optic tectum (OT) of a 7 dpf larva (scale bar, 125 μ m). (B) Representative fragment of a 10-minute recording (scale bar; 1.5mV – 1 min) of a homozygous larva with enlargement of a polyspiking event (scale bar; 0.5mV – 0.2s). (C) The percentage of 7 dpf WT (n=18), *tsc2*^{+/-} (n=12) and *tsc2*^{-/-} (n=26) larvae displaying epileptiform activity. (D) The average number of epileptiform events per 10-minute recording. (E) The average duration of epileptiform events per 10-minute recording. (F) The cumulative duration of epileptiform events per 10-minute recording. (D-F) Data are expressed as mean \pm SEM. Statistical analyses: (C) Fisher's exact test with Bonferroni correction for multiple testing,

4.4 Characterization of the zebrafish transcriptome

RNA-Sequencing (RNA-Seq) was performed on the heads of WT, *tsc2*^{+/-} and *tsc2*^{-/-} zebrafish larvae at 7 dpf. On average ~24 million single-end reads were produced per sample of which over 21 million passed quality control and filtering. For each sample approximately 88% of the filtered reads aligned to the zebrafish genome (GRCz10).

Overall, 20,781 genes were expressed in at least one of the three genotypes, 16,874 of these genes were protein-coding, 156 were long intergenic non-coding RNAs (lincRNAs), 313 were from a variety of other RNAs species and 3,438 were un-annotated genes (henceforth referred to as novel) (Fig 5, Panel A). Of the novel genes ~14% were classed as having strong protein-coding potential, the remaining 86% showed none to weak protein-coding potential, and thus could possibly fall into varying classes of long non-coding RNAs. Further, the novel genes had a greater level of genotype specific expression than the protein-coding genes (Fig 5, Panel B). While 91% of all protein-coding genes were expressed in all three genotypes, only 68% of the novel genes were expressed in all three genotypes. Conversely, much higher percentages of the novel genes were expressed in one or two of the genotypes than the protein-coding genes. The number of genotypes that each gene was expressed in was dependent on whether the gene was protein-coding or novel (Chi-squared *p*-value < 0.00001).

4.4.1 Differentially expressed genes

Unsupervised hierarchical clustering (Manhattan distance) of samples based on the gene expression profiles revealed two divergent groups (S1 Fig). The biological replicates from the *tsc2*^{+/-} and WT samples clustered together forming a distinct group from the *tsc2*^{-/-} samples. This grouping was further reflected in the testing for differentially expressed genes (DEGs). Analysis of the gene expression profiles of WT and *tsc2*^{+/-} revealed 117 DEGs, while between WT and *tsc2*^{-/-} and *tsc2*^{+/-} and *tsc2*^{-/-} there were 1,414 and 1,079 DEGs respectively (Fig 5, Panel C and S2 and S3 Figs). The 1,414 DEGs between WT and *tsc2*^{-/-} included 735 genes (179 novel genes) that were down-regulated in *tsc2*^{-/-} and 679 genes (66 novel genes) that were up-regulated in *tsc2*^{-/-}. The top 10 up- and down-regulated protein-coding genes sorted by fold-change are listed in table 1 (S1 Table for complete lists).

Next, the expression levels of 84 genes related to the mTOR pathway were assessed in the transcriptome comparison between WT and *tsc2*^{-/-} larvae. These 84 genes were selected based on the probes present on the zebrafish mTOR-pathway Qiagen RT² profiler PCR array (for the full list of genes see S5 Table). Using the cutoff of absolute fold-change of 2, and a Benjamini-Hochberg (BH) corrected *p*-value < 0.05 the genes insulin receptor b (-2.2-fold), Ras-related GTP binding Ca (2.1-fold) and vascular endothelial growth factor Aa (2-fold) were differentially expressed. When the cut-offs were relaxed to all genes with a BH corrected *p*-value < 0.05, a further 15 genes were considered differentially expressed (S5 Table). Of the 18 mTOR genes that had perturbed expression 6 were down-regulated and 12 were up-regulated. Analysis of the expression of *tsc2* showed that there was no difference in the expression level of *tsc2* across any of the three genotypes (S4 Fig).

Table 1: The top 10 up- and down-regulated genes sorted by fold change are listed.

Top 10 up-regulated protein-coding genes					
Gene ID	Ensembl ID	Gene Name	Chromosome	Fold-Change	Adjusted <i>p</i> -value
si:ch211-125e6.5	ENSDARG00000069381	si:ch211-125e6.5	Chr9	Unique to <i>tsc2</i> ^{-/-}	0.001
mfsd9	ENSDARG00000074728	major facilitator superfamily domain containing 9	Chr9	4.74	0.001
isg15	ENSDARG00000086374	ISG15 ubiquitin-like modifier	Chr5	4.14	0.001
MDP1	ENSDARG00000088040	si:dkeyp-27c8.2	Chr23	4.05	0.001
slc1a4	ENSDARG00000000551	solute carrier family 1 member 4	Chr13	3.73	0.001
sesn2	ENSDARG00000070012	Sestrin 2	Chr19	3.70	0.001
si:ch73-236c18.2	ENSDARG00000103829	Si:ch73-236c18.2	Chr1	3.69	0.001
si:ch1073-140o9.2	ENSDARG00000101804	Si:ch1073-140o9.2	Chr17	3.59	0.001
tcn1	ENSDARG00000068088	Transcobalamin like	Chr5	3.55	0.001
CU633981.1	ENSDARG00000090361	Cu633981.1.	Chr2	3.52	0.001
Top 10 down-regulated protein-coding genes					
Gene ID	Ensembl ID	Gene Name	Chromosome	Fold-Change	Adjusted <i>p</i> -value
zgc:92137	ENSDARG00000009443	Zgc:92137	Chr17	-7.71	0.013
si:dkey-117n7.2	ENSDARG00000093135	Si:dkey-117n7.2	Chr4	-6.13	0.001
slc23a3	ENSDARG00000088891	Solute carrier family 23, member 3	Chr9	-5.37	0.001
ela2l	ENSDARG00000056765	Elastase 2 like	Chr8	-5.12	0.047
gria4b	ENSDARG00000059368	Glutamate receptor, ionotropic, AMPA 4b	Chr21	-4.57	0.001
CELA1 (1 to many)	ENSDARG00000017314	zgc:92041	Chr22	-4.51	0.001
prss59.1	ENSDARG00000079274	Protease, serine, 59, tandem duplicate 1	Chr16	-4.32	0.001
ctrl	ENSDARG00000068680	Chymotrypsin-like	Chr15	-4.19	0.001
ela2	ENSDARG00000056744	Elastase 2	Chr8	-4.18	0.001
si:dkey-182g1.10	ENSDARG00000099577	Si:dkey-182g1.10	Chr22	-3.95	0.001

4.4.2 RT-qPCR validation of RNA-Seq data

A set of seven genes, complement C1q B chain (*c1qb*), calcium channel voltage-dependent type alpha 1D subunit (*cacna1da*), a serpin peptidase inhibitor clade A (alpha-1 antitrypsin, antitrypsin) member 7 (*serpina7*), cathepsin S ortholog2 tandem duplicate 1 (*ctss2.1*), sodium channel voltage-gated type 1 like alpha b (*scn1lab*), ribosomal protein S6 kinase polypeptide 5 (*rps6ka5*) and glycyl-tRNA synthetase (*qars*), was selected for validation using RT-qPCR in a cohort of 11 samples (3 WT, 4 *tsc2^{+/-}* and 4 *tsc2^{-/-}*). The Kruskal-Wallis test revealed significant differences in the median expression levels of *ctss2.1*, *scn1lab*, *rps6ka5* and *qars* between the different groups analyzed. Using the Dunn's post-hoc test or the Mann-Whitney U test to analyze the differences between individual groups, *scn1lab* and *rps6ka5* were found to be significantly down-regulated in *tsc2^{-/-}* compared to the *tsc2^{+/-}* group. On the other hand, *ctss2.1* was significantly up-regulated in *tsc2^{-/-}* compared to WT while *qars* was up-regulated in *tsc2^{-/-}* compared to the *tsc2^{+/-}* group. On the whole, the expression pattern of all the genes selected for validation mirrored the results obtained by RNA sequencing (S5 Fig, S2 Table).

4.4.3 Enriched gene ontology terms and pathways

A gene ontology (GO) enrichment analysis revealed distinct GO terms enriched in the up- and down-regulated gene lists from the WT and *tsc2^{-/-}* transcriptome analysis (S3 Table). Amongst the up-regulated genes 16 GO terms were strongly enriched (adjusted p -value < 0.05) forming two major clusters (Fig 5, panel D). The first cluster contained terms related to ligase activity and aminoacylation, terms in the second cluster pertained to peptidase, hydrolase and lysosome activity. For the down-regulated genes there was one significant cluster with GO terms related to calcium channels and ions. The only common enriched GO terms shared by both the up- and down-regulated gene lists were peptidase and hydrolase activity. While there were more down-regulated genes than up-regulated genes, there were more significantly enriched GO terms amongst the up-regulated genes.

Pathway analysis identified 14 enriched pathways (p -value < 0.05) from the up-regulated genes (Fig 5, Panel E). Two interesting pathways amongst this list were lysosome and phagosome. Lysosome, which also appeared amongst the enriched GO terms, was the most enriched pathway. Further, ~5% of the significant up-regulated genes were involved in this pathway at various points. Amongst the down-regulated genes there were 6 enriched pathways (p -value < 0.05) (Fig 5, Panel E). Interesting terms from this list were the MAPK signaling pathway and the calcium-signaling pathway.

4.4.4 Genes related to inflammation and immune response differentially expressed in the zebrafish model

When the GO terms produced from the up-regulated DEGs from *tsc2*^{-/-} larvae were combined into “annotation clusters”, based on similarity of gene lists and functionality, an enriched annotation cluster that included the GO terms chemokine activity, inflammatory response, chemokine-mediated signaling pathway, neutrophil chemotaxis, immune response and G-protein coupled receptor signaling pathway was revealed (Fig 5, Panel F and S4 Table). This annotation cluster of inflammation and immune response related GO terms was made up of 15 distinct genes, with three genes encoding for various chemokine ligands represented in all six GO terms. This suggests that the inflammation and immune response are activated in the *tsc2*^{-/-} larvae.

4.4.5 Up-regulation of *ctss2.1* in the *tsc2* homozygous larvae

One particular gene that was strongly up-regulated in *tsc2*^{-/-} zebrafish was *ctss2.1*. From the RNA-Seq data *ctss2.1* was expressed at 6.19 and 7.43 fpkm in the WT and *tsc2*^{+/-} zebrafish respectively, in the *tsc2*^{-/-} zebrafish the expression levels increased to 28.11 fpkm. In both cases this increase in expression was statistically significant (adjusted *p*-value < 0.002). This result was confirmed with RT-qPCR, showing a statistically significant increase in *ctss2.1* in the *tsc2*^{-/-} relative to both the WT and *tsc2*^{+/-} zebrafish (S5 Fig). *Ctss2.1* was also identified as being involved in immune response in zebrafish (Fig 5, panel F) and in five of the 16 strongly enriched GO clusters from the up-regulated genes (adjusted *p*-value < 0.05), including lysosome, hydrolase and peptidase and both of the up-regulated pathways; lysosome and phagosome. The mammalian ortholog for *ctss2.1* is the gene cathespain S (*ctss*). *Ctss* is a lysosomal cysteine proteinase that may participate in the degradation of antigenic proteins to peptides for presentation on MHC class II molecules (179).

4.4.6 Prediction of pharmacological targets for TSC

To demonstrate the utility of the *tsc2*^{-/-} zebrafish in the identification of possible new treatment targets for TSC, the DEGs from the RNA-Seq comparison between WT and *tsc2*^{-/-} zebrafish were subjected to drug-gene interaction analysis. First, the zebrafish DEGs were converted to their human orthologs; of the 1,168 annotated DEGs expressed 1,052 distinct human orthologs were identified. Of these 1,052 human orthologs, 216 were associated with various numbers of drug-gene interactions (S5 Table). Interestingly, for *CTSS* the human ortholog for *ctss2.1* eight different drug-gene interactions were identified.

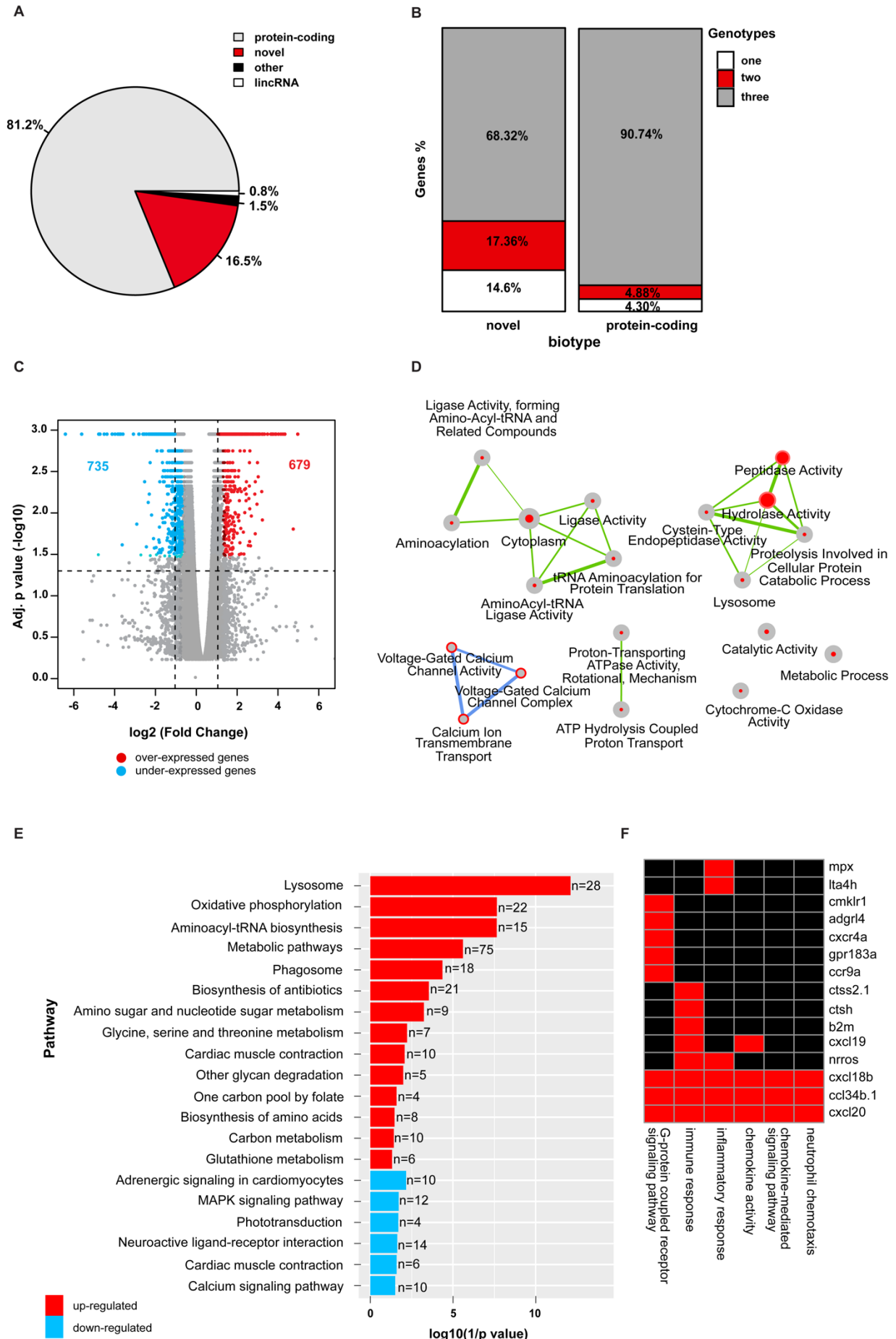


Figure 5: Transcriptional analysis of *tsc2* homozygous, *tsc2* heterozygous and WT zebrafish. (A) Biotypes of genes identified as expressed in at least one of the zebrafish genotypes. 81.2% of the expressed genes were protein-coding genes, 0.8% were lincRNAs, 1.5% belonged to other biotype categories, and 16.5% were previously unidentified genes and were classed as novel genes. (B) Percentages of novel and protein-coding genes that were expressed across genotypes. A disproportionately high percentage of novel genes appeared in only 1 (p -value < 0.001, Chi-squared test) and 2 (p -value < 0.001, Chi-squared test) of the genotypes, when compared to the protein-coding genes. (C) Volcano plot of differentially expressed genes between the wild-type and the *tsc2*^{-/-} zebrafish. 735 genes were down-regulated and 679 genes were up-regulated. Cut-offs of an absolute fold-change of 2, and a Benjamini-Hochberg corrected p -value < 0.05 were applied. (D) Gene Ontology (GO) enrichment map from up- and down-regulated genes when the wild-type were compared to the *tsc2*^{-/-}. Each node represents a different GO term, the red centre of node indicates enrichment in up-regulated genes, the red outside of the node indicates enrichment in down-regulated genes. The larger the node the greater the number of genes in the enriched GO term. Green connections indicate common genes shared between the nodes from the up-regulated list. Blue connections indicate common genes shared between the nodes from the down-regulated list. The thicker the connection the more genes in common. The more intense the red of the node the lower the p -value. (E) Enriched pathways from differentially expressed genes when the wild-type was compared to the *tsc2*^{-/-} zebrafish. Enriched pathways from the up-regulated genes are in red, enriched pathways from the down-regulated genes are in blue. The x-axis is the $\log_{10}(1/p\text{-value})$, n is equal to the number of genes that appear in each category. (F) Enriched annotation cluster of related GO terms based on gene list similarities. The differentially expressed genes are listed on the y-axis and the associated GO terms are on the x-axis. Red indicates that the gene was allocated to the GO term, black indicates that the gene was not. The majority of these genes and terms are related to inflammatory responses or immune system activation.

4.5 Pharmacological validation

In order to pharmacologically validate the model, we first investigated the effect of rapamycin, that was pericardially micro-injected (1 nl) at 3 dpf in a non-genotyped mixture of WT, *tsc2*^{+/-} and *tsc2*^{-/-} larvae (offspring of heterozygous adults, so theoretically present for 25%, 50% and 25%, respectively) on survival and locomotor behavior (see above). Rapamycin treatment significantly increased the survival of the larvae at 10 dpf (100% for 1mg/kg rapamycin (n=59), 93% for 0.3mg/kg rapamycin (n=44) as compared to 71% for VHC-treated (n=38), Fig6 Panel A). Furthermore, we observed a statistically significant rescue of the reduced locomotor behavior in Dark1 with the highest dose of rapamycin (p < 0.001, Dark1 and p < 0.05, Dark2; Fig6 Panel B). Next, we investigated the effect of pericardially micro-injected rapamycin (1mg/kg) on the levels of phosphorylated mTOR (pmTOR) and phosphorylated S6, both markers of catalytically active mTOR (180), and LC3B-II as a marker of cellular autophagy (181) (Fig6, Panel C). Rapamycin treatment significantly reduced the elevated pS6 protein levels in the heads of 7dpf *tsc2*^{-/-} larvae to a level comparable to those found in VHC-treated WT and *tsc2*^{+/-} larvae (Fig6, Panel D). Moreover, it also normalized the levels of pmTOR that was increased in case of 7dpf *tsc2*^{-/-} larvae (Fig6, Panel E). No statistically significant effect of rapamycin could be observed on the protein levels of the autophagy marker LC3B-II (Fig6, Panel F).

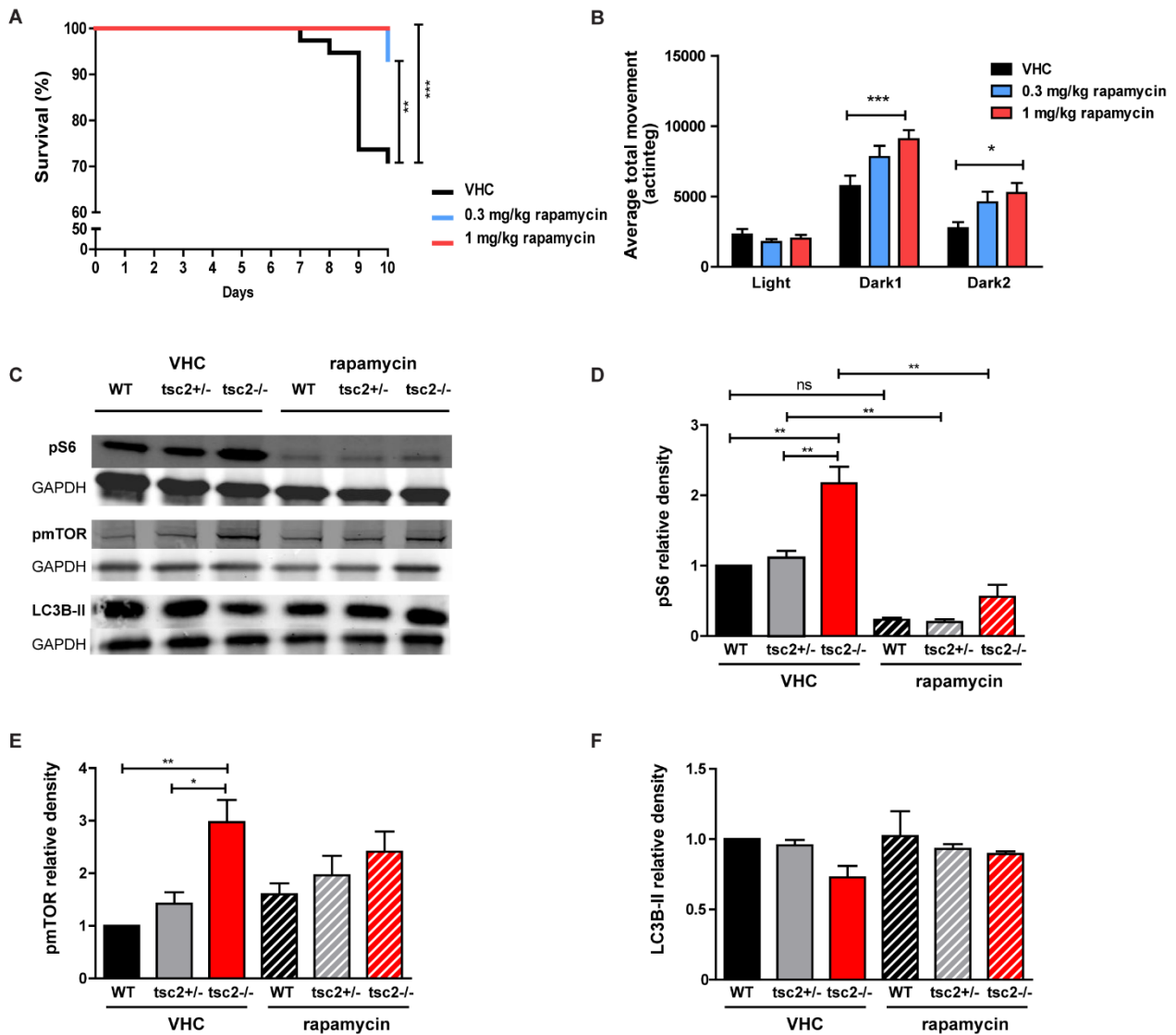


Figure 6: Pharmacological validation with rapamycin. (A) Survival rate curves of larvae (mixture of WT, *tsc2*^{+/-} and *tsc2*^{-/-}) pericardially injected with vehicle (n=38), 0.3 mg/kg rapamycin (n=44) and 1 mg/kg rapamycin (n=59) at 3 dpf. (B) Locomotor behavior of 7 dpf larvae (mixture of WT, *tsc2*^{+/-} and *tsc2*^{-/-}) pericardially injected with vehicle (n=38), 0.3 mg/kg rapamycin (n=44) and 1 mg/kg rapamycin (n=59) at 3 dpf. Data are expressed as mean \pm SEM (C) Representative blots of the western blot analyses of pS6, pmTOR and LC3B-II. (D-F) Semi-quantification of the relative densities of pS6 (D), pmTOR (E) and LC3B-II (F) expression normalized against the VHC-treated WT condition. The relative densities are expressed as mean \pm SEM (n=3). Statistical analysis: (A) Chi Square test, (B) two-way ANOVA, (D-F) one-way ANOVA (Graphpad Prism 5). * $p \leq 0,05$; ** $p \leq 0,01$; *** $p \leq 0,001$.

5. Discussion

In the present study, we performed a phenotypic, transcriptomic and pharmacological analysis of the *tsc2^{-/-}* zebrafish with the aim of elucidating the underlying mechanisms of TSC pathophysiology. Patients with TSC are characterized by the presence of abnormal brain structure, intractable epilepsy and TAND (182). Here we focus on the brain-related pathological aspects of the *tsc2^{-/-}* larvae and correlated the outcome with a transcriptome-based integrated pathway analysis. Behavioral readout tests were used based on the PMR, touch response and locomotor activity of the embryo's and larvae. As innate behavior depends on sensory input, neuronal connectivity of the hindbrain and spinal cord and multiple neurotransmitter pathways, these assays represent a straightforward way to test the correct development and function of the nervous system (183-185).

First, we confirmed the up-regulation of mTORC1 in the brain of *tsc2^{-/-}* larvae at 7 dpf. Further, we show that the *tsc2^{-/-}* larvae consistently display abnormal local field potentials (LFP) that are associated with a substantially reduced response of locomotor activity to a light-dark stimulus, as compared to the *tsc2^{+/-}* and WT larvae. Of interest, the former larvae also displayed a higher occurrence of non-inflated swim bladders. This situation, however did not affect the outcome of the locomotor assay as a lack of functional swim bladder results in subtle movements as a consequence of maintaining balance and not in seizing-like behavior or reduced locomotor activity (95). Moreover, all *tsc2^{-/-}* larvae showed a normal touch response at 7 dpf, which corroborates the idea that the underlying neural circuitry is intact (186). Of interest, when investigating the PMR response, a behavior that is used to determine early neuromodulatory effects, no differences were observed between the 32 hpf, *tsc2^{-/-}*, *tsc2^{+/-}* and WT embryos. This outcome likely demonstrates that at least the first two days post fertilization the *tsc2^{-/-}* larvae behave normally. Possibly, this is the consequence of the presence of maternal *tsc2* mRNA in the early developmental stages (118, 187). Furthermore, *tsc2^{-/-}* larvae also displayed a MEG phenotype at 7 dpf. MEG/HMEG (hemimegalencephaly) has been observed in patients with mutations in multiple PI3K-AKT-mTOR pathway components (188-190), but also in TSC patients (191-193). Previously MEG has been reported in mice models in which the *Tsc1* or *Tsc2* gene was deleted selectively in neural progenitors (194) or glial fibrillary acidic protein (GFAP)-positive cells (195, 196).

To gain more insight into the molecular basis underlying the major differences observed in the *tsc2^{-/-}* larvae, we further studied these differences at the transcriptome level. Previously, it has been demonstrated in human TSC patients that even in the absence of tissue pathology, gross transcriptome alterations are present (197). In the aforementioned study, up-regulation of genes related to immune and inflammatory response and down-regulation of genes involved in ion channels were seen. In the presented study, the *tsc2^{-/-}* larvae had large perturbation of the transcriptome when compared to the WT

or *tsc2*^{+/-} larvae. Many of the differentially expressed genes were involved in inflammation, immune response and calcium channels, demonstrating that the *tsc2*^{-/-} zebrafish models aspects of the human TSC condition (197-200).

Calcium signals are vital information carriers and regulators of various biochemical processes in virtually all cells (201). Nuclear calcium appears to be a master regulator of neuronal gene expression (202). Malfunctioning of calcium signaling toward and within the cell nucleus may have deleterious effects leading to cell death (202). In fact, dysfunction of nuclear calcium signaling leads to decreases in dendrite length and complexity, synapse loss, increased mitochondrial vulnerability, neurodegeneration, memory impairments, cognitive dysfunction and a decrease in reactive oxygen species defense (203). While not investigated specifically in TSC, there appears to exist a link between calcium signaling, astrocytes and neuronal excitability and thus epilepsy (204, 205). Here, there was a strong down-regulation of genes related to voltage-gated calcium channel activity, voltage-gated calcium channel complex and calcium ion transmembrane transport, suggesting dysfunction of calcium ion channels and calcium signaling. This could be directly related to the abnormal brain activity seen in the *tsc2*^{-/-} zebrafish larvae. Investigation of the role of calcium signaling in TSC warrants further investigation.

Importantly, there was a direct response (up-regulation) of numerous genes associated with inflammation, inflammatory molecules and immune responses in the *tsc2*^{-/-} zebrafish larvae. Similar responses have been documented throughout the literature in gene expression profiles of both rodent models of epilepsy and in human epilepsy tissue (206, 207). Further, inflammatory and immune responses appear to be one of the major hallmarks in human TSC patients (197). The role of the immune response in zebrafish TSC pathology is highlighted by the up-regulation of the *ctss2.1*. The mammalian ortholog for *ctss2.1* is the lysosomal cysteine proteinase *ctss*. *Ctss* is expressed throughout the rodent brain, particularly in microglia and at the subcellular level accumulates in granules, indicating a lysosomal localization (208). Up-regulation of *ctss2.1* may suggest the activation of microglia in the zebrafish brains, a process seen during epileptogenesis in a mouse model of TSC (209, 210). *Ctss* also appears to play a significant role as a regulator of the innate immune response, regulation of interleukin 1 beta (IL1B) release and inflammatory responses (208, 211). Further, increased expression of *ctss* has been implicated in Alzheimer's disease and Down-syndrome, where it appears to localize with tangle-bearing neurons, astrocytes and senile plaques (212). High expression of *ctss* has been identified in human and murine tumors, and selective depletion of *ctss* impairs angiogenesis and tumor cell proliferation (209, 210). *Ctss* has not been investigated in the pathogenesis of TSC, although studies from other disease contexts demonstrate that it would be relevant. Thus, this finding highlights the potential of using the zebrafish *tsc2*^{-/-} model to identify new genes for therapeutic targeting that are related to TSC pathology.

In this study, the *tsc2*^{+/-} zebrafish larvae were very similar to the WT larvae, both morphologically and at the transcriptome level. This suggests that inactivation of just one of the *tsc2* alleles is not sufficient to cause any significant pathogenesis. Instead, a biallelic inactivation appears to be a requirement for mTOR hyper-activation in zebrafish. Significantly, in mice it has been shown that a biallelic deletion of *tsc1* resulted in activation of the mTOR pathway (158). While loss of heterozygosity (LOH) and second hit mutations at either the *TSC1* or *TSC2* has been demonstrated in humans in both TSC subependymal giant cell astrocytomas and tubers (213-215), this model remains controversial and no consensus exists (157). The morphological and transcriptome changes seen in the *tsc2*^{-/-} zebrafish support the idea that at least in zebrafish inactivation of both *tsc2* alleles is a requirement for the hyper-activation of mTOR.

Finally, we were able to demonstrate that rapamycin, a very well-known mTOR inhibitor that together with its analogue everolimus has been used in humans to treat SEGAs (40), renal angiomyolipomas (41), pulmonary lymphangiomyomatosis (41), facial angiofibromas (42) and epilepsy (43), has a very dramatic effect on two selected behavioral read-outs (locomotor and survival) of the *tsc2* mutant zebrafish model. Of importance, for that purpose the offspring of heterozygous adults were pharmacologically treated as a whole. Homozygous *tsc2*^{-/-} larvae are theoretically present for 25% in this mixture, and since these larvae show dramatically different results for the selected assays as compared to the WT and *tsc2*^{+/-} zebrafish larvae, any treatment effect that rescues the homozygous fish can be observed easily and in a sensitive way. Notably, the methodology described herein does not necessitate genotyping neither selection of the *tsc2*^{-/-} zebrafish larvae, and in this way provides a straightforward *in vivo* phenotype-driven screening platform for medium-throughput testing of TSC-related compounds.

Furthermore, the treatment effects of rapamycin were assessed at the molecular level by means of western blotting. Rapamycin functions as a mTOR inhibitor by the formation of a complex with FK506 binding protein 12 (FKBP12) and by binding of this complex to the FKBP12-rapamycin binding (FRB) domain of mTOR (216, 217). It is assumed that rapamycin does not directly inhibit the kinase activity of mTOR, but more likely acts by blocking interactions with other regulatory proteins (216). Therefore, it is expected to block the activation of downstream mediators such as p70S6K and consequently to decrease the level of pS6 (152). Previously it has been shown that mTOR is phosphorylated at Ser2448 by p70S6K and that this phosphorylation is rapamycin-sensitive (180, 218). Our results show indeed that rapamycin normalizes the hyperactive mTORC1 signaling in the *tsc2*^{-/-} larvae, as shown by the protein levels of pS6 and pmTOR.

The effect of rapamycin on autophagy was studied as well, since mTORC1 is a potent inhibitor of this self-degradative process (181). This inhibition occurs by phosphorylation and inactivation of ULK-1 (a serine/threonine protein kinase) and autophagy-related protein 13 (Atg13), two components that

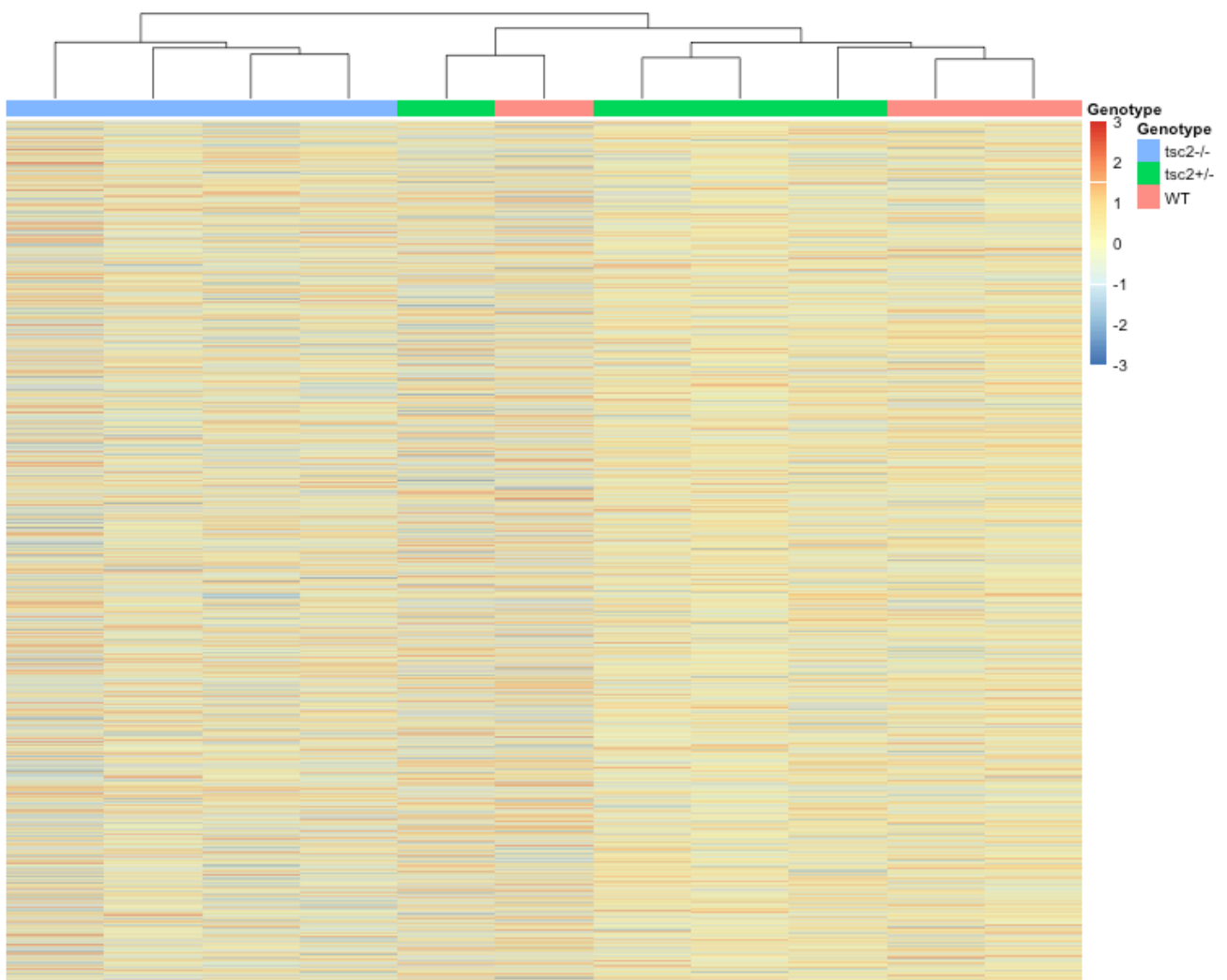
together with FAK family kinase-interacting protein of 200kDa (FIP200) form the ULK1-Atg13-FIP200 complex, indispensable for the initiation of autophagosome formation (219, 220). To investigate the effect of rapamycin treatment on the level of autophagy present in the larval heads, we choose LC3B-II, an integral component of the autophagosome membrane, as a marker (181, 221). However, as we only observed a small and statistically not significant decline in LC3B-II present the VHC-treated *tsc2*^{-/-} larvae, we could not demonstrate any effect of rapamycin in these conditions.

Taken together, our phenotypic, transcriptomic and pharmacological analysis identified the *tsc2*^{-/-} zebrafish as a preclinical model that mirrors well aspects of the human condition. This has allowed for not only the confirmation of TSC related pathology, but also for the identification of novel areas of investigation, including dysfunction of calcium ion channels and calcium signaling and up-regulation of *ctss2.1*. This suggests that the zebrafish model may be an interesting tool for future investigations with the aim to provide further pathomechanistic insights in TSC. The identification of 216 human orthologs with possible drug targets, including CTSS demonstrates the potential use of the *tsc2*^{-/-} zebrafish in the identification of therapeutic treatments.

6. Supplementary information

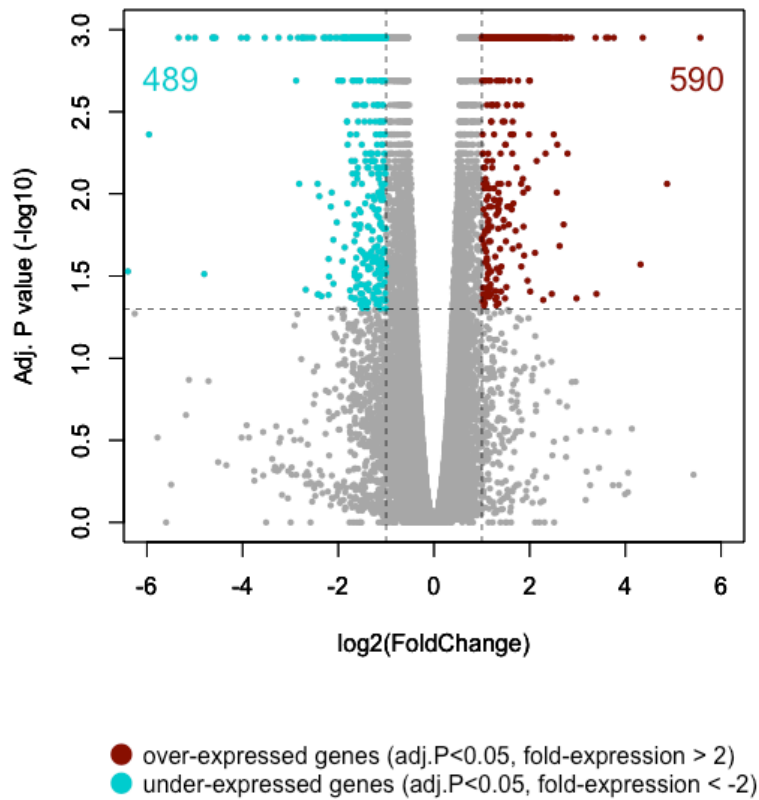
6.1 S1 figure: Heatmap of the complete transcriptome profile of each sequenced replicate

Two distinct clusters, based on the Euclidean distance, were formed, one containing entirely *tsc2*^{-/-} (blue), the second was made up of both samples from the wild-type (pink) and *tsc*^{+/-} (green) zebrafish. Gene expression was the scaled $\log_{10}(\text{FPKM}+1)$.



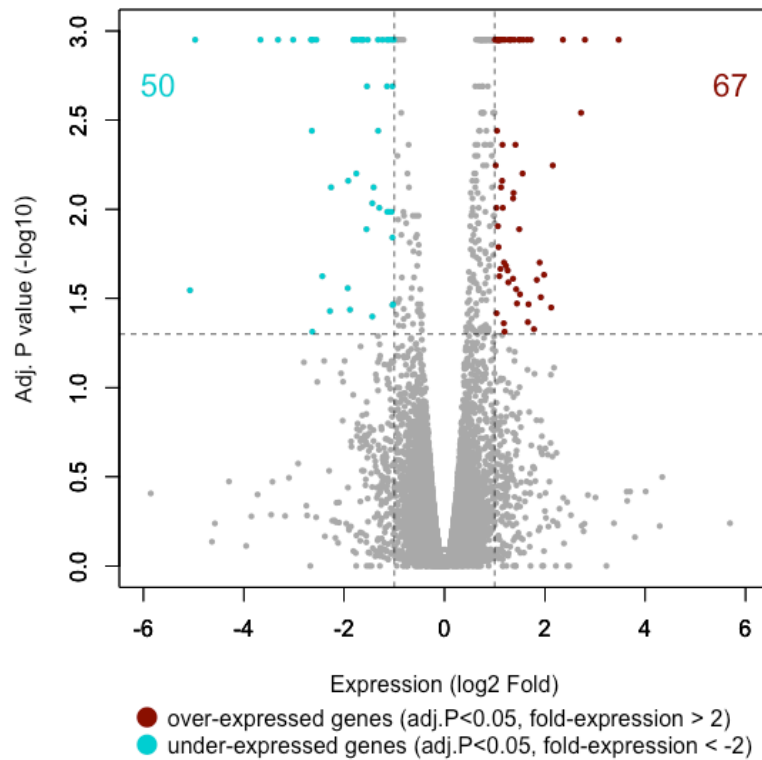
6.2 S2 figure: Volcano plot of differentially expressed genes between the *tsc2*^{+/-} and the *tsc2*^{-/-} zebrafish

489 genes were down-regulated and 590 genes were up-regulated. Cut-offs of an absolute fold-change of 2, and a Benjamini-Hochberg corrected p -value < 0.05 were applied.



6.3 S3 figure: Volcano plot of differentially expressed genes between the wild-type and the *tsc2*^{+/-} zebrafish

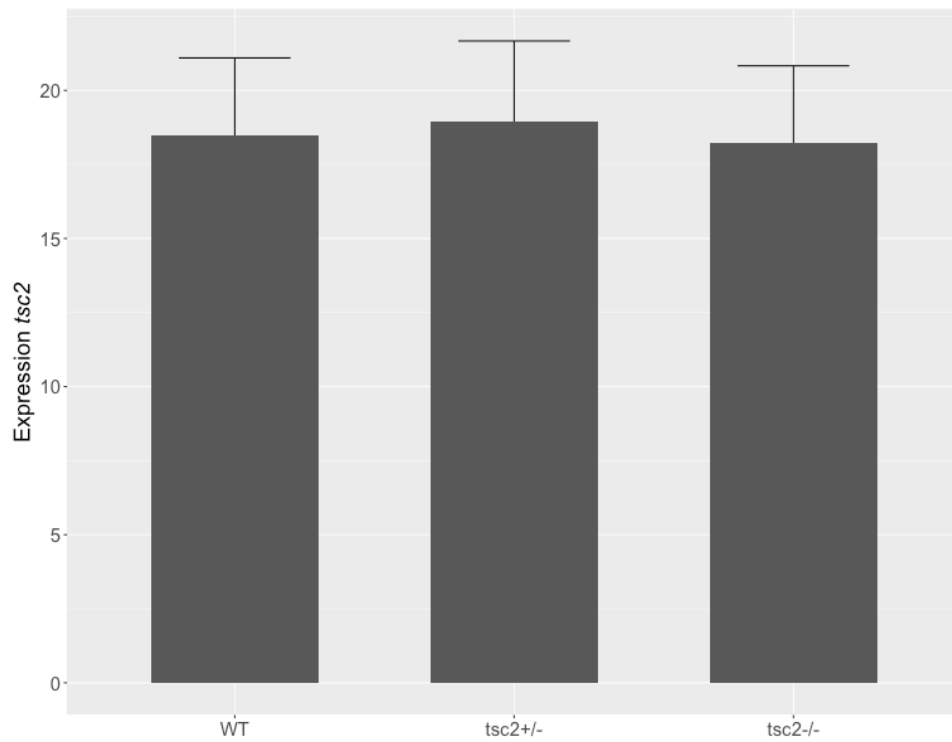
50 genes were down-regulated and 67 genes were up-regulated. Cut-offs of an absolute fold-change of 2, and a Benjamini-Hochberg corrected p -value < 0.05 were applied.



6.4 S4 figure: The expression of *tsc2* in each of the genotypes

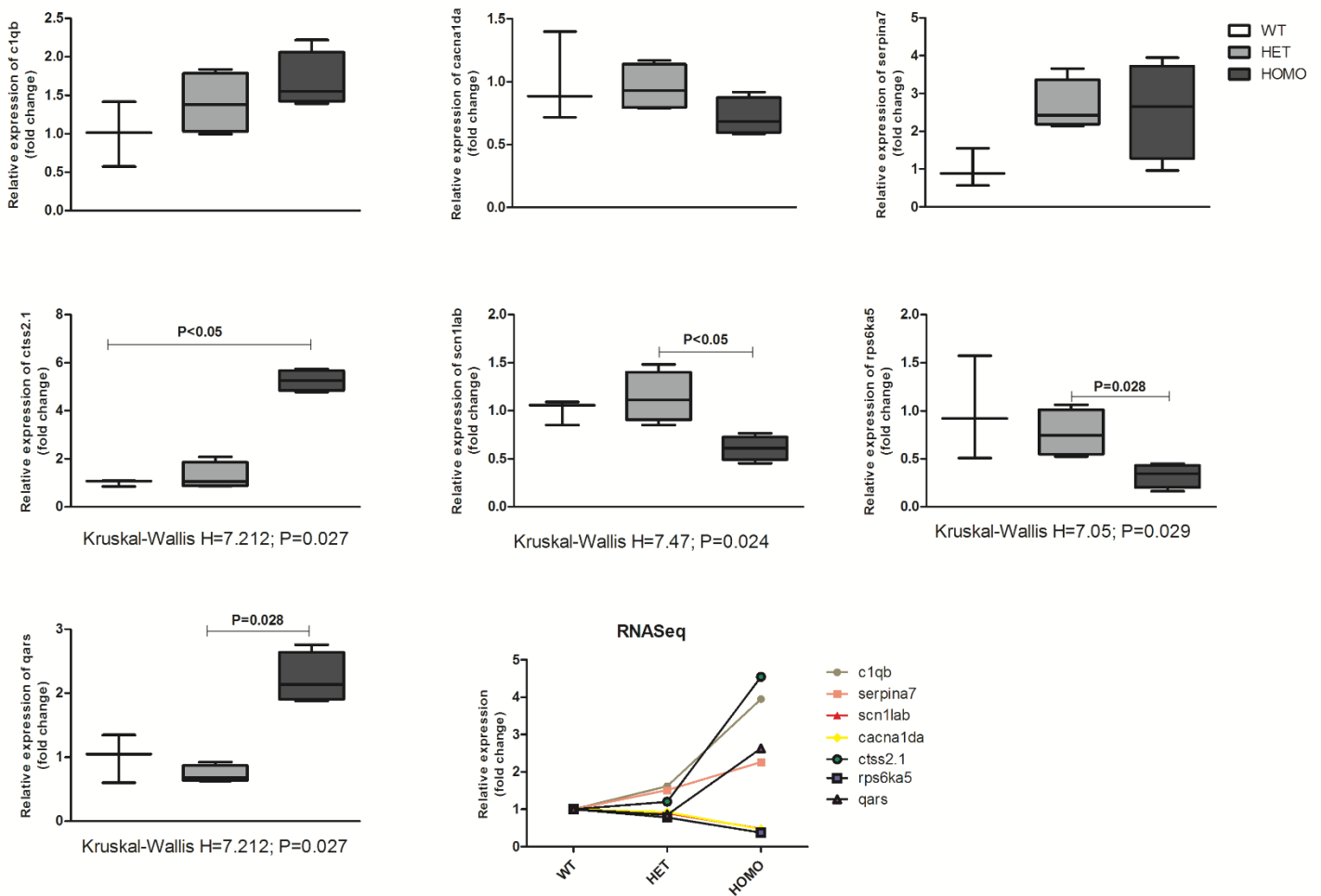
There was no difference in *tsc2* expression across any of the samples. Expression on the y-axis is FPKM.

Data are expressed as mean \pm SD.



6.5 S5 figure: RT-qPCR validation of selected genes

Seven genes were selected from the RNA-Seq for validation. Data are expressed as box and whiskers plots. The fold-change is relative to the expression of the gene in the wild-type group. The statistical test used was the Kruskal-Wallis followed by the Dunn's post-hoc test or the Mann-Whitney U test. The expression RNA-Seq expression levels are shown in the final panel (labeled RNA-Seq). Overall, the expression patterns mirrored the results obtained from RNA-Seq.



6.6 Supplementary tables

Supplementary tables are available online, through the following link:

<https://www.sciencedirect.com/science/article/pii/S0969996117302127?via%3Dihub>

- S1 table: Up- and down-regulated protein coding genes between WT and *tsc2*^{-/-} sorted by fold change
- S2 table: List of RT-qPCR primers used for validation. The forward and reverse primers are listed, written in 5' to 3' direction.
- S3 table: GO terms enriched in the up- and down-regulated gene lists from the WT and *tsc2*^{-/-} transcriptome analysis
- S4 table: List of up-regulated genes from the *tsc2*^{-/-} samples belonging to the cluster of inflammation and immune response related GO terms
- S5 table: List of the expression levels of 84 mTOR-related genes, assessed in the transcriptome comparison between WT and *tsc2*^{-/-} larvae

7. Acknowledgements

This work was supported by the European Union Seventh Framework Programme FP7/2007-2013 under the project EPISTOP (grant agreement n: 602391). A. Siekierska is a postdoctoral fellow of the Research Foundation–Flanders (FWO Vlaanderen).

CHAPTER V

General discussion

1. Challenges in anti-seizure drug discovery

Two induced acute rodent seizure models have been widely used and were recognized as standard procedures for ASD discovery: the MES test and the PTZ test (45, 222, 223). In brief, the MES test results in seizure induction by applying a short 60 Hz electrical stimulus of 50 mA (for mice) or 150 mA (for rats) via electrodes to the cornea of the animals (44), whereas chemical induction of seizures is established by a subcutaneous injection of the pro-convulsant PTZ (224). Despite the successes of ASD discovery using these animal models, one third of epilepsy patients remains drug-resistant (47, 48, 50). The problems associated with these simple acute seizure models is that they do not mirror epilepsy, since seizures are induced in ‘normal’ non-epileptic brains, possibly resulting in false positive and false negative findings (50, 222). Moreover, it has been argued that the further use of these models would only give rise to ‘me-too’ drugs and will not facilitate the discovery of drugs that have an effect on drug-resistant epilepsies (50). One of the major aims of the Epilepsy Therapy Screening Program (ETSP) is to identify drugs for the treatment of drug-resistant epilepsies. To this end, more complex chronic and drug-resistant models (*e.g.* 6 Hz model) were included in the ASD screening process (47, 222, 225). For ASD testing, the ETSP proposes a battery of rodent and *in vitro* tests, grouped into an ‘Identification’ and ‘Differentiation’ phase, where the models of the latter group are more resource-intensive and lower throughput, *e.g.* the post-kainic acid status epilepticus rat as a model of chronic epilepsy (47, 225).

Where the rodent models, as proposed by the ETSP, focus on the modeling of different drug-resistant human seizure types in general, zebrafish as a tractable genetic model organism are increasingly used to model a specific epileptic syndrome with the associated pathophysiology and drug-resistance of epilepsy (up to 66% in case of TSC patients). Therefore, the use of these genetic zebrafish epilepsy models in high-throughput screening would result in a more ‘personalized’ medicine and could potentially aid the discovery of treatments for drug-resistant epilepsy in general.

1.1 Potential of genetic zebrafish epilepsy models in anti-seizure drug discovery

The *scn1Lab* mutant zebrafish model is the first example of a genetic zebrafish epilepsy model implemented in high-throughput screening of a repurposed drug library (55). The human ortholog of *scn1Lab* is the *SCN1A* gene encoding the alpha subunit of the voltage-gated sodium channel 1.1 (Na_v1.1). Mutations in *SCN1A* have been linked to Dravet syndrome, a drug-resistant epileptic encephalopathy, starting within the first year of life (226-228). The *scn1Lab* homozygous larvae showed, when compared to WT and *scn1Lab* heterozygous larvae, a distinct behavior typified by hyperactivity and whole-body convulsions. In addition to this seizure behavior the larvae also demonstrated epileptiform discharges, underscoring the relevance of zebrafish in mimicking the Dravet syndrome-associated epilepsy. High-throughput screening of 320 FDA approved compounds was

performed in 96-well plates with one larva per well, a starting concentration of 667 μ M, and each compound being tested on a minimum of six homozygous larvae. Screening was based on the locomotor activity of the larvae (hyperactive seizure behavior), where a compound that was able to reduce the behavior to the control level was identified as a positive hit. The initial screening revealed 18 hits that subsequently were retested at three different concentrations. From those, four out of 18 compounds were efficient in reducing seizure behavior at all tested concentrations and were therefore further investigated by means of local field potential recordings. Finally, only clemizole sustained both seizure activity tests and forms the first proof-of-principle of the successful implementation of genetic zebrafish epilepsy models in drug discovery (55).

1.2 *fhl1* mutant zebrafish model

In our research, we investigated the disease-causative nature of a mutation in *FHF1*. Therefore, we established an overexpression model of the patients' *FHF1* mutation in zebrafish and as such were able to confirm a causal link between the specific mutation and the early-onset epileptic encephalopathy (EOEE) with cerebellar atrophy. Of interest, more recently six additional patients have been reported carrying the exact same mutations in the *FHF1* gene (229-231). All patients suffer(ed) from an early-onset intractable epilepsy and most of them also showed a moderate to severe intellectual disability. However, while in our case the disease course was very progressive and associated with early lethality, the six more recently identified patients are still alive (229-231) (Fig. 1).

EPILEPSY	P1(7y)	P2 (3y)	P3 (11m)	P4 (15y)	P5 (3y)	P6 (16y)	P7 (18y)	P8 (5y)
Onset before 1 month	black	black	black	black	black	white	black	black
Frequent SE	black	black	white	white	black	black	black	white
Response to sodium channel blockers	white	white	black	dark grey	white	white	dark grey	black
Response to VNS	light gray	black	black	light gray				
DEVELOPMENT								
Intellectual disability	death	death	normal	moderate	severe	severe	moderate	moderate
BRAIN MRI								
Initially normal	black	black	black	black	black	black	black	black
Progressive cortical/cerebellar atrophy	black	black	white	white	black	black	dark grey	white

Figure 1: Clinical picture of the 8 reported *FHF1* p.R52H patients. Squares: black (true), dark grey (partially true), light gray (not tested) and white (false/absent). P1-P2 (our study), P3-P4 (215), P5-P7 (214), P8 (216). SE = status epilepticus, VNS = vagus nerve stimulation. Adapted from Villeneuve *et al.* 2017 *European Journal of Pediatric Neurology* (231).

In the case of our *fhl1* overexpression larvae, a moderate- to high-throughput ASD screening similar to the one described by Baraban *et al.* could be done. To this end, the Tol2-microinjected larvae with bright red fluorescent brains will have to be raised until adulthood and incrossed to obtain F1 larvae that

homogenously overexpress the patients' *FHF1* mutation in the brain. The generation of this stable transgenic line will lower the labor-intensivity by eliminating the need for repetitive microinjections. Moreover, the expression of the transgene is more homogenous in the F1 offspring compared to the founders (148). Compounds identified in this 'personalized' model of intractable epilepsy might as well be of interest for other drug-resistant epilepsies. A factor that might limit the generation of this line is that transgenic animals could show an early lethal phenotype. Also, the use of this line for ASD screening depends on the availability of a good read-out, preferably at the behavioral level.

Of interest, the identification of *FHF1* as a novel predisposing gene for EOEE in zebrafish is one of the first examples of rapid bedside-to-bench-to-bedside translational research. With back-to-bedside, we refer to the importance of a complete diagnosis for the patient and his family. From a pharmacological point of view, however, there is no translation to the clinic yet. Nevertheless, the search for improved therapy starts with an improved understanding of the disease. Other examples are the discovery of *CHD2* as a novel predisposing gene for an epileptic encephalopathy with generalized seizures, sharing features with Dravet Syndrome (90) and the identification of *STX1B* as a novel predisposing gene for fever-associated epilepsy syndromes (128). These studies demonstrate that modeling of *de novo* disease-causative mutations in zebrafish is clinically important for a fast patient diagnosis and genetic counseling. Moreover, knowing the defected gene might open the opportunity for a more targeted treatment approach, where known drugs could be used that target the pathway in which the diseased gene is involved. This approach assumes knowledge of the pathway of the gene of interest and the availability of drugs that are known to interact with this pathway.

1.3 *tsc2* mutant zebrafish model

We demonstrated the validity of the *tsc2* zebrafish model as a model recapitulating certain brain-related clinical features of the human disease, i.e. megalencephaly and epileptiform activity associated with a change in neurobehavior. Other similarities to the human condition are the beneficial effect of rapamycin treatment and the upregulation of genes related to inflammation and immune response. Additionally, transcriptome profiling showed the potential of the model (i) to improve understanding of the pathogenesis and to find novel areas of investigation, i.e. dysfunction of calcium ion channels and calcium signaling, and (ii) to identify possible drug targets, i.e. upregulation of *ctss2.1*. Although transcriptomics has proven its utility, one of the downsides is that only gene expression and not post-translational modifications are detected, meaning that the transcriptomic data should be interpreted with some caution. Therefore, ideally, in order to fully characterize a model, transcriptome studies should be complemented with a study of the proteome (identify proteins) and metabolome (link proteins to metabolic pathways) (115). With regards to ASD discovery, the potential of this model is explored in detail below.

1.3.1 Challenges for mutant zebrafish epilepsy models in ASD discovery

The discovery of clemizole as an ASD for treatment of drug-resistant epilepsy in Dravet syndrome using the *scn1Lab* mutant zebrafish model underscores the relevance of genetic zebrafish epilepsy models in high-throughput ASD screening. Of importance, only homozygous larvae were incorporated in the screening assay, rendering it to be as efficient as possible. The *scn1Lab* homozygotes were characterized by hyperpigmentation, allowing selection based on their black appearance (55). Other examples of mutant zebrafish epilepsy models that could be used for ASD screening are the *stxbp1b* and the *mind bomb* mutant, showing a reduced locomotor response to a dark-flash and hyperactivity respectively. The *stxbp1b* homozygous mutant is characterized by a black appearance, while the *mind bomb* homozygous mutants are typified by their deformed heads, smaller eyes and a curled body axis (91, 94). These morphological features can be used as a selection tool to pick out the homozygous mutants from the mixture of offspring.

However, not all mutant zebrafish epilepsy models possess an obvious morphological marker that allows easy selection of the homozygous larvae. This is exemplified by the *tsc2* mutant which does not show gross morphological alterations, although enlarged brains were observed in the homozygous larvae. However, this morphological difference is too subtle to be visually determined and necessitates brain size measurements. Therefore, it was considered to be not fit for use as a selection marker.

The question arises whether the *tsc2* mutant in particular, and a model without a selection marker in general, can be used as a high-throughput cost- and time- efficient drug discovery platform. Such a model necessitates genotyping to select the homozygous larvae. However, ideally genotyping is avoided because of its labor-intensiveness and associated costs.

Therefore, alternatively, the possibility to use a genotyping-free approach based on a mixture of WT, heterozygous and homozygous larvae is investigated below. In our thought process, we choose locomotor behavior as high-throughput readout for screening since it was shown to be reduced in the homozygous *tsc2* larvae following a light-dark switch and in general is altered in the context of epilepsy. This approach assumes the locomotor activity of the homozygous larvae to be sufficiently distinct to affect the total behavior of the mixture of WT, heterozygous and homozygous larvae. A compound will be identified as a positive hit when it rescues the altered movement of the homozygous larvae and thus increases the total behavior of the mix in case of the *tsc2* zebrafish model. First, the required sample size for this genotyping-free approach is calculated. Second, the costs and benefits of this method are compared to those associated with genotyping.

1.3.1.1 Sample size

Based on the drug screening performed by Baraban *et al.* using the *scn1Lab* model, we conclude that the number of homozygous animals needed to test 1 compound should at least equal six (55). Assuming a mendelian distribution of genotypes in the offspring of heterozygous parents, i.e. 25% WT, 50% heterozygous and 25% homozygous animals, the group size should be 24 larvae in order to have six homozygotes per treatment.

However, what is the chance of exactly obtaining 25% of homozygotes in a given sample size? This is where probability calculations come into the picture. And more specifically calculations of combinations, since the order of selecting the homozygotes has no importance. Assuming 100 embryos as the total number of offspring (= the population) from heterozygous parents, one can calculate the probability of obtaining a homozygosity rate of 25% within a specific group size (= sample taken from the population). The probability of having exactly 25% homozygotes in a group size of 24 embryos, i.e. six homozygous embryos, is calculated as follows. All favorable combinations are those in which six homozygotes out of 24 embryos are selected from the population of 100 embryos, thus combinations that contain six homozygous and 18 non-homozygous embryos. The number of these combinations is divided by the total number of combinations possible when selecting 24 embryos (sample size) from 100 embryos (population) (Fig. 2). The calculated probability is 0.212 or 21.2%, meaning that when 24 embryos are selected from a population of 100 embryos in which mendelian distribution is assumed, there is only a 21.2% chance of having six homozygotes within this group size.

$$\frac{\text{number of favorable combinations}}{\text{total number of combinations}} = \frac{\binom{25}{6} \binom{75}{18}}{\binom{100}{24}}$$

Figure 2: Example of the probability calculation in a group size of 24 larvae.

These calculations can also be made for other group sizes: n=12, n=36, n=48, n=60, n=72, n=84, n=96, n=99 and n=100. The probabilities of having exactly 25% homozygotes within each group size are plotted in figure 3. These probabilities decrease to 18.2% in a group of 48 larvae, after which the probability increases with increasing group size.

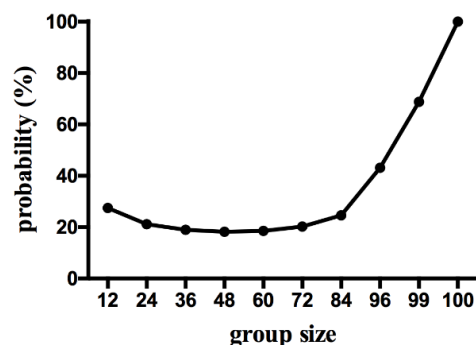


Figure 3: The probability of obtaining exactly 25% homozygotes in different group sizes.

These calculations show that the probabilities of obtaining exactly 25% homozygotes are low, e.g. $p = 43.1\%$ for a group size of 96 larvae. Therefore, we choose an interval of 21% to 29% of homozygotes as an acceptable approximation of the expected 25% and recalculate the probabilities of having between 21% and 29% of homozygotes within each group size (Fig. 4A).

The fact that only natural numbers of embryos are included, results in a correlation that is not perfectly linear and slightly underestimates the real probability (Fig. 4B). Nevertheless, these results show that the probability of having between 21% and 29% homozygotes increases with increasing group size. The chance of having between 21 – 29% homozygotes quadruples from $n=24$ (21.23%) to $n=72$ (80.27%). Based on these results, we would recommend for a genotyping-free assay to use a group size of 72 larvae to test one compound instead of the 24 suggested earlier.

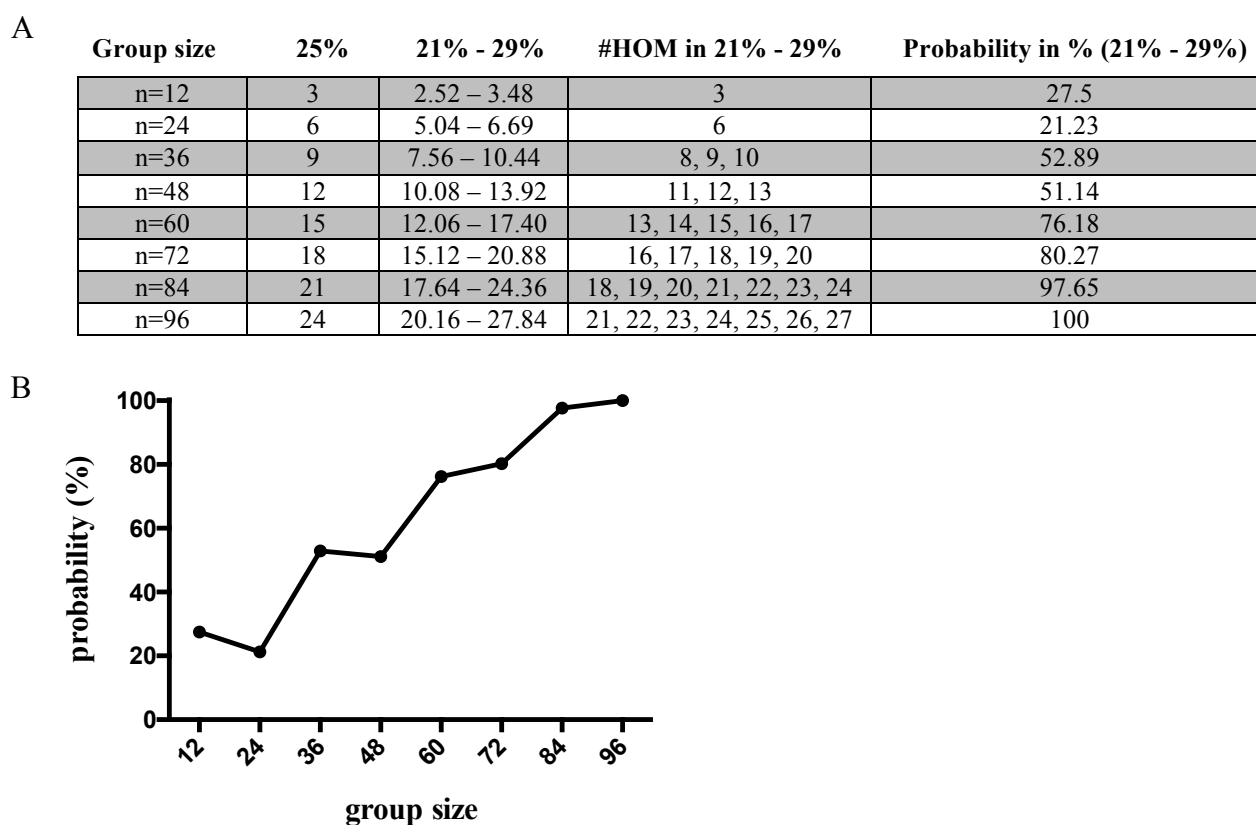


Figure 4: The probability of obtaining homozygotes in an interval of 21% to 29% for different group sizes. (A) The table shows calculations of 25%, the range 21% - 29%, the number of homozygotes falling in between the calculated range and the probability of having a % of homozygotes between 21% and 29% for different group sizes. (B) The probability of obtaining 21% - 29% homozygotes is plotted for each group size. HOM = homozygotes.

1.3.1.2 *Cost-benefit analysis: genotyping-free vs genotyping*

For screening, larvae are generally arrayed in 96-well plates and behaviorally analyzed using an automated tracking device. In case of the *tsc2* larvae every plate would be tracked twice, a first time to determine the baseline movement of the larvae (internal controls) and a second time after addition of the compounds. The protocol to detect locomotor behavior takes 35 minutes. Thus, meaning that 12 runs, i.e. six plates before and after treatment, can be performed daily. This experimental approach is widely applicable for zebrafish-based screening. Below, the costs and benefits of a genotyping-free approach are compared to the ones associated with genotyping, assuming the screening of a library of 1,000 compounds.

Genotyping-free approach: n=72

In case of a genotyping-free approach, the group size needs to be increased to enlarge the chance of having an approximation of 25% homozygotes per group. Based on our probability calculations, a group size of 72 larvae is considered to be appropriate. In order to screen a library of 1,000 compounds, 72,000 larvae and 125 days or approximately six months are needed. No costs or time related to genotyping have to be taken into account (Table 2).

Genotyping preceding the screening n=6

Another approach is to determine the genotype upfront and then only use the homozygous larvae for screening. This could be realized by means of chorion- or tissue-genotyping, an approach that relies on microfluid technology to extract genetic material from the chorionic fluid or fin tissue without harming the embryo. Genotyping is performed using PCR amplification and high resolution melt analysis (232). The preselection of homozygous larvae for screening allows a reduction of the group size to six larvae per group. This would necessitate the use of only 6,000 homozygous larvae, which equals 63 plates and 11 days to perform the locomotor screening. Nevertheless, to obtain 6,000 homozygotes, genotyping of more or less 24,000 embryos is needed. The most time-consuming step in this genotyping procedure will be the extraction of embryonal DNA. An educated estimation of the time and costs linked to the genotyping-before-screening approach of 24,000 embryos would be 2,250 man hours and 3,000 euros respectively (Table 2).

The screening approaches are compared in terms of the number of embryos used for screening, the number of compounds that can be tested daily and the associated workload and costs (Table 2). Clearly, the method that includes genotyping is associated with a higher cost and workload compared to the genotyping-free assay. However, the latter one uses much more larvae per group (n=72), meaning that daily only 8 compounds can be tested, which questions the high-throughputness of this approach. Thus, in contrast to zebrafish models that contain a selection marker, none of these approaches leads to a high-throughput time- and cost-efficient screening with genetic zebrafish epilepsy models that lack an obvious morphological marker. Nevertheless, as soon as advances enable automatized extraction of

embryonal genetic material, the genotyping approach would be useful, as daily up to 96 compounds can be tested.

Table 2: Comparison of the different approaches with regards to the number of embryos used for screening, the number of compounds that can be tested daily, the workload and costs.

	# embryos used for screening	# compounds tested daily	Workload (months)	Total cost (euros)
Genotyping-free (n=72)	72,000	8	6	No costs related to genotyping
Genotyping preceding the screening (n=6)	6,000 (although 24000 for genotyping)	96	9	3000

2. Conclusion and future perspectives

With the discovery of clemizole using the *scn1Lab* zebrafish mutant, genetic zebrafish epilepsy models have proven to be very well suited for innovative high-throughput ASD discovery purposes. Similar to the *scn1Lab* mutant zebrafish larvae, the *fhf1* mutant model, which became one of the first examples of rapid bedside-to-bench-to-bedside translation, can be implemented in high-throughput ASD screening. While the zebrafish *tsc2* mutant model was used primarily to model features of the human disease and is useful to better understand the pathophysiology and identify possible drug targets, we also reflected on the potential of this model for high-throughput drug discovery. After comparing two approaches for screening, we concluded that genetic zebrafish epilepsy models that lack a selection marker like the *tsc2* mutant, are not time- and cost-efficient for high-throughput screening. Nonetheless, such models remain valuable for directed testing of compounds for which evidence exists that they might work in these models, i.e. by using insights from fundamental research. Moreover, technological advances for genotyping that reduce the associated labor-intensiveness and costs, could pave the way for these mutant models to be used as high-throughput ASD discovery platform.

This research provides a proof-of-concept of the translational potential of zebrafish to model human genetic epilepsies. However, our interest is not limited to the modeling of drug-resistant epilepsy caused by mutations in specifically *TSC2* or *FHF1*. Therefore, we would invest in the generation of a platform of ‘personalized’ zebrafish models, reflecting the multiplicity of drug-resistant epilepsies. This will include the modeling of both existing drug-resistant epilepsy syndromes and candidate-epilepsy genes, discovered by Next-Generation Sequencing. If no zebrafish mutant is commercially available, these models will be generated using CRISPR/Cas9 methodology. Next, they can serve for fundamental research aiming at elucidation of the pathophysiology and ASD screening purposes, ideally with the availability of a morphological marker, rendering genotyping unneeded. With regards to ASD screening, the developed zebrafish platform can be positioned next to the rodent platform, proposed by the ETSP, as both aim at identifying treatments with improved efficacy against drug-resistant seizures. Of course, the success of this approach will rely on the availability of suitable rodent models for further preclinical drug development.

REFERENCES

1. Singh A, Trevick S. The Epidemiology of Global Epilepsy. *Neurologic Clinics*. 2016;34(4):837-47.
2. Fisher RS, Acevedo C, Arzimanoglou A, Bogacz A, Cross JH, Elger CE, et al. ILAE official report: a practical clinical definition of epilepsy. *Epilepsia*. 2014;55(4):475-82.
3. Fisher RS, Cross JH, French JA, Higurashi N, Hirsch E, Jansen FE, et al. Operational classification of seizure types by the International League Against Epilepsy: Position Paper of the ILAE Commission for Classification and Terminology. *Epilepsia*. 2017;58(4):522-30.
4. Scheffer IE, Berkovic S, Capovilla G, Connolly MB, French J, Guilhoto L, et al. ILAE classification of the epilepsies: Position paper of the ILAE Commission for Classification and Terminology. *Epilepsia*. 2017;58(4):512-21.
5. Falco-Walter JJ, Scheffer IE, Fisher RS. The new definition and classification of seizures and epilepsy. *Epilepsy Research*. 2018;139:73-9.
6. Blume WT, Luders HO, Mizrahi E, Tassinari C, van Emde Boas W, Engel J, Jr. Glossary of descriptive terminology for ictal semiology: report of the ILAE task force on classification and terminology. *Epilepsia*. 2001;42(9):1212-8.
7. Nehring WM, Faux SA. Clinical genetics: an overview. *Journal of Cardiovascular Nursing*. 1999;13(4):19-33.
8. Seyhan AA. RNAi: a potential new class of therapeutic for human genetic disease. *Human Genetics*. 2011;130(5):583-605.
9. Aiello LB, Chiatti BD. Primer in Genetics and Genomics, Article 4-Inheritance Patterns. *Biological Research for Nursing*. 2017;19(4):465-72.
10. Nightingale H, Pfeffer G, Bargiela D, Horvath R, Chinnery PF. Emerging therapies for mitochondrial disorders. *Brain*. 2016;139(Pt 6):1633-48.
11. Veltman JA, Brunner HG. De novo mutations in human genetic disease. *Nature Review Genetics*. 2012;13(8):565-75.
12. Crow JF. The origins, patterns and implications of human spontaneous mutation. *Nature Review Genetics*. 2000;1(1):40-7.
13. Ku CS, Vasiliou V, Cooper DN. A new era in the discovery of de novo mutations underlying human genetic disease. *Human Genomics*. 2012;6:27.
14. Goldfarb M, Schoorlemmer J, Williams A, Diwakar S, Wang Q, Huang X, et al. Fibroblast growth factor homologous factors control neuronal excitability through modulation of voltage-gated sodium channels. *Neuron*. 2007;55(3):449-63.
15. Itoh N. Hormone-like (endocrine) Fgfs: their evolutionary history and roles in development, metabolism, and disease. *Cell and Tissue Research*. 2010;342(1):1-11.
16. Olsen SK, Garbi M, Zampieri N, Eliseenkova AV, Ornitz DM, Goldfarb M, et al. Fibroblast growth factor (FGF) homologous factors share structural but not functional homology with FGFs. *The Journal of biological chemistry*. 2003;278(36):34226-36.
17. Zhang J, Li Y. Therapeutic uses of FGFs. *Semin Cell Dev Biol*. 2016;53:144-54.
18. Goldfarb M. Fibroblast growth factor homologous factors: evolution, structure, and function. *Cytokine & Growth Factor Reviews*. 2005;16(2):215-20.
19. Siekierska A, Isrie M, Liu Y, Scheldeman C, Vanthillo N, Lagae L, et al. Gain-of-function FHF1 mutation causes early-onset epileptic encephalopathy with cerebellar atrophy. *Neurology*. 2016;86(23):2162-70.
20. Caban C, Khan N, Hasbani DM, Crino PB. Genetics of tuberous sclerosis complex: implications for clinical practice. *The Application of Clinical Genetics*. 2017;10:1-8.
21. De Waele L, Lagae L, Mekahli D. Tuberous sclerosis complex: the past and the future. *Pediatric nephrology (Berlin, Germany)*. 2015;30(10):1771-80.
22. Crino PB, Nathanson KL, Henske EP. The tuberous sclerosis complex. *The New England Journal of Medicine*. 2006;355(13):1345-56.

23. Curatolo P, Moavero R, de Vries PJ. Neurological and neuropsychiatric aspects of tuberous sclerosis complex. *The Lancet Neurology*. 2015;14(7):733-45.
24. de Vries PJ, Whittemore VH, Leclezio L, Byars AW, Dunn D, Ess KC, et al. Tuberous sclerosis associated neuropsychiatric disorders (TAND) and the TAND Checklist. *Pediatric neurology*. 2015;52(1):25-35.
25. Gipson TT, Johnston MV. New insights into the pathogenesis and prevention of tuberous sclerosis-associated neuropsychiatric disorders (TAND). *F1000Research*. 2017;6.
26. Curatolo P. Mechanistic target of rapamycin (mTOR) in tuberous sclerosis complex-associated epilepsy. *Pediatric neurology*. 2015;52(3):281-9.
27. Thiele EA. Managing and understanding epilepsy in tuberous sclerosis complex. *Epilepsia*. 2010;51 Suppl 1:90-1.
28. Kingswood JC, Bruzzi P, Curatolo P, de Vries PJ, Fladrowski C, Hertzberg C, et al. TOSCA - first international registry to address knowledge gaps in the natural history and management of tuberous sclerosis complex. *Orphanet Journal of Rare Diseases*. 2014;9:182.
29. Northrup H, Krueger DA, International Tuberous Sclerosis Complex Consensus G. Tuberous sclerosis complex diagnostic criteria update: recommendations of the 2012 International Tuberous Sclerosis Complex Consensus Conference. *Pediatric neurology*. 2013;49(4):243-54.
30. Huang J, Manning BD. The TSC1-TSC2 complex: a molecular switchboard controlling cell growth. *The Biochemical journal*. 2008;412(2):179-90.
31. Qin J, Wang Z, Hoogeveen-Westerveld M, Shen G, Gong W, Nellist M, et al. Structural Basis of the Interaction between Tuberous Sclerosis Complex 1 (TSC1) and Tre2-Bub2-Cdc16 Domain Family Member 7 (TBC1D7). *Journal of Biological Chemistry*. 2016;291(16):8591-601.
32. van Slegtenhorst M, de Hoogt R, Hermans C, Nellist M, Janssen B, Verhoef S, et al. Identification of the tuberous sclerosis gene TSC1 on chromosome 9q34. *Science (New York, NY)*. 1997;277(5327):805-8.
33. European Chromosome 16 Tuberous Sclerosis C. Identification and characterization of the tuberous sclerosis gene on chromosome 16. *Cell*. 1993;75(7):1305-15.
34. Laplante M, Sabatini DM. mTOR signaling at a glance. *Journal of Cell Science*. 2009;122(20):3589.
35. Crino PB. The mTOR signalling cascade: paving new roads to cure neurological disease. *Nature reviews Neurology*. 2016;12(7):379-92.
36. Switon K, Kotulska K, Janusz-Kaminska A, Zmorzynska J, Jaworski J. Molecular neurobiology of mTOR. *Neuroscience*. 2017;341:112-53.
37. Laplante M, Sabatini DM. mTOR signaling in growth control and disease. *Cell*. 2012;149.
38. Dibble CC, Elis W, Menon S, Qin W, Klekota J, Asara JM, et al. TBC1D7 is a third subunit of the TSC1-TSC2 complex upstream of mTORC1. *Molecular Cell*. 2012;47(4):535-46.
39. Santiago Lima AJ, Hoogeveen-Westerveld M, Nakashima A, Maat-Kievit A, van den Ouweland A, Halley D, et al. Identification of regions critical for the integrity of the TSC1-TSC2-TBC1D7 complex. *PLoS One*. 2014;9(4):e93940.
40. Franz DN, Belousova E, Sparagana S, Bebin EM, Frost M, Kuperman R. Efficacy and safety of everolimus for subependymal giant cell astrocytomas associated with tuberous sclerosis complex (EXIST-1): a multicentre, randomised, placebo-controlled phase 3 trial. *Lancet*. 2013;381.
41. Bissler JJ, Kingswood JC, Radzikowska E, Zonnenberg BA, Frost M, Belousova E, et al. Everolimus for angiomyolipoma associated with tuberous sclerosis complex or sporadic lymphangiomyomatosis (EXIST-2): a multicentre, randomised, double-blind, placebo-controlled trial. *Lancet (London, England)*. 2013;381(9869):817-24.
42. Koenig MK, Hebert AA, Roberson J, Samuels J, Slopis J, Woerner A, et al. Topical rapamycin therapy to alleviate the cutaneous manifestations of tuberous sclerosis complex: a double-blind, randomized, controlled trial to evaluate the safety and efficacy of topically applied rapamycin. *Drugs in R&D*. 2012;12(3):121-6.
43. French JA, Lawson JA, Yapici Z, Ikeda H, Polster T, Nabbout R, et al. Adjunctive everolimus therapy for treatment-resistant focal-onset seizures associated with tuberous sclerosis (EXIST-

- 3): a phase 3, randomised, double-blind, placebo-controlled study. *Lancet* (London, England). 2016.
44. Raol YH, Brooks-Kayal AR. Experimental models of seizures and epilepsies. *Progress in Molecular Biology and Translational Science*. 2012;105:57-82.
 45. Loscher W. Critical review of current animal models of seizures and epilepsy used in the discovery and development of new antiepileptic drugs. *Seizure*. 2011;20(5):359-68.
 46. Cunliffe VT, Baines RA, Giachello CN, Lin WH, Morgan A, Reuber M, et al. Epilepsy research methods update: Understanding the causes of epileptic seizures and identifying new treatments using non-mammalian model organisms. *Seizure*. 2015;24:44-51.
 47. Loscher W. Animal Models of Seizures and Epilepsy: Past, Present, and Future Role for the Discovery of Antiseizure Drugs. *Neurochemical Research*. 2017;42(7):1873-88.
 48. Loscher W. Fit for purpose application of currently existing animal models in the discovery of novel epilepsy therapies. *Epilepsy Research*. 2016;126:157-84.
 49. Grone BP, Baraban SC. Animal models in epilepsy research: legacies and new directions. *Nature Neuroscience*. 2015;18(3):339-43.
 50. Bialer M, White HS. Key factors in the discovery and development of new antiepileptic drugs. *Nature Reviews Drug Discovery*. 2010;9(1):68-82.
 51. MacRae CA, Peterson RT. Zebrafish as tools for drug discovery. *Nature Reviews Drug Discovery*. 2015;14(10):721-31.
 52. Schubert J, Siekierska A, Langlois M, May P, Huneau C, Becker F, et al. Mutations in STX1B, encoding a presynaptic protein, cause fever-associated epilepsy syndromes. *Nature Genetics*. 2014;46(12):1327-32.
 53. Stewart AM, Desmond D, Kyzar E, Gaikwad S, Roth A, Riehl R, et al. Perspectives of zebrafish models of epilepsy: what, how and where next? *Brain research bulletin*. 2012;87(2-3):135-43.
 54. Stewart AM, Braubach O, Spitsbergen J, Gerlai R, Kalueff AV. Zebrafish models for translational neuroscience research: from tank to bedside. *Trends in Neurosciences*. 2014;37(5):264-78.
 55. Baraban SC, Dinday MT, Hortopan GA. Drug screening in Scn1a zebrafish mutant identifies clemizole as a potential Dravet syndrome treatment. *Nature communications*. 2013;4:2410.
 56. Liew WC, Orban L. Zebrafish sex: a complicated affair. *Briefings in Functional Genomics*. 2014;13(2):172-87.
 57. Wyatt C, Bartoszek EM, Yaksi E. Methods for studying the zebrafish brain: past, present and future. *European Journal of Neuroscience*. 2015;42(2):1746-63.
 58. Grunwald DJ, Eisen JS. Headwaters of the zebrafish -- emergence of a new model vertebrate. *Nature Reviews Genetics*. 2002;3(9):717-24.
 59. Santoriello C, Zon LI. Hooked! Modeling human disease in zebrafish. *The Journal of Clinical Investigation*. 2012;122(7):2337-43.
 60. Ablain J, Zon LI. Of fish and men: using zebrafish to fight human diseases. *Trends in cell biology*. 2013;23(12):584-6.
 61. Kimmel CB, Ballard WW, Kimmel SR, Ullmann B, Schilling TF. Stages of embryonic development of the zebrafish. *Developmental Dynamics*. 1995;203(3):253-310.
 62. Singleman C, Holtzman NG. Growth and maturation in the zebrafish, *Danio rerio*: a staging tool for teaching and research. *Zebrafish*. 2014;11(4):396-406.
 63. Orban L, Sreenivasan R, Olsson PE. Long and winding roads: testis differentiation in zebrafish. *Molecular and Cellular Endocrinology*. 2009;312(1-2):35-41.
 64. Nagabhushana A, Mishra RK. Finding clues to the riddle of sex determination in zebrafish. *Journal of Biosciences*. 2016;41(1):145-55.
 65. Lieschke GJ, Currie PD. Animal models of human disease: zebrafish swim into view. *Nature Reviews Genetics*. 2007;8(5):353-67.
 66. Dooley K, Zon LI. Zebrafish: a model system for the study of human disease. *Current Opinion in Genetics and Development*. 2000;10(3):252-6.
 67. Goldsmith JR, Jobin C. Think small: zebrafish as a model system of human pathology. *Journal of Biomedicine and Biotechnology*. 2012;2012:817341.

68. Howe K, Clark MD, Torroja CF, Torrance J, Berthelot C, Muffato M, et al. The zebrafish reference genome sequence and its relationship to the human genome. *Nature*. 2013;496(7446):498-503.
69. Doke SK, Dhawale SC. Alternatives to animal testing: A review. *Saudi Pharmaceutical Journal*. 2015;23(3):223-9.
70. Strahle U, Scholz S, Geisler R, Greiner P, Hollert H, Rastegar S, et al. Zebrafish embryos as an alternative to animal experiments--a commentary on the definition of the onset of protected life stages in animal welfare regulations. *Reproductive toxicology (Elmsford, NY)*. 2012;33(2):128-32.
71. Tamplin OJ, White RM, Jing L, Kaufman CK, Lacadie SA, Li P, et al. Small molecule screening in zebrafish: swimming in potential drug therapies. *Wiley Interdisciplinary Reviews Developmental Biology*. 2012;1(3):459-68.
72. Nishimura Y, Murakami S, Ashikawa Y, Sasagawa S, Umemoto N, Shimada Y, et al. Zebrafish as a systems toxicology model for developmental neurotoxicity testing. *Congenital Anomalies (Kyoto)*. 2015;55(1):1-16.
73. Guo S. Using zebrafish to assess the impact of drugs on neural development and function. *Expert opinion on drug discovery*. 2009;4(7):715-26.
74. Delvecchio C, Tiefenbach J, Krause HM. The zebrafish: a powerful platform for in vivo, HTS drug discovery. *Assay and drug development technologies*. 2011;9(4):354-61.
75. Taylor JS, Braasch I, Frickey T, Meyer A, Van de Peer Y. Genome duplication, a trait shared by 22000 species of ray-finned fish. *Genome Research*. 2003;13(3):382-90.
76. Wong K, Stewart A, Gilder T, Wu N, Frank K, Gaikwad S, et al. Modeling seizure-related behavioral and endocrine phenotypes in adult zebrafish. *Brain Research*. 2010;1348:209-15.
77. Pitkänen A, Buckmaster PS, Galanopoulou AS, Moshé SL. *Models of seizures and epilepsy*. Second edition. ed. London: Elsevier/Academic Press; 2017. xxvi, 1151 pages p.
78. Baraban SC, Taylor MR, Castro PA, Baier H. Pentylentetrazole induced changes in zebrafish behavior, neural activity and c-fos expression. *Neuroscience*. 2005;131(3):759-68.
79. Mussulini BH, Leite CE, Zenki KC, Moro L, Baggio S, Rico EP, et al. Seizures induced by pentylentetrazole in the adult zebrafish: a detailed behavioral characterization. *PLoS One*. 2013;8(1):e54515.
80. Alfaro JM, Ripoll-Gomez J, Burgos JS. Kainate administered to adult zebrafish causes seizures similar to those in rodent models. *European Journal of Neuroscience*. 2011;33(7):1252-5.
81. Leclercq K, Afrikanova T, Langlois M, De Prins A, Buenafe OE, Rospo CC, et al. Cross-species pharmacological characterization of the allylglycine seizure model in mice and larval zebrafish. *Epilepsy Behavior*. 2015;45:53-63.
82. Tiedeken JA, Ramsdell JS. Embryonic exposure to domoic Acid increases the susceptibility of zebrafish larvae to the chemical convulsant pentylentetrazole. *Environmental Health Perspectives*. 2007;115(11):1547-52.
83. Tiedeken JA, Ramsdell JS. DDT exposure of zebrafish embryos enhances seizure susceptibility: relationship to fetal p,p'-DDE burden and domoic acid exposure of California sea lions. *Environmental Health Perspectives*. 2009;117(1):68-73.
84. Vermoesen K, Serruys AS, Loyens E, Afrikanova T, Massie A, Schallier A, et al. Assessment of the convulsant liability of antidepressants using zebrafish and mouse seizure models. *Epilepsy Behavior*. 2011;22(3):450-60.
85. Afrikanova T, Serruys AS, Buenafe OE, Clinckers R, Smolders I, de Witte PA, et al. Validation of the zebrafish pentylentetrazole seizure model: locomotor versus electrographic responses to antiepileptic drugs. *PLoS One*. 2013;8(1):e54166.
86. Hunt RF, Hortopan GA, Gillespie A, Baraban SC. A novel zebrafish model of hyperthermia-induced seizures reveals a role for TRPV4 channels and NMDA-type glutamate receptors. *Experimental Neurology*. 2012;237(1):199-206.
87. Teng Y, Xie X, Walker S, Rempala G, Kozlowski DJ, Mumm JS, et al. Knockdown of zebrafish *Lgila* results in abnormal development, brain defects and a seizure-like behavioral phenotype. *Human Molecular Genetics*. 2010;19(22):4409-20.
88. Chege SW, Hortopan GA, M TD, Baraban SC. Expression and function of KCNQ channels in larval zebrafish. *Developmental neurobiology*. 2012;72(2):186-98.

89. Ramirez IB, Pietka G, Jones DR, Divecha N, Alia A, Baraban SC, et al. Impaired neural development in a zebrafish model for Lowe syndrome. *Human Molecular Genetics*. 2012;21(8):1744-59.
90. Suls A, Jaehn JA, Kecskes A, Weber Y, Weckhuysen S, Craiu DC, et al. De novo loss-of-function mutations in CHD2 cause a fever-sensitive myoclonic epileptic encephalopathy sharing features with Dravet syndrome. *American Journal of Human Genetics*. 2013;93(5):967-75.
91. Grone BP, Marchese M, Hamling KR, Kumar MG, Krasniak CS, Sicca F, et al. Epilepsy, Behavioral Abnormalities, and Physiological Comorbidities in Syntaxin-Binding Protein 1 (STXBP1) Mutant Zebrafish. *PLoS One*. 2016;11(3):e0151148.
92. Mahmood F, Mozere M, Zdebik AA, Stanescu HC, Tobin J, Beales PL, et al. Generation and validation of a zebrafish model of EAST (epilepsy, ataxia, sensorineural deafness and tubulopathy) syndrome. *Disease Models & Mechanisms*. 2013;6(3):652-60.
93. Zdebik AA, Mahmood F, Stanescu HC, Kleta R, Bockenbauer D, Russell C. Epilepsy in *kcj10* morphant zebrafish assessed with a novel method for long-term EEG recordings. *PLoS One*. 2013;8(11):e79765.
94. Hortopan GA, Dinday MT, Baraban SC. Spontaneous seizures and altered gene expression in GABA signaling pathways in a mind bomb mutant zebrafish. *Journal of Neuroscience*. 2010;30(41):13718-28.
95. Zhang Y, Kecskes A, Copmans D, Langlois M, Crawford AD, Ceulemans B, et al. Pharmacological characterization of an antisense knockdown zebrafish model of Dravet syndrome: inhibition of epileptic seizures by the serotonin agonist fenfluramine. *PLoS One*. 2015;10(5):e0125898.
96. Griffin A, Krasniak C, Baraban SC. Advancing epilepsy treatment through personalized genetic zebrafish models. *Progress in brain research*. 2016;226:195-207.
97. Bedell VM, Westcot SE, Ekker SC. Lessons from morpholino-based screening in zebrafish. *Briefings in Functional Genomics*. 2011;10(4):181-8.
98. Bill BR, Petzold AM, Clark KJ, Schimmenti LA, Ekker SC. A primer for morpholino use in zebrafish. *Zebrafish*. 2009;6(1):69-77.
99. Schulte-Merker S, Stainier DY. Out with the old, in with the new: reassessing morpholino knockdowns in light of genome editing technology. *Development*. 2014;141(16):3103-4.
100. Kok FO, Shin M, Ni CW, Gupta A, Grosse AS, van Impel A, et al. Reverse genetic screening reveals poor correlation between morpholino-induced and mutant phenotypes in zebrafish. *Developmental Cell*. 2015;32(1):97-108.
101. Doyon Y, McCammon JM, Miller JC, Faraji F, Ngo C, Katibah GE, et al. Heritable targeted gene disruption in zebrafish using designed zinc-finger nucleases. *Nature Biotechnology*. 2008;26(6):702-8.
102. Meng X, Noyes MB, Zhu LJ, Lawson ND, Wolfe SA. Targeted gene inactivation in zebrafish using engineered zinc-finger nucleases. *Nature Biotechnology*. 2008;26(6):695-701.
103. Huang P, Xiao A, Zhou M, Zhu Z, Lin S, Zhang B. Heritable gene targeting in zebrafish using customized TALENs. *Nature Biotechnology*. 2011;29(8):699-700.
104. Sander JD, Cade L, Khayter C, Reyon D, Peterson RT, Joung JK, et al. Targeted gene disruption in somatic zebrafish cells using engineered TALENs. *Nature Biotechnology*. 2011;29(8):697-8.
105. Wiedenheft B, Sternberg SH, Doudna JA. RNA-guided genetic silencing systems in bacteria and archaea. *Nature*. 2012;482(7385):331-8.
106. Barrangou R, Fremaux C, Deveau H, Richards M, Boyaval P, Moineau S, et al. CRISPR provides acquired resistance against viruses in prokaryotes. *Science (New York, NY)*. 2007;315(5819):1709-12.
107. Shah AN, Davey CF, Whitebitch AC, Miller AC, Moens CB. Rapid reverse genetic screening using CRISPR in zebrafish. *Nature Methods*. 2015;12(6):535-40.
108. Hwang WY, Fu Y, Reyon D, Maeder ML, Tsai SQ, Sander JD, et al. Efficient genome editing in zebrafish using a CRISPR-Cas system. *Nature Biotechnology*. 2013;31(3):227-9.
109. Kawakami K. Tol2: a versatile gene transfer vector in vertebrates. *Genome Biology*. 2007;8 Suppl 1:S7.

110. Suster ML, Kikuta H, Urasaki A, Asakawa K, Kawakami K. Transgenesis in zebrafish with the tol2 transposon system. *Methods in Molecular Biology*. 2009;561:41-63.
111. Altman RB. Translational bioinformatics: linking the molecular world to the clinical world. *Clinical Pharmacology and Therapeutics*. 2012;91(6):994-1000.
112. Kouskoumvekaki I, Shublaq N, Brunak S. Facilitating the use of large-scale biological data and tools in the era of translational bioinformatics. *Briefings in Bioinformatics*. 2014;15(6):942-52.
113. Allcock RJ. Production and analytic bioinformatics for next-generation DNA sequencing. *Methods in Molecular Biology*. 2014;1168:17-29.
114. Ideker T, Galitski T, Hood L. A new approach to decoding life: systems biology. *Annual Review of Genomics and Human Genetics*. 2001;2:343-72.
115. Mushtaq MY, Verpoorte R, Kim HK. Zebrafish as a model for systems biology. *Biotechnology and Genetic Engineering Reviews*. 2013;29:187-205.
116. Alawieh A, Sabra Z, Nokkari A, El-Assaad A, Mondello S, Zaraket F, et al. Bioinformatics approach to understanding interacting pathways in neuropsychiatric disorders. *Methods in Molecular Biology*. 2014;1168:157-72.
117. Huang da W, Sherman BT, Lempicki RA. Systematic and integrative analysis of large gene lists using DAVID bioinformatics resources. *Nature Protocols*. 2009;4(1):44-57.
118. Kim SH, Speirs CK, Solnica-Krezel L, Ess KC. Zebrafish model of tuberous sclerosis complex reveals cell-autonomous and non-cell-autonomous functions of mutant tuberin. *Disease Models & Mechanisms*. 2011;4(2):255-67.
119. Berg AT, Berkovic SF, Brodie MJ, Buchhalter J, Cross JH, van Emde Boas W, et al. Revised terminology and concepts for organization of seizures and epilepsies: report of the ILAE Commission on Classification and Terminology, 2005-2009. *Epilepsia*. 2010;51(4):676-85.
120. Tavyev Asher YJ, Scaglia F. Molecular bases and clinical spectrum of early infantile epileptic encephalopathies. *European Journal of Medical Genetics*. 2012;55(5):299-306.
121. Veeramah KR, O'Brien JE, Meisler MH, Cheng X, Dib-Hajj SD, Waxman SG, et al. De novo pathogenic SCN8A mutation identified by whole-genome sequencing of a family quartet affected by infantile epileptic encephalopathy and SUDEP. *American Journal of Human Genetics*. 2012;90(3):502-10.
122. Estacion M, O'Brien JE, Conravey A, Hammer MF, Waxman SG, Dib-Hajj SD, et al. A novel de novo mutation of SCN8A (Nav1.6) with enhanced channel activation in a child with epileptic encephalopathy. *Neurobiology of Disease*. 2014;69:117-23.
123. Ohba C, Kato M, Takahashi S, Lerman-Sagie T, Lev D, Terashima H, et al. Early onset epileptic encephalopathy caused by de novo SCN8A mutations. *Epilepsia*. 2014;55(7):994-1000.
124. Li H, Durbin R. Fast and accurate short read alignment with Burrows-Wheeler transform. *Bioinformatics*. 2009;25(14):1754-60.
125. McKenna A, Hanna M, Banks E, Sivachenko A, Cibulskis K, Kernytsky A, et al. The Genome Analysis Toolkit: a MapReduce framework for analyzing next-generation DNA sequencing data. *Genome Research*. 2010;20(9):1297-303.
126. Wang K, Li M, Hakonarson H. ANNOVAR: functional annotation of genetic variants from high-throughput sequencing data. *Nucleic Acids Research*. 2010;38(16):e164.
127. Rozen S, Skaletsky H. Primer3 on the WWW for general users and for biologist programmers. *Methods in Molecular Biology*. 2000;132:365-86.
128. Schubert J, Siekierska A, Langlois M, May P, Huneau C, Becker F, et al. Mutations in STX1B, encoding a presynaptic protein, cause fever-associated epilepsy syndromes. *Nature Genetics*. 2014;46(12):1327-32.
129. Goetz R, Dover K, Laezza F, Shtraizent N, Huang X, Tchetchik D, et al. Crystal Structure of a Fibroblast Growth Factor Homologous Factor (FHF) Defines a Conserved Surface on FHF for Binding and Modulation of Voltage-gated Sodium Channels. *The Journal of biological chemistry*. 2009;284(26):17883-96.
130. Wang C, Chung BC, Yan H, Lee SY, Pitt GS. Crystal structure of the ternary complex of a NaV C-terminal domain, a fibroblast growth factor homologous factor, and calmodulin. *Structure*. 2012;20(7):1167-76.
131. Adzhubei IA, Schmidt S, Peshkin L, Ramensky VE, Gerasimova A, Bork P, et al. A method and server for predicting damaging missense mutations. *Nature Methods*. 2010;7(4):248-9.

132. Schwarz JM, Cooper DN, Schuelke M, Seelow D. MutationTaster2: mutation prediction for the deep-sequencing age. *Nature Methods*. 2014;11(4):361-2.
133. Shakkottai VG, Xiao M, Xu L, Wong M, Nerbonne JM, Ornitz DM, et al. FGF14 regulates the intrinsic excitability of cerebellar Purkinje neurons. *Neurobiology of Disease*. 2009;33(1):81-8.
134. Venkatesan K, Liu Y, Goldfarb M. Fast-onset long-term open-state block of sodium channels by A-type FHF_s mediates classical spike accommodation in hippocampal pyramidal neurons. *Journal of Neuroscience*. 2014;34(48):16126-39.
135. Smallwood PM, Munoz-Sanjuan I, Tong P, Macke JP, Hendry SH, Gilbert DJ, et al. Fibroblast growth factor (FGF) homologous factors: new members of the FGF family implicated in nervous system development. *Proceedings of the National Academy of Sciences U S A*. 1996;93(18):9850-7.
136. Morcos PA. Achieving targeted and quantifiable alteration of mRNA splicing with Morpholino oligos. *Biochemical and Biophysical Research Communications*. 2007;358(2):521-7.
137. Moulton JD. Making a Morpholino Experiment Work: Controls, Favoring Specificity, Improving Efficacy, Storage, and Dose. *Methods in Molecular Biology*. 2017;1565:17-29.
138. Hillman RT, Feng BY, Ni J, Woo WM, Milenkovic L, Hayden Gephart MG, et al. Neuropilins are positive regulators of Hedgehog signal transduction. *Genes & Development*. 2011;25(22):2333-46.
139. Mangos S, Lam PY, Zhao A, Liu Y, Mudumana S, Vasilyev A, et al. The ADPKD genes *pkd1a/b* and *pkd2* regulate extracellular matrix formation. *Disease Models & Mechanisms*. 2010;3(5-6):354-65.
140. San Antonio JD, Zoeller JJ, Habursky K, Turner K, Pimtong W, Burrows M, et al. A key role for the integrin $\alpha 2\beta 1$ in experimental and developmental angiogenesis. *American Journal of Pathology*. 2009;175(3):1338-47.
141. Place ES, Smith JC. Zebrafish *atoh8* mutants do not recapitulate morpholino phenotypes. *PLoS One*. 2017;12(2):e0171143.
142. Jobst-Schwan T, Schmidt JM, Schneider R, Hoogstraten CA, Ullmann JFP, Schapiro D, et al. Acute multi-sgRNA knockdown of KEOPS complex genes reproduces the microcephaly phenotype of the stable knockout zebrafish model. *PLoS One*. 2018;13(1):e0191503.
143. Dauber A, Golzio C, Guenot C, Jodelka FM, Kibaek M, Kjaergaard S, et al. SCRIB and PUF60 are primary drivers of the multisystemic phenotypes of the 8q24.3 copy-number variant. *American Journal of Human Genetics*. 2013;93(5):798-811.
144. Stankiewicz P, Khan TN, Szafranski P, Slattery L, Streff H, Vetrini F, et al. Haploinsufficiency of the Chromatin Remodeler BPTF Causes Syndromic Developmental and Speech Delay, Postnatal Microcephaly, and Dysmorphic Features. *American Journal of Human Genetics*. 2017;101(4):503-15.
145. Golzio C, Willer J, Talkowski ME, Oh EC, Taniguchi Y, Jacquemont S, et al. KCTD13 is a major driver of mirrored neuroanatomical phenotypes of the 16p11.2 copy number variant. *Nature*. 2012;485(7398):363-7.
146. Kluver N, Ortmann J, Paschke H, Renner P, Ritter AP, Scholz S. Transient overexpression of *adh8a* increases allyl alcohol toxicity in zebrafish embryos. *PLoS One*. 2014;9(3):e90619.
147. Hogan BM, Verkade H, Lieschke GJ, Heath JK. Manipulation of gene expression during zebrafish embryonic development using transient approaches. *Methods in Molecular Biology*. 2008;469:273-300.
148. Cho YS, Lee SY, Kim YK, Kim DS, Nam YK. Functional ability of cytoskeletal beta-actin regulator to drive constitutive and ubiquitous expression of a fluorescent reporter throughout the life cycle of transgenic marine medaka *Oryzias dancena*. *Transgenic Research*. 2011;20(6):1333-55.
149. Kondrychyn I, Garcia-Lecea M, Emelyanov A, Parinov S, Korzh V. Genome-wide analysis of Tol2 transposon reintegration in zebrafish. *BMC Genomics*. 2009;10:418.
150. Trudeau MM, Dalton JC, Day JW, Ranum LP, Meisler MH. Heterozygosity for a protein truncation mutation of sodium channel *SCN8A* in a patient with cerebellar atrophy, ataxia, and mental retardation. *Journal of medical genetics*. 2006;43(6):527-30.
151. Larsen J, Carvill GL, Gardella E, Kluger G, Schmiedel G, Barisic N, et al. The phenotypic spectrum of *SCN8A* encephalopathy. *Neurology*. 2015;84(5):480-9.

152. Shimobayashi M, Hall MN. Making new contacts: the mTOR network in metabolism and signalling crosstalk. *Nature Reviews Molecular Cell Biology*. 2014;15(3):155-62.
153. Ma XM, Blenis J. Molecular mechanisms of mTOR-mediated translational control. *Nature Reviews Molecular Cell Biology*. 2009;10(5):307-18.
154. Crino PB, Nathanson KL, Henske EP. The Tuberous Sclerosis Complex. *New England Journal of Medicine*. 2006;355(13):1345-56.
155. De Waele L, Lagae L, Mekahli D. Tuberous sclerosis complex: the past and the future. *Pediatric Nephrology*. 2015;30(10):1771-80.
156. Curatolo P, Moavero R, de Vries PJ. Neurological and neuropsychiatric aspects of tuberous sclerosis complex. *The Lancet Neurology*. 2015;14(7):733-45.
157. Qin W, Chan JA, Vinters HV, Mathern GW, Franz DN, Taillon BE, et al. Analysis of TSC cortical tubers by deep sequencing of TSC1, TSC2 and KRAS demonstrates that small second-hit mutations in these genes are rare events. *Brain pathology (Zurich, Switzerland)*. 2010;20(6):1096-105.
158. Abs E, Goorden SM, Schreiber J, Overwater IE, Hoogeveen-Westerveld M, Bruinsma CF, et al. TORC1-dependent epilepsy caused by acute biallelic Tsc1 deletion in adult mice. *Annals of neurology*. 2013;74(4):569-79.
159. Lozovaya N, Gataullina S, Tsintsadze T, Tsintsadze V, Pallesi-Pocachard E, Minlebaev M, et al. Selective suppression of excessive GluN2C expression rescues early epilepsy in a tuberous sclerosis murine model. *Nature communications*. 2014;5:4563.
160. Marcotte L, Aronica E, Baybis M, Crino PB. Cytoarchitectural alterations are widespread in cerebral cortex in tuberous sclerosis complex. *Acta neuropathologica*. 2012;123(5):685-93.
161. Okanishi T, Akiyama T, Tanaka S, Mayo E, Mitsutake A, Boelman C, et al. Interictal high frequency oscillations correlating with seizure outcome in patients with widespread epileptic networks in tuberous sclerosis complex. *Epilepsia*. 2014;55(10):1602-10.
162. Kalueff AV, Stewart AM, Gerlai R. Zebrafish as an emerging model for studying complex brain disorders. *Trends in pharmacological sciences*. 2014;35(2):63-75.
163. Nasevicius A, Ekker SC. Effective targeted gene "knockdown" in zebrafish. *Nature Genetics*. 2000;26(2):216-20.
164. Zon LI, Peterson RT. In vivo drug discovery in the zebrafish. *Nature Reviews Drug Discovery*. 2005;4(1):35-44.
165. Bedell VM, Wang Y, Campbell JM, Poshusta TL, Starker CG, Krug RG, 2nd, et al. In vivo genome editing using a high-efficiency TALEN system. *Nature*. 2012;491(7422):114-8.
166. Nishimura Y, Murakami S, Ashikawa Y, Sasagawa S, Umemoto N, Shimada Y, et al. Zebrafish as a systems toxicology model for developmental neurotoxicity testing. *Congenital Anomalies*. 2015;55(1):1-16.
167. Hortopan GA, Dinday MT, Baraban SC. Zebrafish as a model for studying genetic aspects of epilepsy. *Disease Models & Mechanisms*. 2010;3(3-4):144-8.
168. Copmans D, Meinel T, Dietz C, van Leeuwen M, Ortmann J, Berthold MR, et al. A KNIME-Based Analysis of the Zebrafish Photomotor Response Clusters the Phenotypes of 14 Classes of Neuroactive Molecules. *Journal of Biomolecular Screening*. 2016;21(5):427-36.
169. Kokel D, Bryan J, Laggner C, White R, Cheung CYJ, Mateus R, et al. Rapid behavior-based identification of neuroactive small molecules in the zebrafish. *Nature chemical biology*. 2010;6(3):231-7.
170. Bolger AM, Lohse M, Usadel B. Trimmomatic: a flexible trimmer for Illumina sequence data. *Bioinformatics*. 2014;30(15):2114-20.
171. Kim D, Pertea G, Trapnell C, Pimentel H, Kelley R, Salzberg SL. TopHat2: accurate alignment of transcriptomes in the presence of insertions, deletions and gene fusions. *Genome Biology*. 2013;14(4):R36.
172. Trapnell C, Roberts A, Goff L, Pertea G, Kim D, Kelley DR, et al. Differential gene and transcript expression analysis of RNA-seq experiments with TopHat and Cufflinks. *Nature Protocols*. 2012;7(3):562-78.
173. Kong L, Zhang Y, Ye ZQ, Liu XQ, Zhao SQ, Wei L, et al. CPC: assess the protein-coding potential of transcripts using sequence features and support vector machine. *Nucleic Acids Research*. 2007;35(Web Server issue):W345-9.

174. Cline MS, Smoot M, Cerami E, Kuchinsky A, Landys N, Workman C, et al. Integration of biological networks and gene expression data using Cytoscape. *Nature Protocols*. 2007;2(10):2366-82.
175. Ramakers C, Ruijter JM, Deprez RH, Moorman AF. Assumption-free analysis of quantitative real-time polymerase chain reaction (PCR) data. *Neuroscience Letters*. 2003;339(1):62-6.
176. Ruijter JM, Ramakers C, Hoogaars WM, Karlen Y, Bakker O, van den Hoff MJ, et al. Amplification efficiency: linking baseline and bias in the analysis of quantitative PCR data. *Nucleic acids research*. 2009;37(6):e45.
177. Durinck S, Moreau Y, Kasprzyk A, Davis S, De Moor B, Brazma A, et al. BioMart and Bioconductor: a powerful link between biological databases and microarray data analysis. *Bioinformatics*. 2005;21(16):3439-40.
178. Wagner AH, Coffman AC, Ainscough BJ, Spies NC, Skidmore ZL, Campbell KM, et al. DGIdb 2.0: mining clinically relevant drug-gene interactions. *Nucleic Acids Research*. 2016;44(D1):D1036-44.
179. Hsing LC, Rudensky AY. The lysosomal cysteine proteases in MHC class II antigen presentation. *Immunological reviews*. 2005;207:229-41.
180. Chiang GG, Abraham RT. Phosphorylation of mammalian target of rapamycin (mTOR) at Ser-2448 is mediated by p70S6 kinase. *The Journal of biological chemistry*. 2005;280(27):25485-90.
181. Varga M, Fodor E, Vellai T. Autophagy in zebrafish. *Methods*. 2015;75:172-80.
182. Crino PB. mTOR: A pathogenic signaling pathway in developmental brain malformations. *Trends in Molecular Medicine*. 2011;17(12):734-42.
183. Saint-Amant L. Development of motor rhythms in zebrafish embryos. *Progress in brain research*. 2010;187:47-61.
184. Kokel D, Dunn TW, Ahrens MB, Alshut R, Cheung CY, Saint-Amant L, et al. Identification of nonvisual photomotor response cells in the vertebrate hindbrain. *Journal of Neuroscience*. 2013;33(9):3834-43.
185. Orger MB, Gahtan E, Muto A, Page-McCaw P, Smear MC, Baier H. Behavioral screening assays in zebrafish. *Methods in cell biology*. 2004;77:53-68.
186. Low SE, Woods IG, Lachance M, Ryan J, Schier AF, Saint-Amant L. Touch responsiveness in zebrafish requires voltage-gated calcium channel 2.1b. *Journal of neurophysiology*. 2012;108(1):148-59.
187. Sapetto-Rebow B, McLoughlin SC, O'Shea LC, O'Leary O, Willer JR, Alvarez Y, et al. Maternal topoisomerase II alpha, not topoisomerase II beta, enables embryonic development of zebrafish top2a^{-/-} mutants. *BMC developmental biology*. 2011;11:71.
188. Lee JH, Huynh M, Silhavy JL, Kim S, Dixon-Salazar T, Heiberg A, et al. De novo somatic mutations in components of the PI3K-AKT3-mTOR pathway cause hemimegalencephaly. *Nature Genetics*. 2012;44(8):941-5.
189. Jansen LA, Mirzaa GM, Ishak GE, O'Roak BJ, Hiatt JB, Roden WH, et al. PI3K/AKT pathway mutations cause a spectrum of brain malformations from megalencephaly to focal cortical dysplasia. *Brain*. 2015;138(Pt 6):1613-28.
190. Capo-Chichi JM, Tcherkezian J, Hamdan FF, Decarie JC, Dobrzyniecka S, Patry L, et al. Disruption of TBC1D7, a subunit of the TSC1-TSC2 protein complex, in intellectual disability and megalencephaly. *Journal of medical genetics*. 2013;50(11):740-4.
191. Maloof J, Sledz K, Hogg JF, Bodensteiner JB, Schwartz T, Schochet SS. Unilateral megalencephaly and tuberous sclerosis: related disorders? *Journal of child neurology*. 1994;9(4):443-6.
192. Griffiths PD, Gardner SA, Smith M, Rittey C, Powell T. Hemimegalencephaly and focal megalencephaly in tuberous sclerosis complex. *American Journal of Neuroradiology*. 1998;19(10):1935-8.
193. Masoumi H, Kinney HC, Chadwick AE, Rubio A, Krous HF. Sudden unexpected death in childhood associated with cardiac rhabdomyoma, involuting adrenal ganglioneuroma, and megalencephaly: another expression of tuberous sclerosis? *Pediatric and developmental pathology : the official journal of the Society for Pediatric Pathology and the Paediatric Pathology Society*. 2007;10(2):129-33.

194. Tee AR, Sampson JR, Pal DK, Bateman JM. The role of mTOR signalling in neurogenesis, insights from tuberous sclerosis complex. *Seminars in Cell & Developmental Biology*. 2016;52:12-20.
195. Zeng L-H, Rensing NR, Zhang B, Gutmann DH, Gambello MJ, Wong M. Tsc2 gene inactivation causes a more severe epilepsy phenotype than Tsc1 inactivation in a mouse model of Tuberous Sclerosis Complex. *Human Molecular Genetics*. 2011;20(3):445-54.
196. Way SW, McKenna J, Mietzsch U, Reith RM, Wu HCJ, Gambello MJ. Loss of Tsc2 in radial glia models the brain pathology of tuberous sclerosis complex in the mouse. *Human Molecular Genetics*. 2009;18.
197. Boer K, Crino PB, Gorter JA, Nellist M, Jansen FE, Spliet WG, et al. Gene expression analysis of tuberous sclerosis complex cortical tubers reveals increased expression of adhesion and inflammatory factors. *Brain Pathology*. 2010;20(4):704-19.
198. Boer K, Jansen F, Nellist M, Redeker S, Ouweland AMW, Spliet WGM. Inflammatory processes in cortical tubers and subependymal giant cell tumors of tuberous sclerosis complex. *Epilepsy Research*. 2008;78.
199. Prabowo AS, Anink JJ, Lammens M, Nellist M, van den Ouweland AM, Adle-Biassette H, et al. Fetal brain lesions in tuberous sclerosis complex: TORC1 activation and inflammation. *Brain Pathology*. 2013;23(1):45-59.
200. Zhang B, Zou J, Rensing NR, Yang M, Wong M. Inflammatory mechanisms contribute to the neurological manifestations of tuberous sclerosis complex. *Neurobiology of Disease*. 2015;80.
201. Berridge MJ, Lipp P, Bootman MD. The versatility and universality of calcium signalling. *Nature Reviews Molecular Cell Biology*. 2000;1(1):11-21.
202. Zhang SJ, Zou M, Lu L, Lau D, Ditzel DA, Delucinge-Vivier C, et al. Nuclear calcium signaling controls expression of a large gene pool: identification of a gene program for acquired neuroprotection induced by synaptic activity. *PLoS Genetics*. 2009;5(8):e1000604.
203. Bading H. Nuclear calcium signalling in the regulation of brain function. *Nature Reviews Neuroscience*. 2013;14(9):593-608.
204. Steinlein OK. Calcium signaling and epilepsy. *Cell and Tissue Research*. 2014;357(2):385-93.
205. Carmignoto G, Haydon PG. Astrocyte calcium signaling and epilepsy. *Glia*. 2012;60(8):1227-33.
206. Gorter JA, van Vliet EA, Aronica E, Breit T, Rauwerda H, Lopes da Silva FH, et al. Potential new antiepileptogenic targets indicated by microarray analysis in a rat model for temporal lobe epilepsy. *Journal of Neuroscience*. 2006;26(43):11083-110.
207. Vezzani A, Granata T. Brain inflammation in epilepsy: experimental and clinical evidence. *Epilepsia*. 2005;46(11):1724-43.
208. Wendt W, Lubbert H, Stichel CC. Upregulation of cathepsin S in the aging and pathological nervous system of mice. *Brain Research*. 2008;1232:7-20.
209. Jedezsko C, Sloane BF. Cysteine cathepsins in human cancer. *Biological Chemistry*. 2004;385(11):1017-27.
210. Jiang Z, Yamauchi K, Yoshioka K, Aoki K, Kuroyanagi S, Iwata A, et al. Support vector machine-based feature selection for classification of liver fibrosis grade in chronic hepatitis C. *Journal of Medical Systems*. 2006;30(5):389-94.
211. Hughes CS, Colhoun LM, Bains BK, Kilgour JD, Burden RE, Burrows JF, et al. Extracellular cathepsin S and intracellular caspase 1 activation are surrogate biomarkers of particulate-induced lysosomal disruption in macrophages. *Particle and Fibre Toxicology*. 2016;13:19.
212. Lemere CA, Munger JS, Shi GP, Natkin L, Haass C, Chapman HA, et al. The lysosomal cysteine protease, cathepsin S, is increased in Alzheimer's disease and Down syndrome brain. An immunocytochemical study. *American Journal of Pathology*. 1995;146(4):848-60.
213. Henske EP, Wessner LL, Golden J, Scheithauer BW, Vortmeyer AO, Zhuang Z. Loss of tuberin in both subependymal giant cell astrocytomas and angiomyolipomas supports a two-hit model for the pathogenesis of tuberous sclerosis tumors. *American Journal of Pathology*. 1997;151.
214. Chan JA, Zhang H, Roberts PS, Jozwiak S, Wieslawa G, Lewin-Kowalik J. Pathogenesis of tuberous sclerosis subependymal giant cell astrocytomas: biallelic inactivation of TSC1 or TSC2 leads to mTOR activation. *Journal of Neuropathology and Experimental Neurology*. 2004;63.

215. Crino PB, Aronica E, Baltuch G, Nathanson KL. Biallelic TSC gene inactivation in tuberous sclerosis complex. *Neurology*. 2010;74.
216. Fingar DC, Blenis J. Target of rapamycin (TOR): an integrator of nutrient and growth factor signals and coordinator of cell growth and cell cycle progression. *Oncogene*. 2004;23.
217. Brown EJ, Beal PA, Keith CT, Chen J, Shin TB, Schreiber SL. Control of p70 s6 kinase by kinase activity of FRAP in vivo. *Nature*. 1995;377(6548):441-6.
218. Holz MK, Blenis J. Identification of S6 kinase 1 as a novel mammalian target of rapamycin (mTOR)-phosphorylating kinase. *The Journal of biological chemistry*. 2005;280(28):26089-93.
219. Boglev Y, Badrock AP, Trotter AJ, Du Q, Richardson EJ, Parslow AC, et al. Autophagy Induction Is a Tor- and Tp53-Independent Cell Survival Response in a Zebrafish Model of Disrupted Ribosome Biogenesis. *PLoS genetics*. 2013;9(2):e1003279.
220. Hosokawa N, Hara T, Kaizuka T, Kishi C, Takamura A, Miura Y, et al. Nutrient-dependent mTORC1 association with the ULK1-Atg13-FIP200 complex required for autophagy. *Molecular biology of the cell*. 2009;20(7):1981-91.
221. Klionsky DJ, Abdelmohsen K, Abe A, Abedin MJ, Abeliovich H, Acevedo Arozena A, et al. Guidelines for the use and interpretation of assays for monitoring autophagy (3rd edition). *Autophagy*. 2016;12(1):1-222.
222. Loscher W, Klitgaard H, Twyman RE, Schmidt D. New avenues for anti-epileptic drug discovery and development. *Nature Reviews Drug Discovery*. 2013;12(10):757-76.
223. Smith M, Wilcox KS, White HS. Discovery of antiepileptic drugs. *Neurotherapeutics : the journal of the American Society for Experimental NeuroTherapeutics*. 2007;4(1):12-7.
224. Mandhane SN, Aavula K, Rajamannar T. Timed pentylenetetrazol infusion test: a comparative analysis with s.c.PTZ and MES models of anticonvulsant screening in mice. *Seizure*. 2007;16(7):636-44.
225. Barker-Haliski ML, Johnson K, Billingsley P, Huff J, Handy LJ, Khaleel R, et al. Validation of a Preclinical Drug Screening Platform for Pharmacoresistant Epilepsy. *Neurochemical Research*. 2017;42(7):1904-18.
226. Claes L, Del-Favero J, Ceulemans B, Lagae L, Van Broeckhoven C, De Jonghe P. De novo mutations in the sodium-channel gene SCN1A cause severe myoclonic epilepsy of infancy. *American Journal of Human Genetics*. 2001;68(6):1327-32.
227. Dravet C, Bureau M, Oguni H, Fukuyama Y, Cokar O. Severe myoclonic epilepsy in infancy: Dravet syndrome. *Advances in Neurology*. 2005;95:71-102.
228. Marini C, Scheffer IE, Nabbout R, Suls A, De Jonghe P, Zara F, et al. The genetics of Dravet syndrome. *Epilepsia*. 2011;52 Suppl 2:24-9.
229. Al-Mehmadi S, Splitt M, For DDDSG, Ramesh V, DeBrosse S, Dessoffy K, et al. FHF1 (FGF12) epileptic encephalopathy. *Neurology Genetics*. 2016;2(6):e115.
230. Guella I, Huh L, McKenzie MB, Toyota EB, Bebin EM, Thompson ML, et al. De novo FGF12 mutation in 2 patients with neonatal-onset epilepsy. *Neurology Genetics*. 2016;2(6):e120.
231. Villeneuve N, Abidi A, Cacciagli P, Mignon-Ravix C, Chabrol B, Villard L, et al. Heterogeneity of FHF1 related phenotype: Novel case with early onset severe attacks of apnea, partial mitochondrial respiratory chain complex II deficiency, neonatal onset seizures without neurodegeneration. *European Journal of Paediatric Neurology*. 2017;21(5):783-6.
232. Samuel R, Stephenson R, Roy P, Pryor R, Zhou L, Bonkowsky JL, et al. Microfluidic-aided genotyping of zebrafish in the first 48 h with 100 % viability. *Biomedical microdevices*. 2015;17(2):43.

© cover image adapted from: 2016 DBCLS 統合 TV, licensed under Creative Commons Attribution 4.0 International License (CC-BY-4.0)

	translational Applications in the brain’ KU Leuven, Leuven
2016	f-TALES ‘Animal models of neurodegeneration’ IMEC, Leuven
2014	3 rd LIND seminar ‘Getting Connected’ LAMOT, Mechelen
2014	Mini-symposium on ADME profiling KU Leuven, Leuven

MENTORING

2017 – 2018	Supervisor of master student Lena Ceyskens (KU Leuven)
2016 – 2017	Supervisor of master student Dieter Willekens (KU Leuven)
2015 – 2016	Supervisor of master student Liesl Jacobs (KU Leuven)

TEACHING

2015 – 2017	Supervisor in laboratory sessions of Biopharmaceutical research
2013 – 2015	Supervisor of LOCO ‘Formulering en bereiding van geneesmiddelen’

EXPERIENCE

June 2014 – present	Dissemination officer within the European research project EPISTOP
2016 – 2017	Chair of the Organizing Committee of the 13 th ULLA Summer School
2015	Supervisor workshop epilepsy research during “G4G Mol 2015” (11-16 year olds) in European School Mol
2015 – 2017	Ombuds person for students of 3 rd bachelor of Pharmaceutical Sciences (KUL)
2013 – 2015	Representative of AAP/BAP in the Council of the Department of the faculty of Pharmaceutical Sciences (KUL)
2012-2013	member of the working group ‘specialisation Drug Development’ (faculty of Pharmaceutical Sciences – KUL)
2011 – 2013	Student Representative, Pharmaceutical Sciences (KUL)
2010 – 2013	Member of the Permanent Education Commission (POC) of the faculty of Pharmaceutical Sciences (KUL)
2006 – 2008	Member of the Council for Tolerance (Secondary education, Sint-Jozefcollege Turnhout)

PUBLICATIONS

Serra I., Scheldeman C., Bazelot M., Whalley B.J., Dallas M.L., de Witte P.A.M., Williams C.M. Cannabidiol reduces pS6 signalling in a zebrafish model of Tuberous Sclerosis Complex. (manuscript in preparation)

Scheldeman C., Mills JD, Siekierska A, Serra I, Copmans D, Iyer AM, et al. mTOR-related neuropathology in mutant tsc2 zebrafish: Phenotypic, transcriptomic and pharmacological analysis. Neurobiol Dis. 2017

Siekierska A*, Isrie M*, Liu Y*, Scheldeman C., Vanthillo N, Lagae L, et al. Gain-of-function FHF1 mutation causes early-onset epileptic encephalopathy with cerebellar atrophy. Neurology. 2016;86(23):2162-70

PERSONAL CONTRIBUTION

Chapter III: The contributions of Chloë Scheldeman were focused on the zebrafish-related research. Chloë Scheldeman, Aleksandra Siekierska and Peter A.M. de Witte were responsible for study design and experimental design. Experiments were performed and data analyzed by Chloë Scheldeman under supervision of Aleksandra Siekierska and Peter A.M. de Witte. Chloë Scheldeman wrote the chapter.

Chapter IV: The contributions of Chloë Scheldeman were focused on the phenotypic and pharmacological validation of the zebrafish model. The contributions of the co-first author James D. Mills were focused on the analysis of the transcriptome data. Chloë Scheldeman and Peter A.M. de Witte were responsible for study design and experimental design. Experiments were performed and data analyzed by Chloë Scheldeman, i.e. Fig1, Fig3, Fig4 and Fig6. Chloë Scheldeman wrote the chapter.

CONFLICT OF INTEREST STATEMENT

Chapter III and IV: No potential conflict of interest was identified.

Chapter III and IV: Funding sources and scientific acknowledgements are described in the acknowledgement section of each chapter.

